INVESTIGATION OF EQUILIBRIUM FLOW IN A SLIGHTLY DIVERGENT CHANNEL

by

J. RAY RUETENIK

Department of Mechanical Engineering

Report I - 19

Performed under
Contract N- onr 248(33)
Office of Naval Research
Navy Department,
Washington, D. C.

August, 1954

The Johns Hopkins University
Department of Mechanical Engineering
Baltimore 18, Maryland

INVESTIGATION OF EQUILIBRIUM FLOW IN A SLIGHTLY DIVERGENT CHANNEL

by

J. Ray Ruetenik

Report I - 19

Performed under
Contract N- onr 248(33)
Office of Naval Research
Navy Department,
Washington, D.C.

August, 1954

Approved by George F. Wislicenus
Dr. George F. Wislicenus
Research Contract Director

INVESTIGATION OF EQUILIBRIUM FLOW IN A SLIGHTLY DIVERGENT CHANNEL by J. R. Ruetenik

ERRATA

1. P. 21, Line 30: Replace "would" by "could".
2. P. 22, Line 26: Replace "6" by "8"
3. P. 23, Line 26: Replace "A_o" by "A_e".
   Line 30: Replace "R_o" by "R_f".
4. P. 25, Line 24: Replace "$-\frac{1}{}$" by "$-\frac{}{}$"
5. P. 26, Line 21: Replace "5" by "15".
   Line 23: Replace "4" by "5".
6. P. 31, Line 12: Define R_λ as on P. VII.
   Line 14: Replace "19" by "20".
   Line 17 & 25: Replace "R_b" by "R".
7. P. 33, Line 20: Replace "27" by "28".
   Line 26: Replace "26" by "27".
8. P. 44: Add to reference 30 "Journal of the Aeronautical Sciences, July 1953, p. 477-82."

ACKNOWLEDGEMENTS

This investigation was conducted in the Laboratory of the Mechanical Engineering Department at Johns Hopkins University under the sponsorship of the Office of Naval Research, Mechanics Branch. The writer wishes to express his appreciation to Professor George F. Wislicenus under whose direction the investigation was conducted, and Professor Stanley Corrsin who conceived the problem and gave continuous guidance and encouragement through every phase of the work. The assistance of many others is appreciated, but due to space mention will be limited to: Messrs. Ronald Stouffer and Lester Jones who helped in the experimental work, Mr. Richard Marks who constructed the instruments, and Mrs. Doris A. Van-Meter and Mrs. Gertrud M. Michelson for the typing.

TABLE OF CONTENTS

SYMBOLS

(as they appear)

U, V, W	Instantaneous velocities in the x, y, and z directions respectively.
$\overline{U}$, $\overline{V}$, $\overline{W}$	Mean velocities in the x, y, and z directions.
u, v, w	Instantaneous values of the velocity fluctuations in the x, y, and z directions
u', v', w'	Root-mean-square values of the velocity fluctuation.
$\overline{P}$	Mean pressure at any point.
P	Instantaneous pressure at any point.
p	Instantaneous value of the pressure fluctuation.
t	Time.
ρ	Air density.
μ	Air viscosity.
ν	Kinematic viscosity of air.
e	Kinetic energy of the turbulent motion: $\frac{1}{2}\rho q^2$
q	Instantaneous value of the speed fluctuation: $\sqrt{u^2 + v^2 + w^2}$
α	Local half-angle between the walls.
R_b	Reynolds number: $\frac{U_o b}{\nu}$
U_o	Mean Velocity at y = o.
P*	A pressure term: $\overline{P} + \overline{\rho v^2}$
τ	Total shearing stress: τ_w is the value at the wall. $\mu \frac{\partial \overline{U}}{\partial y} - \rho \overline{uw}$
y'	Distance from the wall: b - y
η	Dimensionless distance from the wall: $\frac{y'}{b}$

c_f — Skin-friction coefficient: $\dfrac{\tau_w}{\rho U_o^2}$

ζ — Dimensionless distance along diffuser:

$$\int_{x=0}^{x} \frac{dx_1}{b(x_1)} \qquad x = 0, \text{(entrance)}$$

k_1 — One-dimensional wave number in x direction.

$F_u(k_1)$, $F_v(k_1)$, $F_w(k_1)$ — Fraction of turbulent energy $\overline{u^2}$, $\overline{v^2}$, $\overline{w^2}$, respectively, associated with k_1:

$$\int_0^\infty F_u(k_1)\,dk_1 = 1, \text{ etc.}$$

λ_u, λ_v, λ_w — Microscales of turbulence:

$$\frac{u'}{\left(\frac{\partial u}{\partial x}\right)'}, \quad \frac{\sqrt{2}\,v'}{\left(\frac{\partial v}{\partial x}\right)'}, \quad \frac{\sqrt{2}\,w'}{\left(\frac{\partial w}{\partial x}\right)'} \qquad \text{respectively.}$$

(P_r) — Rate of production of turbulent energy:

$$-\frac{b}{U_o^3}\left[\overline{uv}\,\frac{\partial \bar{U}}{\partial y} + \left(\overline{u^2} - \overline{v^2}\right)\frac{\partial \bar{U}}{\partial x}\right]$$

$(P_r)_2$ — Portion of rate of production of turbulent energy:

$$-\frac{b}{U_o^3}\left(\overline{u^2} - \overline{v^2}\right)\frac{\partial \bar{U}}{\partial x}$$

(C) — Rate of convection of turbulent energy by mean motion:

$$\frac{b}{U_o^3}\left[\bar{U}\,\frac{\partial\left(\frac{1}{2}\overline{q^2}\right)}{\partial x} + \bar{V}\,\frac{\partial\left(\frac{1}{2}\overline{q^2}\right)}{\partial y}\right]$$

(T) — Rate of pressure work plus turbulent diffusion:

$$\frac{b}{U_o^3}\,\frac{\partial}{\partial y}\left\{\overline{v\left(\tfrac{1}{2}q^2 + \frac{p}{\rho}\right)}\right\}$$

(V) — Rate of "viscous work":

$$-\frac{b^2}{U_o^2 R_b}\,\frac{\partial^2\left(\frac{1}{2}\overline{q^2}\right)}{\partial y^2}$$

(W) — Rate of "dissipation":

$$\frac{b^2}{U_o^2 R_b}\,\overline{\left(\frac{\partial u_i}{\partial x_k}\right)\left(\frac{\partial u_i}{\partial x_k}\right)}$$

R_λ	Reynolds number of microscale: $\frac{1}{3\nu}\frac{\overline{q^2}}{\sqrt{\left(\frac{\partial u}{\partial x}\right)^2}}$
u_*	Wall shear-stress velocity: $\sqrt{\left\|\frac{\tau_w}{\rho}\right\|}$
y_*	Dimensionless distance from the wall: $\frac{y' u_*}{\nu}$
γ	Fluid weight density.
h	Height of fluid column in manometer - capillarity absent.
S	Surface tension, force per unit length.
M	Dimensionless meniscus parameter.
h_c	Additional height of liquid column due to capillarity.
A, B	Coefficients in King's Equation
Φ	Hot-wire Correction

INTRODUCTION

The early attempts towards a representation of turbulent shear flow were by the so-called phenomenological theories. They were developed during the late twenties and early thirties, and enjoyed some success at predicting mean-velocity distributions, but it became apparent that their basic assumptions were in conflict with observations. The assumptions and discrepancies were clearly reviewed by Batchelor (ref. 1).

This phase of development emphasized the fact that the effects of turbulent motion (transport of stream properties and conversion of energy to heat) required the investigation of the dynamics of the fluctuating motion. The simple case of isotropic turbulence had been studied in more detail, and some success has been realized in applying the results of isotropic theory to limited portions of shearing flow. But the production of turbulent energy from the mean motion and the transport of mean momentum by the fluctuating motion, important to shearing flows, is absent in the isotropic case. In fact the transport of all mean properties may be different in the shearing flow.

It became apparent some years ago that some simple and clearly defined turbulent shearing flows should be set up in the laboratory in order to accumulate more data on the statistical properties of the turbulent motion preliminary to formulating a theory of the mechanism of turbulent motion. The circular jet has been explored by Corrsin and Uberoi (ref. 2, et. al.); the half-jet by Liepmann and Laufer (ref. 3); the two-dimensional wake by Townsend (ref. 4, et. al.); the channel (ref. 5) and pipe (ref. 6) by Laufer; the boundary layer by Townsend (ref. 7), and Klebanoff and Diehl (ref. 8); and the boundary layer in an adverse pressure gradient by Schubauer and Klebanoff (ref. 9), Ludwieg and Tillmann (ref. 10), and Clauser (ref. 11). (The last two were restricted to measurements of the mean motion but were included as they made significant contributions to the general understanding of the important parameters.)

The boundary layer on a solid surface, which is important in engineering and convenient to explore experimentally, is characterized by a rising Reynolds number in the direction of the flow. This implies, as pointed out by Townsend (ref. 7) and Clauser (ref. 11). that a state of dynamic equilibrium cannot exist in the turbulent boundary layer (without bleeding). There would be a progressive change in the direction of the flow between the large-scale and the small-scale structure of the motion, e. g. the ratio of an "integral scale" to a "microscale". This complication motivated Laufer to investigate the flow in a channel with a rectangular cross-section (ref. 5) and a pipe (ref. 6) where the Reynolds number of the flow far from the entrance remains constant. The latter two investigations are closest to the present experiment, so will serve as the principal basis for comparison.

The diverging channel is a next logical investigation following the channel and pipe since the characteristic overall dimension of the flow, the channel width, is varied in the direction of the flow, but the dynamic equilibrium is retained by keeping the channel essentially two-dimensional (for which the Reynolds number is constant) and the walls plane. Beside the basic significance of such an investigation, it is believed that the systematic study of this equilibrium flow affords the soundest approach to such an engineering problem as maintaining unseparated flow in a diffuser.

Previous measurements had been reported in a diverging channel by Dönch (ref. 12) and Nikuradse (ref. 13) but they were limited to mean-velocities. Furthermore, there is considerable doubt whether the flow in reference 13 had reached equilibrium (discussed further in Appendix I). Therefore little reference will be made to these two sources.

The two most important forces on a turbulent flow are the pressure and wall shear stress. In Laufer's two experiments these were in balance. Logically one might investigate the case where the pressure force is absent -- a very small positive-angle diffuser -- but it was felt that the more interesting flow is that where the pressure forces are large. Therefore a two-dimensional diffuser was

built with provision for a half-angle of divergence from zero to 6 degrees. At a 1 degree half-angle, which is the angle reported here, the pressure force was 7 times larger than the wall-shear force.

Considerable effort was spent to attain an equilibrium state by the downstream region of the diffuser. A parallel-wall channel was placed ahead of the diffuser to give the flow a head start towards equilibrium, and the diffuser test section is 117 half-widths (ξ, defined later) long, more than three times that of reference 13. The steps taken to establish the equilibrium flow are discussed in detail in Appendix I. The flow was in equilibrium, determined by the mean velocity and turbulence-level profiles, in a considerable portion of the diffuser.

Townsend (ref. 7) first demonstrated the importance of the turbulent region very near the solid surface. Later Laufer confirmed the observation in the channel (ref 5) and the pipe (ref.6) where he demonstrated that the rate of production, diffusion, and dissipation of turbulent energy reach a sharp maximum at the outer edge of the laminar sublayer and are much larger than in the other regions. It appears that this region deserves intensive investigation. This contention has guided the work in the present investigation. The diffuser is about 8 inches wide at the downstream end and very small probes were constructed to enable measurements into the laminar sublayer.

ANALYTICAL CONSIDERATIONS

Equations of Motion for Flow in a Two-Dimensional Converging or Diverging Channel with a Small Angle.

The mean - and fluctuating velocity components are represented by $\bar{U}_i$ and u_i respectively in x_i Cartesian coordinate and pressure is P. Repeated indices indicate summation. The time (or ensemble) average is indicated by a bar, so for stationary flow

$$U_i(x_i,t) = \bar{U}_i(x_i) + u_i(x_i,t)$$

$$P(x_i,t) = \bar{P}(x_i) + p(x_i,t)$$

where $\bar{u}_i \equiv \bar{p}_i \equiv 0$ by definition. The continuity equation (1), Reynolds equations (2), and turbulent kinetic-energy equation (3) are

$$\frac{\partial \bar{U}_i}{\partial x_i} = 0 \tag{1}$$

$$\rho \frac{\partial \bar{U}_i \bar{U}_k}{\partial x_k} = -\frac{\partial \bar{P}}{\partial x_i} + \frac{\partial}{\partial x_k}\left(\mu \frac{\partial \bar{U}_i}{\partial x_k} - \rho \overline{u_i u_k}\right) \tag{2}$$

$$\bar{U}_k \frac{\partial \bar{e}}{\partial x_k} = -\rho \overline{u_i u_k} \frac{\partial \bar{U}_i}{\partial x_k} - \frac{\partial}{\partial x_k}\left[\overline{u_k (e+p)}\right] + \nu \frac{\partial^2 \bar{e}}{\partial x_j \partial x_j} - \mu \overline{\left(\frac{\partial u_i}{\partial x_k}\right)\left(\frac{\partial u_i}{\partial x_k}\right)} \tag{3}$$

where

$$e \equiv \frac{1}{2} \rho u_i u_i$$

Henceforth, U, V, and W will replace U_i in the respective directions x, y, and z, which replace x_i . The coordinate x is in the direction of flow and along the line of symmetry; y is the transverse coordinate in the plane of flow; and z is normal thereto.

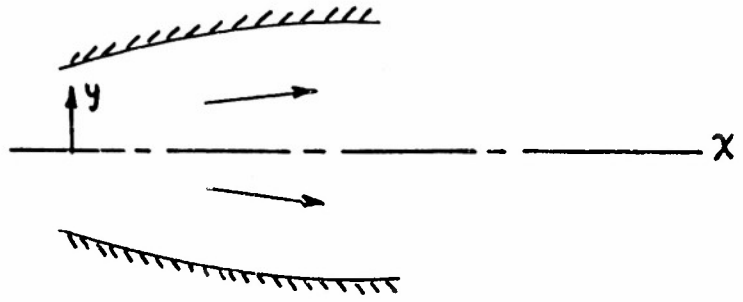

For flow in a two-dimensional converging or diverging (henceforth "diverging" will be used to imply both) channel at a small angle

(a) $\overline{W} = 0$

(b) $\frac{\partial(\bar{\ })}{\partial z} = 0$, where $(\bar{\ })$ is any term.

(c) $\alpha \ll 1$, where α is the local half-angle between the walls.

Equation (1) reduces by (b) to

$$\frac{\partial \bar{U}}{\partial x} + \frac{\partial \bar{V}}{\partial y} = 0 \qquad (4)$$

The following assumptions are made regarding the turbulent motion:

(d) $\overline{u^2}$, $\overline{v^2}$, $\overline{w^2}$, and $\overline{uv}$ are of the same order of magnitude. This was found to be the case, except very near the wall where $\overline{u^2}$ dominates, and at the center where $\overline{uv}$ goes to zero.

(e) $\overline{u^2} \ll \overline{U}^2$. This is not universally valid for turbulent flows; for example in the outer region of a jet entering a fluid at rest, near a separation point, or possibly in a channel at sufficiently low Reynolds number. However Laufer (ref. 5) found $\overline{u^2} < 0.1\,\overline{U}^2$ everywhere in the channel at $R_\delta > 3\times10^4$. This was confirmed in the present experiment.

Since $\alpha \ll 1$ it is reasonable to make the approximation that

$$\frac{\partial \xi}{\partial x} \ll \frac{\partial \xi}{\partial y}$$

where ξ refers to any velocity term. This will be called the "boundary-layer approximation". Note that the boundary-layer approximation is invalid at the axis of symmetry. In this region other assumptions will be called upon. Using the boundary-layer approximation in equation (4) one deduces that $\overline{V} \ll \overline{U}$. At the centerline $\overline{V} \ll \overline{U}$ by reason of symmetry, so it applies to the whole region of flow.

The x-momentum and y-momentum equation become

$$\overline{U}\frac{\partial \overline{U}}{\partial x} + \overline{V}\frac{\partial \overline{U}}{\partial y} = -\frac{1}{\rho}\frac{\partial \overline{P}}{\partial x} + \nu\frac{\partial^2 \overline{U}}{\partial y^2} - \frac{\partial \overline{uv}}{\partial y} \qquad (5a)$$

$$\frac{1}{\rho}\frac{\partial}{\partial y}\left(\overline{P} + \rho\overline{v^2}\right) = 0 \qquad (5b)$$

So $\bar{P} + \rho\overline{v^2}$, called P^* is a function of x alone. By (d) and (e) $\frac{\partial}{\partial x}(\rho\overline{v^2})$ is small in equation (5a) so it becomes

$$\bar{U}\frac{\partial \bar{U}}{\partial x} + \bar{V}\frac{\partial \bar{U}}{\partial y} = -\frac{1}{\rho}\frac{dP^*}{dx} + \nu\frac{\partial^2 \bar{U}}{\partial y^2} - \frac{\partial \overline{uv}}{\partial y} \qquad (6)$$

The turbulent kinetic-energy equation (3) by assumptions (a), (b), (c), and (d) is:

$$-\rho\overline{uv}\frac{\partial \bar{U}}{\partial y} = \bar{U}\frac{\partial \bar{e}}{\partial x} + \bar{V}\frac{\partial \bar{e}}{\partial y} + \frac{\partial}{\partial x}\left\{\overline{u(e+p)}\right\} + \frac{\partial}{\partial y}\left\{\overline{v(e+p)}\right\} - \nu\left\{\frac{\partial^2 \bar{e}}{\partial x^2} + \frac{\partial^2 \bar{e}}{\partial y^2}\right\} + \mu\overline{\left(\frac{\partial u_i}{\partial x_k}\right)\left(\frac{\partial u_i}{\partial x_k}\right)}$$

The fourth term is negligible compared to the fifth term by the boundary-layer approximation, except at the channel center where the fifth term goes to zero. However in this region the fourth term is negligible compared to the second term as (e) becomes so strong that $u' \ll \bar{U}$. Laufer (ref. 6) found that in a pipe $\nu\frac{\partial^2 \bar{e}}{\partial y^2}$ was important very near the wall so it will be kept in the equation. This was confirmed in the present case. However even there it does not dominate the equation, so the term $\nu\frac{\partial^2 \bar{e}}{\partial x^2}$ would be negligible by the boundary-layer approximation. The latter term at the channel center is small compared to $\bar{U}\frac{\partial \bar{e}}{\partial x}$ for a high Reynolds number, therefore it will be neglected. *

*The term $\overline{(u^2 - v^2)}\frac{\partial \bar{U}}{\partial x}$ should be neglected by the boundary-layer approximation. This was substantiated everywhere with the exception of a small region near the wall where (1) $\overline{u^2} \gg \overline{uv}$, or $\overline{v^2}$, and (2) the orientation of the coordiantes on the centerline makes $\frac{\partial \bar{U}}{\partial x}$ somewhat larger than if oriented on the wall. The latter demonstrates the inherent advantage of cylindrical-polar coordiantes in this problem. There was insufficient time when this was discovered to make such a revision, and furthermore, the term is negligible in the integral form.

The turbulent kinetic-energy equation for the diverging channel becomes

$$-\rho\overline{u'v'}\frac{\partial\bar{U}}{\partial y} = \bar{U}\frac{\partial\bar{e}}{\partial x} + \bar{V}\frac{\partial\bar{e}}{\partial y} + \frac{\partial}{\partial y}\left\{\overline{v'(e+p)}\right\} - \nu\frac{\partial^2\bar{e}}{\partial y^2} + \mu\overline{\left(\frac{\partial u_i}{\partial x_k}\right)\left(\frac{\partial u_i}{\partial x_k}\right)} \tag{7}$$

The terms are, in order: the production of turbulent energy from the mean motion, convection, diffusion by turbulent motion, and the last two terms combine the diffusion by viscous forces and dissipation to heat. The identification of the last two terms is given in reference 14. Equations (4), (6), and (7) comprise the differential equations for the diverging channel.

Integral Equations

The integral equations will now be derived after von Karman's method for mean motion (ref. 15) and Corrsin's extension to turbulent motion (ref. 16). Equation (4) upon integration across the channel and the use of Leibnitz' rule becomes

$$\frac{d}{dx}\int_0^{b(x)}\bar{U}\,dy - \bar{U}_b\frac{db}{dx} + \bar{V}_b - \bar{V}_o = 0$$

where b (x) is the duct half-width, $\bar{U}_b$ and $\bar{V}_b$ are at the wall and $\bar{V}_o$ is at $y = 0$. The wall no-slip condition and symmetry of the flow about $y = 0$ reduce this equation to

$$\frac{d}{dx}\int_0^{b(x)}\bar{U}\,dy = 0 \tag{8}$$

By the same reasoning the integral of the x-momentum equation (6) becomes

$$\frac{1}{\bar{U}_o^2}\frac{d}{dx}\int_0^{b(x)}\bar{U}^2 dy = -\frac{b}{\rho\bar{U}_o^2}\frac{d\bar{P}^*}{dx} + \frac{\tau_b}{\rho\bar{U}_o^2} \qquad (9)$$

where $\tau = \mu\frac{\partial\bar{U}}{\partial y} - \rho\overline{u v}$. The integral of the turbulent energy (7) is

$$-\int_0^{b(x)}\overline{u v}\frac{\partial\bar{U}}{\partial y}dy = \frac{1}{2}\frac{d}{dx}\int_0^{b(x)}\bar{U}\overline{q^2}dy + \nu\int_0^{b(x)}\overline{\left(\frac{\partial u_i}{\partial x_k}\right)\left(\frac{\partial u_i}{\partial x_k}\right)}dy \qquad (10)$$

the only terms remaining being: the production, the longitudinal gradient of turbulent energy, and the term entering dissipation.

At this point an interesting comparison can be made between the relative magnitude of energy going to turbulence and the energy going directly from the mean motion to heat for the flow in the parallel channel. For this purpose the so-called mechanical - energy equation is derived by multiplying each term in equation (6) by $\bar{U}$ and then integrating. Following the above procedure one obtains:

$$-\frac{d}{dx}\int_0^{b(x)}\bar{U}\left(\frac{\bar{P}}{\rho}+\frac{1}{2}\bar{U}^2\right)dy = \int_0^{b(x)}\left(\nu\frac{\partial\bar{U}}{\partial y} - \overline{u v}\right)\frac{\partial\bar{U}}{\partial y}dy \qquad (11)$$

The terms are respectively: the work done by the mean pressure , the longitudinal decrease in the flux of mean

energy, the energy fed to turbulence, and the direct dissipation to heat. The last two-terms are

$$I_T \equiv \int_0^{b(x)} (-\rho\overline{uv}) \frac{d\bar{U}}{dy}\, dy = \frac{b\tau_w^2}{\mu\rho} \int_0^1 \frac{\tau_T \tau_L}{\tau_w^2}\, d\eta$$

$$I_H \equiv \int_0^{b(x)} \mu \left(\frac{d\bar{U}}{dy}\right)^2 dy = -\frac{b\tau_w^2}{\mu\rho} \int_0^1 \left(\frac{\tau_L}{\tau_w}\right)^2 d\eta$$

where

$$\tau_L = \mu \frac{d\bar{U}}{dy} \qquad \tau_T = -\rho\overline{uv}$$

$$\eta = \frac{y'}{b} \qquad y' = b - y$$

suppose (1) that all the mean-flow dissipation and turbulent energy production occur within a region of thickness ϵ adjacent to the wall, and (2) that the laminar shear stress is approximately

$$\frac{\tau_L}{\tau_w} = 1 - \eta \frac{b}{\epsilon} \qquad \text{if} \qquad 0 \le \eta \le \frac{\epsilon}{b}$$

$$= 0 \qquad \text{if} \qquad \frac{\epsilon}{b} \le \eta \le 1$$

Then

$$\tau \equiv \tau_L + \tau_T$$
$$= (1-\eta)\tau_w$$

in the $\alpha = 0$ channel. Evaluation of the integrals gives

$$I_H = \frac{1}{3}\frac{\epsilon}{b}k \qquad I_T = \left(\frac{b}{\epsilon} - 1\right)\frac{1}{b}\left(\frac{\epsilon}{b}\right)^2 k$$

$$\frac{I_H}{I_T} = \frac{2}{1 - \frac{\epsilon}{b}} \doteq 2 \qquad \text{if} \qquad \frac{\epsilon}{b} \ll 1$$

This means that, to an order of magnitude, the dissipation of energy directly to heat is as large as the energy that goes directly to turbulence.

Longitudinal Similarity

The integral equations will now be further reduced by making the assumption that the flow in succeeding sections is similar. By this is meant that distribution of all the time-averaged properties, both mean and fluctuating, across any section is identical at successive sections if made dimensionless by the appropriate characteristic quantities. This will be called "longitudinal similarity", and it is in contrast to the Karman type wherein each small region is considered to be similar to every other small region even if the regions are at the same longitudinal station.

The argument for the existence of simple similarity is the following. Consider a region in the plane of flow bounded by the channel walls and two transverse sections a small distance apart (an isosceles trapezoid). The equations of motion (Reynolds equations) are characterized by a Reynolds Number, which can be formed from the channel half-width , b, and spatial-mean longitudinal velocity across the section. By continuity, equation (8), this Reynolds number has the same value for all such regions in a two-dimensional channel for any wall configuration. Therefore the equation is identical in all regions. If the

walls are plane then each region is geometrically similar, that is the physical boundaries of each region are also identical. Therefore one expects that the flow would be independent of the particular value of x. There are two other possibilities. A longitudinal periodicity may set in, but this appears unlikely; or the flow may progressively change until it reaches some state of breakdown such as separation. The latter is expected to happen as the angle between the walls is increased.

It should be noted that the flow in an axially-symmetric diffuser or the boundary layer on a flat plate would not be expected to exhibitlongitudinal similarity since the Reynolds numbers changes in the direction of flow.

It is also worth mentioning that if the laminar sub-layer has a characteristic Reynolds number then the ratio of the thickness of the sub-layer to the half-width, b, in the two-dimensional diffuser would be constant in the direction of flow, compatible with the previous remarks.

Simple similarity implies.

$$\frac{\bar{U}}{U_0} = f(\eta)\ ,\quad \frac{\overline{uv}}{U_0^2} = g(\eta)\ ,\quad \frac{\overline{q^2}}{U_0^2} = h(\eta)\ ,\quad \frac{\lambda}{b} = j(\eta)$$

where we recall $\eta = \frac{y'}{b}$ The following integrals will be useful:

$$I_1 = \int_0^{'} f(\eta)\,d\eta \qquad I_2 = \int_0^{'} f^2\,d\eta \qquad I_3 = \int_0^{'} g f'\,d\eta$$

$$I_4 = \int_0^{'} f h\,d\eta \qquad I_5 = \int_0^{'} h\,d\eta \qquad I_6 = \int_0^{'} j h\,d\eta$$

The equations of continuity (8), momentum (9), and turbulent energy (10) become respectively

$$I_1 = A \ CONSTANT \tag{12}$$

$$\frac{b}{\rho U_o^2}\frac{dp^*}{dx} = I_2\alpha + \frac{\tau_w}{\rho U_o^2} \tag{13}$$

$$I_3 = -I_4\alpha + \frac{I_5}{R_b}\left[\frac{b}{2}\frac{d\alpha}{dx} + \alpha^2\right] + \frac{\nu}{U_o^3}\int_0^b \overline{\left(\frac{\partial u_i}{\partial x_k}\right)\left(\frac{\partial u_i}{\partial x_k}\right)}\, dy$$

where α is the diffuser half-angle. Let us proceed without making the restriction of geometric similarity, i.e. $\frac{db}{dx} = A \ CONSTANT$, to see whether similarity could exist for a more general wall shape. Generally $I_5 = 0\{I_4\}$. If there are no large gradients of α then for a large Reynolds number the turbulent energy equation becomes

$$I_3 = -I_4\alpha + \frac{\nu}{U_o^3}\int_0^b \overline{\left(\frac{\partial u_i}{\partial x_k}\right)\left(\frac{\partial u_i}{\partial x_k}\right)}\, dy \tag{14}$$

One can now determine the conditions for longitudinal similarity by two methods.

(1) Consider equation (13). For smooth surfaces and similar profiles $\frac{\tau_w}{\rho U_o^2}$ would be a constant. Clauser (ref. 11) presents arguments to show that $\frac{(a\ length)}{\tau_w}\frac{dp^*}{dx}$ would have a constant value for similar profiles in the turbulent boundary layer. In the present case all lengths would remain proportional, therefore b is selected. From this equation (13) shows $\frac{db}{dx}$ would be a constant, that is the walls must be plane.

(2) Consider equation (14). Define a length λ by

$$\overline{\left(\frac{\partial u_i}{\partial x_k}\right)\left(\frac{\partial u_i}{\partial x_k}\right)} = \frac{5\overline{q^2}}{\lambda^2}$$

If $\frac{\lambda}{\delta}$ is also to follow longitudinal similarity (a particular case is λ independent of y (ref. 16), then

$$I_4 \frac{db}{dx} = -I_3 + \frac{5}{R_b} I_5$$

or $\frac{db}{dx}$ is a constant, as before. Therefore similarity would exist only for the plane-wall case.

EQUIPMENT

Wind Tunnel

A blowing-type wind tunnel was constructed for the present investigation (figure 1). The room air passes through a cloth filter, 3 axial flow fans, and a settling chamber. This and the remainder of the tunnel is 67in. high. The stream then passes through a 1in. wide parallel-wall channel and enters the test section. The fan speed was controlled to keep a constant Reynolds number in the test section with day-to-day changes in density and viscosity of the air.

The test section is 16ft. long. The side walls swing laterally on a sheet-metal hinge attached to the parallel section. Considerable care was taken to make the walls smooth and plane. Each wall is a symmetrical-sandwich type construction with 1/4in. tempered masonite faces and 3/4in. marine plywood ribbing on 1ft. spacing. Surveys were made of the channel width at $\alpha = 0$ over a wide range of atmospheric conditions (temperature and humidity) and the variations in the lengthwise direction were less than 1:500 (width variation/ unit length) which is equivalent to 0.1 degree. The pressure drop was measured at $\alpha = 0$ and $b = \frac{1}{2}$ in. The computed value of c_f was 20% higher than Laufer (ref. 5) reported, but only 6% higher than Skinner (ref. 17) measured later in the same tunnel as ref. 5. Since a 2% error in b would account for the latter difference it was not pursued further. The walls were then waxed and polished, and are dusted before each run.

Considerable effort was spent attaining acceptable two-dimensionality of the flow in the test section. The channel is pressurized by a throttle at the outlet, and air is bled (an estimated one percent of the total flow) from all four corners by 0.010 in. gaps running the full length of the test section. In addition a laminar boundary-layer tripper was installed in the parallel section to remove more momentum from the mid-plane by hastening the onset of turbulence. The whole program is discussed in detail in Appendix I. But the final result is that even with the above steps the growth of the floor and ceiling boundary layer causes some momentum to be convected into the mid-plane by vertical flow so that the two-dimensional momentum equation is in error by about 10% of the largest terms at the furthest downstream station. Total pressure probes were installed permanently at three elevations of the furthest downstream station and the flow is regularly checked during each run. A 5ft. wall was added to the downstream end of the test section to extend the diffuser and reduce upstream effects of the throttle.

Traversing Apparatus

The probes are posited by a traversing mechanism with a micrometer head graduated in 0.001 in., similar to the one described in reference 5. The distance between the probe and its image reflected in the wall was measured by a telescope during each run so that the distance from the wall was estimated to be accurate to 0.001 in. for the impact probe and 0.002 in. for the single-wire hot wire. The hot-wire holders could be rotated in the horizontal and vertical planes to align with the stream direction. The line of traverse was always normal to the centerline of the channel.

Mean Velocity and Pressure Instruments

A flattened hypodermic needle was used for most of the mean-velocity measurements. The opening was 0.007 in. x 0.042 in. and the wall thickness was 0.004 in. Near the surface several measurements were made with a 0.0005 in. dia. platinum hot-wire. The wire was 5/16 in. long and held taut by two small-diameter needles. The mean resistance of the wire was kept constant throughout the flow traverse.

Static pressure was measured by static taps, each made of a 1/8in. dia. rod threaded into the wall and held securely by a jam nut glued into place. The orfice was 0.020 in. in dia. and finished smooth on the air flow side. There are 51 static taps and 7 traversing points in all.

Due to the low velocities in the downstream portion of the test section it was necessary to develop a very accurate pressure measuring instrument. This is discussed in detail in Appendix II. Water and a wetting agent were used in an inclined manometer with an 18:1 slope. By locating the meniscus with a traveling microscope an accuracy in pressure of 10^{-4} in. of water was attained, which is quite satisfactory. An attempt was made to reduce the meniscus motion due to pressure fluctuations by placing constrictions in the connecting lines so the whole system had a time constant of 1 minute. The fluctuations of the meniscus were sufficiently damped to identify mean values within the desired accuracy, but the effect of the non-zero influx and efflux at the probe is still in question.

Hot-Wire Equipment

The compensating amplifier and associated control unit, calibration unit, and power supplies are essentially duplicates of those described by Kovasznay in reference 18. It is a constant-current type. Compensation for the hot-wire thermal lag is adjusted manually using the square-wave technique. In the present

case a single amplifier channel was employed. Of importance to this investigation is the fact that the amplifier frequency range extends down to 2 cycles per second. The amplifier output filter was kept on position "A" which has a response of ± 3 percent from 2 to 2500 cycles per second. At station 5 the signal was submerged into the noise between 2000 and 3000 cps. The calibration of the amplifier is shown in figure 3.

All output readings were taken by a vacuum thermocouple and millivoltmeter. A block diagram is shown in figure 4. The u', v', w', and $\overline{uv}$ signals were fed directly from the amplifier to the vacuum thermocouple.

An R-C circuit was found most suitable for differentiation. The complete differentiating circuit was linear from 20 to 1000 cycles per second and had only a 15 percent departure at 2000 cycles where the hot-wire signal generally was at the noise level. Spectrum measurements were made using a Hewlett-Packard Model 300A harmonic analyzer with a nominal frequency range of 30 to 16,000 cycles per second. A cathode follower was added to the output stage, to accommodate the relatively low resistance of the vacuum thermocouple. All measurements were made with the 30 and 145 nominal half-band widths.

Platinum wires made by the Wollaston process were used exclusively for the probes. They were etched then soft soldered to the prongs. For u' in the channel center the wires were nominally 0.00015 in. in dia., 0.04 in. long, and attached to fine sewing needles; near the wall the wires were 0.01 in. long and attached to fine jeweler's broaches to reduce aerodynamic interference. Also to measure near the wall the x-meter probe holder used for all the v', w', and $\overline{uv}$ measurements was constructed of fine jewelers broaches. They were spaced 0.025 in. apart and 0.015 in. between pairs. Each wire was 0.00015 in. in dia. and inclined approximately 40 degrees to the free stream to increase the lateral sensitivity compared to the longitudinal. The time constant for all the above probes was 0.5 to 0.8 milliseconds.

For measurement of the $\frac{\partial u}{\partial t}$ a 0.00005 in. dia. wire was used. Its time constant was 0.1 milliseconds and the noise was reduced to 2 percent of the output signal, compared to 10 percent when differentiating v and w as measured with the larger wires. The same wire was used to measure the spectrum nearest the wall. All wires were "overheated" 50 percent above the cold resistance.

Preliminary Measurements in 1 in. Channel

The preliminary measurements in the 1 inch channel were made at $\alpha = 0°$. The longitudinal static-pressure distribution, mean-velocity distribution, and centerline trubulence level were measured at $R_b = 12{,}200$ and compared to Laufer's values (ref. 5) in the straight channel.

The static-pressure distribution is shown in figure 5. The gradient is quite smooth. The computed value of $\frac{\tau_w}{\rho U_o^2}$ was somewhat higher than Laufer obtained but the difference is probably within the limits of the experimental accuracy (see p. 19).

The mean-velocity distribution at $\frac{x}{b} = 283$ is compared in figure 6 to Laufer s distribution. The values nearer the wall tend to be high, but this may be attributable to the difference between the hot wire (ref. 5) and the total-head probe (present experiment), although the correction of page 21 applied to the hot-wire measurements of reference 5 increased $\frac{u}{U_o}$ at $\frac{y}{b} = 0.1$ by only 0.6 percent. The total-head distribution was repeated several times, but the profiles duplicated. The cause of the difference is an unsettled question.

The turbulence level was $\frac{u'}{U} = .036$ at $\frac{y}{b} = 1$, compared to $\frac{u'}{U} = .035$ for reference 5. The difference is within the experimental accuracy.

PROCEDURE AND RESULTS

Mean Velocity and Static Pressure

All measurements were made at $\alpha = 1$ deg. and $R_b = 31,400$, the latter value to compare to one of Laufer's experiments at $\alpha = 0$ deg. U_o is 125 feet per second at the inlet of the test section and decreases to 16 feet per second at station 5.

The mean static-pressure distribution along the wall of the diffuser at the midplane is shown in figure 7. The slope of the faired line corresponds to $\frac{b}{\rho U_o^2}\frac{dp}{dx} = 0.010$. The pressure was measured by the difference between stations along the test section.

The mean-velocity distribution is shown in figures 8 and 9. At stations 2, 3, and 4 traverses were made in the center of the channel for similarity comparisons. The most complete traverse was made at station 5 where all of the data near the wall, figure 9, were obtained. The nearly-straight line from the wall in figure 9 represents the (laminar) velocity distribution computed from $\mu\frac{d^2\bar{U}}{dy^2} = \frac{dP}{dx}$ (the inertia term is negligible in this region) where $\frac{d\bar{U}}{dy}$ at the wall corresponds to $\frac{\tau_w}{\rho U_o^2} = 0.0013$, arrived at later in this report.

The profile was symmetrical on opposite sides of the channel at station 5 within 1/2 percent of $\frac{\bar{U}}{U_o}$. The accuracy in measuring $\frac{\bar{U}}{U_o}$ decreases downstream. At station 5 the probable error (0.675 x std. deviation) of $\frac{\bar{U}}{U_o}$ is estimated to be 0.005 at $\frac{y'}{b} = 0.1$ diminishing towards the center.

Most of the mean velocities were computed from the total-head probe measurement and the wall static pressure to which the following corrections were applied:

1.) Non-linear response of probe to magnitude and direction of velocity. The total-head probe was tested for directional sensitivity, and with the probe axis oriented in the x-direction it was found essentially insensitive to V and W over a range of $\pm$ 30 deg. in each plane. (i.e. the probe has a cosine-squared response to rotation in a uniform stream.)

To estimate the effect of velocity fluctuations we will limit our considerations to the external flow at the probe, i.e., we will ignore the dynamics of the fluid within the probe, tubes, and manometer. We will also assume that the pressure response at the probe, $R(t)$, is in equilibrium with the local instantaneous velocity and pressure.* Then neglecting size affects and including the above directional response

$$R(t) = \tfrac{1}{2}\rho U^2(t) + P(t)$$

$$= \tfrac{1}{2}\rho\left[\bar{U} + u(t)\right]^2 + P(t)$$

Define an apparent-mean velocity, $\bar{U}_{app}$, by

$$\tfrac{1}{2}\rho \bar{U}_{app}^2 = \overline{R(t) - P(t)}$$

so

$$\bar{U}_{app} = \bar{U}\left[1 + \frac{\overline{u^2}}{\bar{U}^2}\right]^{\frac{1}{2}}$$

For a low turbulence level

$$\bar{U} \doteq \bar{U}_{app}\left[1 - \frac{\overline{u^2}}{\bar{U}^2}\right]^{\frac{1}{2}}$$

which was the form employed, where $\frac{\overline{u^2}}{\bar{U}^2}$ was measured by the hot-wire anemometer. The correction was in the order of 5 percent or less.

2.) Finite probe width. Essentially the correction of Young and Maas (ref.19) was employed to account for the finite probe width in a transverse velocity gradient, except that the minimum probe width was used in place of the tube diameter. The correction takes the form of a shift in the apparent centerline of the probe. The maximum shift was

$$\frac{\Delta y}{b} = 0.00065,$$

which is a large correction in the laminar sublayer. The presence of the wall exposes this correction to some question.

3.) Reynolds number of probe. Due to the very low velocities near the wall the viscous effects around the probe were examined. A correction was made following the method of Hurd, Chesky, and Shapiro (ref. 20), where, again, the minimum width of the probe was employed in place of a tube diameter. The maximum correction was 2 percent.

---

*The quasi-equilibrium analysis requires justification.

Equation (5b) indicates a transverse difference in the pressure due to $\overline{v^2}$. This correction to the mean velocity would be nearly everywhere in the order of 0.6 percent going to zero towards the wall. It was considered negligible compared to $\frac{\overline{v}}{v_0}$.

In view of the large corrections to the total-head measurement near the wall the mean velocity was also measured with a hot-wire. The nonlinearity of the latter is such that the values tend to be low, so the following correction was employed:

The method will be merely outlined since it is considered tentative pending an analysis for large fluctuations as existed in the laminar sublayer. The method includes the other leg of the bridge and essentially fits a parabola to King's law (current vs. velocity) about the point of the mean velocity for the response to fluctuations. This assumption is limited to small fluctuations. For a wire oriented in the z direction the "apparent" mean velocity (corresponding to the mean current and mean resistance in King's equation) is

$$\frac{U - U_{app}}{\bar{U}} = \frac{1}{2}\left\{\frac{1}{2}\left(1 + \frac{1}{1 + \frac{A}{B\sqrt{U_{app}}}}\right)\right\}\frac{\overline{u^2}}{\bar{U}^2} - \frac{1}{2}\frac{\overline{w^2}}{\bar{U}^2}$$

where A and B are the constants in King's equation

$$\frac{I^2 R}{R - R_A} = A + B\sqrt{U}$$

The wire hot and cold resistances are R and R_A respectively. The correction was in the order of five percent or less.

It is to be noted that the velocities measured by the hot wire also fall below the curve obtained from the wall shear stress. The wire was calibrated at velocities in excess of 10 feet per second and used down to 1 foot per second, so an error would have been incurred in extrapolation. Also a possibility of error exists due to the determination of $y' = 0$;

0.003 in. would put the points on the curve. The difference between the wire positions could be measured very accurately, however, so the velocity gradient was relied upon. Moreover, two extreme extrapolations of the hot-wire calibration changed the computed gradient by only two percent.

In a recent private communication Mr. Richard Cox indicated that some measurements he made in Göttingen show:

(a) that the correction for velocity fluctuations is larger than computed above,

(b) the conduction to the wall is measurable to at least 50 wire diameters from the wall ($y'/b = 0.006$).

The exact magnitude of these corrections is not known more definately by this writer so they could not be applied. However, qualitatively they do account for the difference of the measured points from the curve. It is planned to investigate this further.

Finally, King's analysis also indicates that the hot-wire equation changes form at a velocity equivalent to $\frac{\overline{U}}{U_c} = 0.1$, where the measured values change slope.

The above comments focus attention on the importance of an intensive investigation of the instrument calibrations at low velocities, near a surface, and with a large gradient in the mean velocity in view of the importance of the laminar sublayer to the whole flow.

The establishment of a fully-developed flow was a prime objective of this investigation. A comparison of the mean-velocity profiles in figure 6 indicates that some peaking of the profile did take place downstream from station 2. But because of the considerable length of the test section it was possible to determine that the change in the profile between stations 2 and 5 was insignificant. This is presented in detail in Appendix I.

It is evident from figure 8 that the difference in the mean velocity destribution between $\alpha = 0$ deg. and $\alpha = 1$ deg. is substantial. This is not surprising inasmuch as the force due to the longitudinal pressure gradient has increased to a value 7 times larger than the wall-shear stress force (which has changed only slightly).

Turbulence Levels and Shearing Stresses

The single-wire probes for measuring u' were calibrated by the constant resistance method of Kovasznay (ref. 21) and used at essentially constant current. Later u' was checked by the x-meter which was calibrated with the current constant, as used, and the values were found to be 25 percent higher over most of the channel. The trouble was finally traced to the dependence of the so-called constant, A, in King's equation (ref. 22) on the wire temperature. It is attributable to the variation in the thermal conductivity of the air surrounding the wire with the wire temperature. This effect had been identified and experimentally evaluated by King, but evidently has been overlooked in a number of intervening turbulence investigations. Since everyone who measures sufficiently close to a surface is faced with this effect, as it increases at low velocities, it will be presented here. The full derivation is given in Appendix III, and will be merely outlined below.

King's equation can be written

$$I^2R = \left\{A(\vartheta) + B\sqrt{U}\right\}(\vartheta - \vartheta_e)$$

where I^2R is the heat input to the wire in equilibrium; $A(\vartheta)$ is the so-called "constant", which, for a given wire, exhibits the dependence upon the wire temperature ϑ ; ϑ_e is the air temperature, assumed constant; B, the velocity coefficient, assumed constant, is only slightly temperature sensitive. King's empirical expression for $A(\vartheta)$ is

$$A = A_0\left[1 + c(\vartheta - \vartheta_e)\right]$$

where $c = 0.00114$ deg. cent.$^{-1}$

Including the second-order coefficient in the thermal resistivity

$$R = R_0\left[1 + \alpha(\vartheta - \vartheta_f) + \beta(\vartheta - \vartheta_f)^2\right]$$

where ϑ_f is the reference temperature for R, and for constant-current, I, operation

$$\frac{dR}{R} = - \frac{a'_w \Xi}{2\left(1 + \frac{\Phi}{\Psi}\right)} \frac{dU}{U}$$

where, very nearly,

$$\Phi = a'_w (1 + a_w) \left\{ \frac{A}{(A + B\sqrt{U}) \left(\frac{\alpha}{c} + a_w - a_e\right)} - \frac{B}{\alpha^2} \right\}$$

and the "overheats" are defined

$$a'_w \equiv \frac{R - R_e}{R_e}$$

$$a_w \equiv \frac{R - R_f}{R_f}$$

$$a_e \equiv \frac{R_e - R_f}{R_e}$$

in which R_e and R_f correspond to ϑ_e and ϑ_f. For the case where A is a constant and $\beta = 0$, $\Phi = 0$, and the equation of ref. 21 is obtained. The value of Φ was 0.16 to 0.24, increasing towards the wall. After this correction was applied the single-wire values increased to within 5 to 10 percent to the x-meter values, the agreement being better near the wall. In a private communication Laufer indicated that he had used $a'_w = 0.2$ in the channel experiment and the velocities were somewhat larger at a corresponding Reynolds number, so the corrections for his data would be in the order of 5 percent. This correction was not applied to his data.

The values of $\frac{u'}{U}$ are given in figure 10 and 11. The profiles at stations 2 and 5 are compared in figure 10 in order to verify that the turbulent motion was also fully-developed, as was the mean velocity. It is interesting that the maximum value

near the wall is nearly equal to Laufer's maximum value, in particular if the above corrections were applies, although somewhat displaced, indicating perhaps that the maximum value of $\frac{u'}{\bar{U}}$ is more sensitive to the Reynolds number than to the pressure gradient.

The method of measuring v', w', and $\overline{uv}$ is similar to the procedure described in reference 23. The probe was placed in a uniform stream and rotated about the neutral position to determine the v- sensitivity (or w - sensitivity), and then the velocity was varied to determine the u -sensitivity, all at essentially constant current. This method is considerably less laborious than calibrating the wires separately, and introduces less possibility of error. Also the probe is calibrated in the circuit exactly as used. With two identical wires the "neutral position", at which the sum and difference of the voltages across the wires would correspond simply to u and v fluctuations respectively, could be easily determined. Actually, since the wires inevitably differ in diameter, length, and straightness it is necessary to make compensations. This is accomplished as follows. Consider the voltage sensitivity of wires no. 1 and no. 2 to fluctuations u and v to be of the form

$$e_1 = a_1 u + b_1 v$$

$$e_2 = a_2 u + b_2 v$$

Then if $a_1 = a_2$ and $b_1 = b_2$

$$\overline{u^2} = \frac{\overline{(e_1 + e_2)^2}}{4a^2}$$

$$\overline{v^2} = \frac{\overline{(e_2 - e_1)^2}}{4b^2}$$

$$\overline{uv} = -\frac{\overline{e_2^2} - \overline{e_1^2}}{4ab}$$

Actually three conditions were satisfied, the third being that the wires had the same overheat. We have 3 degrees of freedom available to satisfy these conditions, provided the differences are small, namely:
(1) the "tap-off" voltage, i.e. a potentiometer to reduce the measured voltage from one wire, (2) the current into each wire by adjustment of the resistance in series with the wire, and (3) the angle of the probe to the air stream. It turned out that for the probe used only adjustments (1) and (3) were necessary to obtain overheating values within 6 percent.

The procedure was to approximate the neutral angle and measure $a_1 - a_2$ keeping the direction constant, and $b_1 - b_2$ keeping the velocity constant. The latter was the most difficult to measure with certainty and consequently set the limit of the final accuracy; the difficulty was in maintaining the velocity sufficiently constant that $e_1 + e_2$ changed due only to v. By knowing the effects of changing the probe angle. etc., which were put into an equation, it was possible to change the angle and tap-off voltage simultaneously so that the conditions were satisfied.

In order to measure $\overline{uv}$ and $\overline{v^2}$ with a 5 percent accuracy the a-coefficients must be matched to approximately 2 percent and the b-coefficients to 4 percent. This corresponds to setting the probe angle to about 1 degree. It is believed the neutral angle could be determined to ± 1-2 deg.

King's law was used to extend the directional sensitivities to the lower mean velocities, but no Φ-correction was necessary. The $\overline{uv}$ signal had large low frequency fluctuations, since it is in the non-isotropic portion of the spectrum, which added to the difficulty in determining the mean values for $\overline{uv}$

but $\overline{v^2}$ readings were quite stable.

The distribution of $\frac{v'}{U}$ and $\frac{w'}{U}$ are given in figure 10, and $\frac{\overline{uv}}{u'v'}$ in figure 12.

The absolute values of $\overline{uv}$ are shown in figure 13. The curve for τ was computed from the pressure gradient and mean-velocity distribution using a form of equation (6) wherin longitudinal similarity was assumed. (A correction was applied due to the vertical flow of momentum by adjusting the value of pressure gradient by 10 percent so $\frac{\tau_w}{\rho U_0^2} = 0.0013$, the value arrived at below.) The dashed line was obtained by subtracting the viscous shear stress and pressure gradient terms.

Of importance to later correlations is the wall shear stress. This was computed from three independent measurements:

1. x-meter. Using the best-fitting curve of $\overline{uv}$ at $\frac{y'}{D} = 0.1$, figure 13, the value at the wall was computed by the momentum equation to be $\frac{\tau_w}{\rho U_0^2} = 0.0014$.

2. Hot-wire. The mean-velocity gradient, figure 9, measured by the the hot wire in the outer region of the laminar sub-layer, corrected for the difference (4 percent) from τ_w due to pressure gradient, gave $\frac{\tau_w}{\rho U_0^2} = 0.00133$

Possibly this is less accurate than 1 in view of the effects mentioned.

3. Total-head probe. This is the most questionable since the probe is 0.015 in. wide compared to a laminar sub-layer of about 0.04 in. The best laminar profile through the three inner points gives $\frac{\tau_w}{\rho U_0^2} = .0011$.

The final value taken, the average of the three, was $\frac{\tau_w}{\rho U_0^2} = 0.0013$. This is estimated to be accurate to 10 percent.

The absolute turbulence values are compared in figures 14 and 15. Important is the fact that the turbulent-energy level is roughly 4 times larger than the $\alpha = 0°$ case over a large region in the center of the channel, decreasing to become equal near the wall. This is a substantially greater effect of the pressure than was exhibited on the mean velocity. Also it is evident that the large scale motion is not isotropic as $\overline{u^2}$ is roughly equal to $\overline{v^2} + \overline{w^2}$ in the central region.

It can be shown from the turbulent energy equations for the individual components that the production occurs in the $\overline{u^2}$ equation and energy is fed to $\overline{v^2}$ and $\overline{w^2}$ through the static pressure fluctuations. Figure 14 shows that the energy is divided equally between $\overline{v^2}$ and $\overline{w^2}$ in the center; towards the wall $\overline{v^2}$ is smaller due to the presence of the surface.

Spectrum

The one dimensional energy spectra of u , v and w are shown in figures 16, 17, and 18. The signals were calibrated by comparing the output at several frequencies in each profile to that for a known sine-wave input. An "effective" (rectangular) band width of 13 c. p. s. was used. This value was obtained by measuring the band-pass shape, and was confirmed by comparing the $\overline{u^2}$ by integrating the whole spectrum to the $\overline{u^2}$ value measured directly. This was carried out in another wind tunnel at a velocity high enough that the energy at lower wave numbers could be measured. Comparing the band-passed signal for a white-noise input would be more dependable, but a suitable noise source was not available at that time. Therefore the absolute level of the energy spectrum is somewhat in question, but the shapes of the spectra should be reliable. The u - spectra were corrected for the wire-length effect by the method of reference 24.

The spectrum is defined, for example, by $F_u(k_1)$ being the fraction of $\overline{u^2}$ at wave number k_1 , and normalized by

$$\int_0^\infty F_u(k_1)\, dk_1 = 1$$

The microscales were computed from the spectra by the well-known relations

$$\lambda_u^2 = \frac{1}{\int_0^\infty k_1^2 F_u(k_1)\, dk_1}$$

$$\lambda_v^2 = \frac{2}{\int_0^\infty k_1^2 F_v(k_1)\, dk_1}$$

$$\lambda_w^2 = \frac{2}{\int_0^\infty k_1^2 F_w(k_1)\, dk_1}$$

They compare very well with the values obtained by differentiation (described below), figure 21.

Production Terms

In the Cartesian coordinate system, as mentioned in the Preliminary Analysis, the following are two of the three production terms (the remaining term, $-\overline{uv}\frac{\partial \bar{v}}{\partial x}$ is negligible)

$$-\overline{uv}\frac{\partial \bar{U}}{\partial y} \quad - \left(\overline{u^2} - \overline{v^2}\right)\frac{\partial \bar{U}}{\partial x}$$

The second term is small everywhere, except near the wall, if the coordinates are parallel to the centerline as defined in this investigation. If the coordinates are aligned parallel to the wall it is small even there. (Of course, the first term increases simultaneously as the sum remains constant). In reality these terms were not all measured in the centerline-coordinate system: Near the wall $\overline{uv}$ was computed from

$$-\overline{uv} = \tau - \mu\frac{\partial^2 \bar{U}}{\partial y^2}$$

Since a hot-wire responds essentially to resultant perpendicular velocity and since very near the wall this is virtually parallel to the wall, the $\overline{uv}$ thus computed is actually in the wall-coordinate system. Therefore, the second production term is negligible, and the production is essentially $-\overline{uv}\frac{\partial \bar{U}}{\partial y}$.

The value of $-\left(\overline{u^2} - \overline{v^2}\right)\frac{\partial \bar{U}}{\partial y}$ in the centerline coordinate system is shown in figure 24.

"Dissipation Terms"

Three of the nine terms in

$$W = \mu\overline{\left(\frac{\partial u_i}{\partial x_k}\right)\left(\frac{\partial u_i}{\partial x_k}\right)}$$

were measured using Taylor's hypothesis (ref. 25),

$$\frac{\partial}{\partial x} \doteq -\frac{1}{\bar{U}}\frac{\partial}{\partial t}$$

following the method of Townsend (ref. 26). The measured terms are $\overline{\left(\frac{\partial u}{\partial x}\right)^2}$, $\overline{\left(\frac{\partial v}{\partial x}\right)^2}$, and $\overline{\left(\frac{\partial w}{\partial x}\right)^2}$.

An estimate of the validity of Taylor's hypothesis was made following the method of Lin (ref. 27). In a shear flow he requires

(1) $$\frac{\overline{u^2}}{\overline{U}^2} << 1$$

(2) $$\left|\overline{U}\frac{\partial u}{\partial x}\right| >> \left|v\frac{\partial \overline{U}}{\partial y}\right|$$

Item (1) is valid with the exception of very near the wall. Item (2) would be expected to hold for wave numbers larger than k_1 (say) where

$$k_1\overline{U} >> \frac{\partial \overline{U}}{\partial y}$$

For a logarithmic mean-velocity distribution

$$k_1\overline{U}y >> y\frac{\partial \overline{U}}{\partial y}$$

For the present mean-velocity distribution this reduces to

$$k_1 b >> \epsilon \equiv$$

where ϵ has the value

$\frac{y'}{b}$	.01	.1	.7	1
ϵ	60	3	.3	0

Figure 19 shows that the greatest portion of $k_1^2 F_u(k_1)$, which is somewhat comparable to the dissipation spectrum, is at higher wave number than ϵ, except for the station y'/b = 0.01. In the latter case $\epsilon(=60)$ bisects the area. With locally isotropic dissipation the dissipation spectrum is actually the second moment of the three-dimensional spectrum, which, for isotropic turbulence, shifts the c.g. to higher wave numbers. In the present experiment the values of the "dissipation" term were most in doubt in this region near the wall due to the large magnitude of the terms which were not measured. The estimating procedures are discussed below.

Having measured three terms in W, the problem was to estimate the other six. Since Laufer had measured the same three terms plus two of the remaining terms in the pipe (ref. 6), his data were employed, on the argument that very near the wall, the boundary curvature should have little effect.

The first step was to select a suitable basis for estimating the unmeasured terms from those measured. The procedure was to divide the channel into two regions: (1) $0.1 \leq y' \leq 1$, where b was used as the characteristic dimension, and (2) $0 \leq y' \leq 0.1$ where $\frac{\nu}{u_*}$ was selected as the characteristic dimension.

In the center region one would expect $R_\lambda \left(= \frac{1}{\sqrt{2}} \frac{\lambda_u u'}{\nu}\right)$ to be a pertinent parameter. The R_λ distribution is shown in figure 19. The values are sufficiently large that one would expect the dissipation terms to receive their principal contribution from the locally isotropic fluctuations. The R_λ values fall between those of the two pipe flows of $R_b = 50,000$ and 500,000. The ratio between terms that we did not measure and those we did measure was essentially the same in the 50,000 and 500,000 flows, so it seems reasonable to guess that the same ratio would apply here. The ratios obtained from the former were used.

In the wall region an assumption of similarity was used. Specifically we assumed that the ratio between the unmeasured and measured terms was the same function of $\frac{y' u_*}{\nu}$ as in the $R_b = 50,000$ pipe. It will be shown later that some of the other turbulent terms (e.g. $\frac{u'}{u_*}$) differ in this region by as much as 30 percent between the two flows. Since the measured terms are considerably smaller than the unmeasured terms the local error in W would be large.

The next step was to select the form of the terms to be compared. The microscales were measured by

$$\lambda_u^2 = \frac{\overline{u^2}}{\left(\frac{\partial u}{\partial x}\right)^2}$$

$$\lambda_v^2 = \frac{2\overline{v^2}}{\overline{\left(\frac{\partial v}{\partial x}\right)^2}} \quad , \quad \lambda_w^2 = \frac{2\overline{w^2}}{\overline{\left(\frac{\partial w}{\partial x}\right)^2}}$$

and are compared in figure 21. The latter two agree very well in the center of the channel, but they are significantly smaller than λ_u, in particular near the wall. The three approach each other near the center of the channel. This difference is expected since the dissipation terms (the derivatives) essentially represent the high wave-number portion, wheras $\overline{u^2}$, $\overline{v^2}$, and $\overline{w^2}$ receive their main contribution from the non-isotropic "feeding" range.

Therefore the "dissipation" terms were compared directly, figure 22. The agreement is good. Therefore the ratios of the dissipation terms measured by Laufer were used to obtain directly $\overline{\left(\frac{\partial u}{\partial y}\right)^2}$ and $\overline{\left(\frac{\partial u}{\partial z}\right)^2}$.

The remaining four terms were obtained, following reference 6, by assuming that the derivatives in the y and z directions individually are equal.

$$\overline{\left(\frac{\partial u}{\partial y}\right)^2} = 2\overline{\left(\frac{\partial v}{\partial y}\right)^2} = \overline{\left(\frac{\partial w}{\partial y}\right)^2}$$

$$\overline{\left(\frac{\partial u}{\partial z}\right)^2} = \overline{\left(\frac{\partial v}{\partial z}\right)^2} = 2\overline{\left(\frac{\partial w}{\partial z}\right)^2}$$

By this procedure W was computed to be within 10 percent of the other terms in the integral energy balance. It should be mentioned that the naive use of the pure isotropic relation

$$W = 15\mu\overline{\left(\frac{\partial u}{\partial x}\right)^2}$$

gave a value of only 60 percent of the remaining energy balance. However considerable question exists concerning the unmeasured terms, so an important item in further work would be to measure at least the terms $\overline{\left(\frac{\partial u}{\partial y}\right)^2}$ and $\overline{\left(\frac{\partial u}{\partial z}\right)^2}$.

DISCUSSION

The turbulent motion will be examined from three principal points of view: (1) by the distribution of energy through the spectrum, (2) through a comparison of the various terms entering the turbulent energy balance, and (3) in the light of the various similarity hypotheses. Each treats the motion from essentially a different aspect so they will be discussed separately.

Throughout the discussion emphasis will be placed on the effect of the adverse pressure gradient on the flow. We have already observed a significant retardation of the whole mean-velocity distribution in comparison to the channel case. Even more striking however, was the rise in the absolute level of the turbulent energy. In fact the relative change in the turbulent energy by the pressure gradient was larger than on the mean motion. Also important was the shift in the location of the maximum shear stress away from the wall to $y'/b \approx 0.35$. We will now examine the other effects.

Spectrum Analysis

Figure 16 reveals that a large portion ($5 < k_1 b < 30$) of the u'-spectrum in the center of the channel varys as the -5/3 power. Naively this could imply, following Kolmogoroff (ref. 27), that local isotropy in this flow extends down to these wave numbers which fall below the dissipation range. But the surprising point is that the -5/3 power extends down to wave lengths equal to half the channel width, i.e. where $\frac{2\pi}{k_1} = b$. It is quite improbable that the fluctations of this wave length are isotropic. A similar situation was noted by Lin (ref. 26) in the turbulent boundary-layer measurements of Klebanoff and Diehl (ref. 8). The wave lengths at the low end of the -5/3 power region were in the order of the boundary layer thickness. An equivalent situation exists in the pipe (ref. 6).

Searching for indications of a true "inertial subrange" of finite spectral extent we must find that the upper limit of the -5/3 range lies at a k_1 large compared with $\frac{2\pi}{b}$. Figure 16 does show such an inequality.

Further, looking at the v' and w' spectra, we note that they both have -5/3 power regions that do not extend to as low wave numbers. In fact, they are so narrow that we cannot vouch for their existence. The same trend is evident for the pipe spectra (ref. 6). Evidently other factors have extended the low end of the -5/3 power region of the u-spectrum (at $y'/b = 0.1$ there is a considerable -5/3 power region in $F_u(k_1)$ and for $F_v(k_1)$ and $F_w(k_1)$ it is non-existent.) However, the u', v' and w' spectra do all "drop away" from the -5/3 slope at about the same k_1, a possible indication of local isotropy for wave numbers higher than this one. The corresponding wave length, $\frac{2\pi}{k_1}$, is roughly $\frac{1}{10}$ of the channel width. The existence of isotropy in the dissipative spectral region has already been pointed out by noting that $\overline{\left(\frac{\partial u}{\partial x}\right)^2}$, $\overline{\left(\frac{\partial v}{\partial x}\right)^2}$, and $\overline{\left(\frac{\partial w}{\partial x}\right)^2}$ are very nearly in agreement with the isotropic laws.

One condition of Kolmogoroff's analysis to be fulfilled in order to have a -5/3 power region is that in addition to being isotropic the so-called inertial subrange be essentially free of dissipative effects. Figure 19 shows that 75 percent of the contribution to

$$\int_0^{k_1^*} F_u(k_1)\, dk, \qquad \text{at} \qquad \frac{y'}{b} = 1.00$$

is from wave numbers greater than those of the -5/3 power region. As before it is expected that even a larger portion of the three-dimensional spectrum, whose second moment gives the dissipation for isotropic turbulence is above the -5/3 power region. Therefore the condition appears to be fulfilled here. The Kolmogoroff condition was not examined at the point nearer the wall in view of the negligible -5/3 power range in their v' and w' spectra.

The u' spectrum at the center of the channel exhibits the -7 power range at the high wave number end. However, the other spectra in the same $k_1 b$ range have slopes with a somewhat more positive trend towards the wall.

In general the shapes of the measured portion of the spectra are similar to the pipe spectra (ref. 6). The diffuser spectra do extend further in the -7 power range, but the measurements were not able to be carried as far into the low wave number end because the air speed was much less. Inasmuch as the spectra in figure 16 tend to be predominantly isotropic, except near the wall where the viscous effects predominate, any influences of the pressure gradient or diverging walls would be expected to manifest themselves in the low wave number end that was not measured.

Incidentally the characteristic of the lengths of the turbulent motion being so near the overall dimensions of the whole turbulent shear region seems to be inherent in the turbulent shear flows. For example, the integral scales in the boundary-layer are not an order of magnitude less than the boundary layer thichness, and the velocity fluctuations are found to be correlated between points all the way across the layer (ref. 9). The longitudinal integral scale was measured in the present experiment by comparing the uncompensated and compensated responses of a hot wire by the method described in reference 5. The distribution is given in figure 23. L_x is nearly everywhere equal to b, even at $y'/b = 0.1$. The values agree within the measurement accuracy to Laufer's values at the same R_b. This discussion emphasizes the inherent weakness of the turbulence "theories" (e. g. mixing-length) which attempt to relate the turbulent motion and the local velocity gradients.

It is well established that the turbulence Reynolds number R_λ is a primary parameter of isotropic turbulence. It is also generally believed to be of great importance in turbulent shear flow, especially in connection with the relative extent of the locally isotropic part of the spectrum. For example, for sufficiently high R_λ it is expected that the dissipation will occur chiefly in the isotropic range; for still higher R_λ, Kolmogoroff's theory anticipates the existence of an extended (-5/3 power) "inertial subrange".

For given boundary conditions R_λ should be uniquely related to R_b, the overall mean flow Reynolds number. Therefore, in seeking the effects of changing boundary conditions (changing the channel half-angle from 0° to 1°) it is important to compare R_λ's at the same value of R_b, or to compare flows with equal R_λ's and different R_b. In figure 20 it is evident that the $R_b = 61,600$ channel and the present experiment have identical distributions over most of the channel. The microscales were computed in both experiments by

$$\lambda_u^2 = \frac{\overline{u^2}}{\left(\frac{\partial u}{\partial x}\right)^2}$$

which essentially compares the contributions from the high and low wave numbers. The λ_u distribution for the two cases are in good agreement, figure 21.

Turbulent Energy Balance

The conclusions that may be drawn from the turbulent-energy balance are somewhat restricted by the method employed to estimate the "dissipation" terms. Furthermore, as mentioned, the true dissipation includes $\overline{\left(\frac{\partial u_i}{\partial x_k}\right)\left(\frac{\partial u_k}{\partial x_i}\right)}$ which are zero in the isotropic case, but not in general. However, they probably are small except near the wall where even the value of $\overline{\left(\frac{\partial u_i}{\partial x_k}\right)\left(\frac{\partial u_i}{\partial x_k}\right)}$ is very uncertain. Nevertheless several interesting conclusions can be drawn from the energy balance, shown in figures 24 and 25.

The flow field seems to divide into four regions:

1. The center of the diffuser, $0.8 < \frac{y'}{b} < 1$ where a net amount of energy is fed in by turbulent convection from the low y' side and by mean flow convection from the upstream side. This latter effect consitiutes a difference from the case of the parallel wall channel.

2. $0.1 < \frac{y'}{b} < 0.8$ This region differs from the channel case in that here (a) the production of energy is mostly balanced locally by the dissipation and (b) the energy convected into the region by mean flow is very nearly offset by the turbulent diffusion and pressure work "outward".

3. $0.05 < \frac{y'}{b} < 0.1$. In this region similar to the pipe (ref. 6), the production and dissipation are in balance and the remaining terms are relatively smaller. This means that the energy produced here is locally dissipated, a result consistent with the cruder assumptions of the mixing-length theories. Hence this may be regarded as consistent with the occurrence of a logarithmic mean-velocity distribution in this region, to be shown later.

4. Wall region. As in the pipe the production reaches a maximum at about $y_* \left(\equiv \frac{y' u_*}{\nu}\right) = 11$, just outside the laminar sublayer. If we assume a qualitative resemblance to the wall region of the pipe, it can be inferred that the energy is transported away by the turbulent diffusion and, to a lesser extent, by the "viscous work" { the true viscous work includes $\overline{\left(\frac{\partial u_i}{\partial x_k}\right)\left(\frac{\partial u_k}{\partial x_i}\right)}$ } However, in contrast to the pipe case, the dissipation in this region exceeds the production, so we must conclude that the feeding of energy into this region by pressure work (Laufer's "pressure diffusion") exceeds the two diffusion effects which tend to drain off the energy. This difference between the wall region of a pipe and diffuser may be important if correct, since it is widely assumed that this small region near the wall is "unaware" of the flow in the large, that is the overall Reynolds number and pressure gradient. Therefore, a more detailed measurement of the dissipation in this should be a part of further work in order to improve the energy balance and thus learn whether this effect of an adverse pressure gradient does exist.

Dimensional Reasoning

It is well-known that the turbulent boundary layer can be separated for analytical purposes into two regions: one comprising all the flow field except a thin layer nearest the wall, which has as a characteristic length the boundary-layer thickness, and velocity u_* ; and the other being the wall region with a characteristic length $\frac{\nu}{u_*}$, and velocity u_* . These correlations will be examined for the channel and diffuser.

1. Center of the channel. The mean velocity is compared on the basis of the velocity-defect law in figure 26. For the turbulent boundary layer this representation of the mean-velocity distribution has been empirically determined to be independent of the Reynolds number and surface roughness, but a function of the pressure gradient. Since all the diffuser tests were conducted at

a constant Reynolds number a single curve is expected. The trend of the channel and diffuser data with an adverse pressure gradient is similar to the boundary layer. Of course, the boundary layer and diffuser data are expected to differ from each other in this region and only the trends are compared. The pressure-gradient parameter, $\frac{\delta}{\tau_w}\frac{dP}{dx}$ was 7.7 for the diffuser, and $\frac{\delta}{\tau_w}\frac{dP}{dx}$ was 12.2-14.8 for the boundary layer.

The turbulence level was compared on a similar basis, figure 27. This emphasizes the larger effect of the pressure gradient on the turbulent fluctuations than on the mean flow.

2. Near the wall the results are considerably more interesting. The mean velocity is compared on the basis of Prandtl's wall-proximity law (ref. 29) in figure 28 using semi-logarithmic coordinates to demonstrate the log-law region. The log law extends over a wide region up to $y_* = 150$. The difference in displacement of the various profiles in this region is probably not significant. In fact all of the points could be collapsed to one curve by admitting a 10 percent error in u_*. Therefore the mean velocity distribution could be said to fulfill the similarity hypothesis out to $y_* \approx 150$.

The turbulence level story, however, is quite different, figure 29. Laufer found good agreement between the channel (ref. 5) and the pipe (ref. 6), with some effect of Reynolds number for $y_* > 30$. But the effect of the pressure gradient is evidently much larger, and it is not attributable to instrument errors. In fact a correction in u_* to bring the channel and diffuser data into better agreement in $\overline{U}$, figure 28, actually increases the discrepancy in u', figure 29. Some unpublished data was obtained from Dr. Clauser's group* which had measured this term in the turbulent boundary layer in an adverse pressure gradient. The values at four stations were all grouped about the $\alpha = 1$ deg. curve. The pressure gradient based on the characteristic quantities in this region was somewhat smaller. The values of $\frac{\nu}{\rho u_*^3}\frac{dP}{dx}$ were:

Turb. b.l.	5.4×10^{-3} to 2.9×10^{-3}
Diffuser	6.8×10^{-3}

*Aeronautics Department, Johns Hopkins University.

An examination was made to ascertain whether u_* is a characteristic velocity of the turbulent region since τ changes across the laminar sublayer. But the variation in τ was only 5 percent, insufficient to account for the difference. The question of local similarity was examined further by comparing $\frac{\overline{uv}}{u'v'}$, which eliminates the characteristic velocity. This is shown in figure 30. The dashed line represents the diffuser values in the wall-coordinate systems. Of course, u_* remains in the abcissa but the difference between the curves is so great that no reasonable shift by adopting a new characteristic velocity could collapse the two to one.

Another approach was then taken. Since only the longitudinal motion faces the mean adverse-pressure gradient the pressure effects may have a preferred direction. The ratio of u' to v' was compared between the pipe flow and the diffuser flow, figure 30, and the agreement in the wall-proximity region is surprising. The conclusion to be drawn evidently is that the pressure gradient does not affect the turbulence levels near the wall, but only their correlation.

The distributions of $\frac{u'}{v'}$ at equal Reynolds numbers are also compared in the center of the channel, pipe, and diffuser in fig. 30. In this region the difference is significant. Evidently the pressure gradient does manifest itself by favoring the fluctuations in the direction of the gradient, perhaps in an indirect way through the energy balance. For example, the production feeds almost purely into u-fluctuations, while turbulent diffusion acts on all three components.

Several oscilloscope traces were made of u(t) within and slightly outside the laminar sublayer, figure 31. The fluctuations inside the sublayer are interesting. They appear to display an intermittancy suggestive of the outer regions of a boundary layer. An important difference is the absence of the sharp demarcations between the turbulent, and in this case, laminar regions, that is evident in boundary-layer intermittancy. Another difference is the fact that the turbulent regions near the wall are generally traveling with excess velocities, whereas in the boundary layer they tend to move slower.

Further Investigations

It seems apparent following the present investigation that further work should pursue the following course.

1. Measure several of the dissipation terms in the direction normal to the main flow, in particular near the region of maximum production.

2. Measure the triple -correlation distribution to identify the pressure- and velocity-diffusion terms. Laufer's pipe data indicate that both of these effects are very large near the maximum-production point.

3. Look for increased skewness in some turbulence properties - a possibility suggested by the unsymmetrizing effect of a large static-pressure gradient.

4. Increase the angle of divergence to find the effect of the pressure gradient as the flow approaches separation. In particular to study the similarity considerations in the wall proximity.

REFERENCES

1. Batchelor, G. K.: Note on Free Turbulent Flows with Special Reference to the Two-Dimensional Wake. Jour. Aero. Sci., Vol. 17, No. 7, July 1950, pp. 441-445.

2. Corrsin, Stanley, and Uberoi, Mahinder S. : Spectra and Diffusion in a Round Turbulent Jet. NACA Rep. 1040, 1951. (Supersedes NACA TN 2124.)

3. Liepmann, Hans Wolfgang, and Laufer, John: Investigations of Free Turbulent Mixing. NACA TN 1257, 1947.

4. Townsend, A. A.: The Fully Developed Turbulent Wake of a Circular Cylinder. Australian Jour. Sci. Res., Ser. A, Vol. 2, No. 4, Dec. 1949, pp. 451-468.

5. Laufer, John : Investigation of a Turbulent Flow in a Two-Dimensional Channel. NACA Rep. 1053, 1951. (Supersedes NACA TN 2123.)

6. Laufer, John : The Structure of Turbulence in Fully Developed Pipe Flow. NACA TN 2954, June 1953.

7. Townsend, A. A. : The Structure of the Turbulent Boundary Layer. Proc. Cambridge Phil. Soc., Vol. 47, Pt. 2, Apr. 1951, pp. 375-395.

8. Klebanoff, P. S. and Diehl, Z. W. : Some Features of Artificially Thickened Fully Developed Turbulent Boundary Layers with Zero Pressure Gradient. NACA TN 2475, Oct. 1951.

9. Schubauer, G. B. and Klebanoff, P. S. : Investigation of Separation of the Turbulent Boundary Layer. NACA TN 2133, Aug. 1950.

10. Ludwieg, H. and Tillmann, W. : Investigations of the Wall-Sheaking Stress in Turbulent Boundary Layers. (Translation) NACA TM 1285, May 1950.

11. Clauser, F.H. : Turbulent Boundary Layers in Adverse Pressure Gradients. Dept. of Aeronautics, Johns Hopkins University, Contract No. AF 33(038)9862, June 1953.

12. Donch, F. : Divergente und Konvergente Turbulente Stromungen mit Kleinen Offnungswinkeln, Forsch Arb. Ger. Ing. Wes., Heft 282, 1926.

13. Nikuradse, Johann : Untersuchungen uber die Strömungen des Wassers in Konvergenten und Divergenten Kanälen. Forsch. Arb. Geb. Ing. Wes., Heft 289, 1929.

14. Corrsin, Stanley : Interpretation of Viscous Terms in the Turbulent Energy Equation. Jour. Aero. Sci., Reader's Forum, Dec. 1953.

15. von Karman, Theo. : Über Laminare und Turbulente Reibung, Z. A. M. M. Vol. 1, No. 1, 1921.

16. Corrsin, Stanley : An Integral Relation from the Turbulent Energy Equation. Jour. Aero. Sc., Reader's Forum, Nov. 1951, pp. 773-74.

17. Skinner, G. T. : Mean-Speed Measurements in Two-Dimensional, Incompressible, Fully-Developed, Turbulent Channel Flow. Thesis, Cal. Ins. of Tech., 1951.

18. Kovasznay, L. S. G. : Development of Turbulence-Measuring Equipment. NACA TN 2839, Jan. 1953.

19. Young A. D. and Maas, J. N. : The Behavior of a Pitot-Tube in a Traverse Pressure Gradient. A. R. C. R. and M. 1770.

20. Hurd, C. W., Chesky, K. P., and Shapiro, A. H. : Influence of Viscous Effects on Impact Tubes. Jour. App. Mech., June 53, pp. 253-56.

21. Kovasznay, Laszlo : Calibration and Measurement in Turbulence Research by the Hot-Wire Method. (Translation) NACA TM-1130, June 1947.

22. King, Louis Vessot : On the Convection of Heat from Small Cylinders in a Stream of Fluid: Determination of the Convection Constants of Small Platinum Wires with Applications to Hot-Wire Anemometry. Phil. Trans. Roy. Soc. (London), Ser. A., Vol. 214, Nov. 12, 1914, pp. 373-432.

23. Schubauer, G. B. and Klebanoff, P. S. : Theory and Application of Hot-Wire Instruments in the Investigation of Turbulent Boundary Layers. NACA W-86, March 1946.

24. Uberoi, M. S., and Kovasznay, L. S. G. : Influence of Resolving Power on Measurement of Correlations and Spectra of Random Fields. Project Squid, Technical Report No. 30.

25. Taylor, G. I. : The Spectrum of Turbulence, Proc. Roy. Soc., A 164, 1938, p. 476-490.

26. Townsend, A. A. : Measurement of Double and Triple Correlation Derivatives in Isotropic Turbulence. Proc. Camb. Phil. Soc., Vol. 43, Pt. 4, Oct. 1947, pp. 560-570.

27. Lin, C. C. : On Taylor's Hypothesis and the Acceleration Terms in the Navier-Stokes Equation. Quar. App. Math. Vol. X, No. 4, Jan. 1953, pp. 295-306.

28. Kolmogoroff, A. : The Local Structure of Turbulence in Incompressible Viscous Fluid for Very Large Reynold's Numbers. Comp. Rend., Acad. Sci. URSS, Vol. 30, No. 4, Feb. 10, 1941, pp. 301-305.

29 Prandtl, L. : Bericht uber Untersuchungen zur Ausgebildeten Turbulenz. Z. A. M. M., Bd. 5, Heft, Apr. 1925, pp. 136-139.

30. Dryden, Hugh L. : Review of Published Data on the Effect of Roughness on Transition from Laminar to Turbulent Flow.

31. Prandtl, L., Tietjens, O. G.: Applied Hydro- and Aero- Mechanics, McGraw-Hill Book Co., 1934, p. 234-39.

32. International Critical Tables, McGraw-Hill Book Co., Ist Edition, 1928, Vol. IV, p. 434.

33. Handbook of Engineering Fundamentals, Ovid W. Eshbach, Editor, John Wiley and Sons, 2nd Edition, 1952, p. 1-147.

34. Wislicenus, George F., and Yeh, Hsuan: A Program of Research in the Field of Turbulent Flow in Ducts, in a Space of Revolution, and in Turbomachinery. Johns Hopkins Univ., Mech. Eng. Dept., Report I-8, Contract Nonr 248(33), Dec. 1952.

APPENDIX I

ESTABLISHMENT OF THE EXPERIMENTAL FLOW

Setting Up The Test Conditions.

The most difficult phase of setting up the test conditions was making the mean flow reasonably two-dimensional. This is apparently a problem characteristic of adverse-pressure gradient flows although it has only recently received attention in the literature. Ludwieg and Tillmann (ref. 10) found that by including the measured secondary flow in a boundary layer in an adverse-pressure gradient the value of C_f computed by von Kármán's momentum equation was reduced by 40 per cent. Clauser (ref.11) found even larger discrepancies with very strong adverse pressure gradients. He indicated the importance of $\frac{\partial w}{\partial z}$ and how it far outweighed the terms mentioned by others.

In the present experiment the steps taken to assure longitudinal-similarity made it difficult to attain two-dimensionality. The parallel-wall approach channel was added ahead of the test section to give the flow a start towards reaching the fully-developed state and to give a previously studied flow field in which measurements could be checked. But inevitably non-uniformities develop in the vertical direction by the time the stream has passed through the parallel channel, and these are amplified in the adverse pressure gradient. The same phenomenon occurs when a boundary layer grows on a flat plate and enters an adverse pressure gradient.

Some physical feeling for the phenomenon can be reached by the following rather rough analysis of the flow in the present diffuser. Consider the stream at two elevations: the midplane ($z=0$) and 2 1/2 in from the ceiling ($z=3$ in). The ratio of the maximum dynamic pressure in the upper profile to the maximum dynamic pressure in the midplane, both at the same x station, will be called the dynamic-pressure ratio, P_r . P_r is unity if the flow is two-dimensional. The measured values of P_r are tabulated in figure 32.

Let us naively invoke the Bernoulli equation for the flow. We will consider the maximum dynamic pressure (presumably at $y=0$) for this approximation. When the walls of the parallel section were smooth the value of P_r 6 in. ahead of the diffuser inlet was 0.96: a velocity defect of only 2 per cent. With $2\alpha = 2$ degrees the width at station 2 is 2.9 times the width in the approach channel, so a Bernoulli - expansion at the midplane would convert 88 per cent of the original dynamic pressure into static pressure, 12 per cent remaining in the dynamic pressure. The upper plane must convert the same amount of energy into static pressure because $\frac{\partial P}{\partial z}$ is small. But it only had 0.96 as much to start with, so Bernoulli-wise P_r would be $\frac{0.96-0.88}{1.00-0.88}$ or 0.67, the value measured. The 33 per cent defect resulted from the small 4 per cent defect at the inlet. At station 5 the dynamic pressure at the top would be negative by Bernoulli's equation, so momentum had evidently been transferred away from the middle region, a condition to be avoided. (Separation did not take place, in fact, anywhere in the diffuser at $2\alpha = 2$ degrees. It did, however, at 3 degrees)

Nikuradse's (ref. 13) furthest downstream station for $2\alpha = 2$ degrees was $\frac{y}{b} = 34.7$, roughly half that of station 2, and he measured $P_r = 0.985$. In his experiment the flow entered the diffuser through a contraction so the velocity distribution was initially uniform. The question arises as to whether he had a fully shearing flow, or just boundary layers.

The measurements of P_r in the approach channel showed that the two-dimensionality troubles were located in the upstream portion. Apparently the following was happening: at the contraction from the plenum chamber the floor and ceiling are plane, the contraction being all in the side walls, therefore the boundary layers on the floor and

ceiling tend to be thicker. Furthermore, the interaction of the corners retards the boundary layers on the ends even more. Therefore transition started first at the floor and ceiling and further downstream at the midplane. Since the coefficient of friction of a boundary layer roughly doubles after passing through transition, the momentum was removed at a faster rate near the floor and ceiling until the flow at the midplane passed through transition.

The transition zone was measured at several elevations by dragging an impact probe along the surface. The method is similar to that employed by Klebanoff and Diehl (ref. 8) with the exception that transition was determined by the total pressure in the present experiment instead of the impact pressure. At the midplane transition started about 12in. downstream from the point where the inlet contraction ends and the parallel wall begins, and had not ended by 20in. from the inlet. At 2 1/2in. from the ceiling transition took place within 4in. downstream of the inlet.

Two methods were tried to improve the two-dimensionality of the flow leaving the approach channel. In the first plan, which was the more conservative, a row of tacks was imbedded in each wall 12in. from the inlet. The heads were 0.22in. dia. and 0.025in. thick and projected entirely above the surface the intent being to remove momentum by the profile drag. The interval between tacks was increased near the floor and ceiling to reduce the momentum removal. It turned out that the improvement of the two-dimensionality was negligible.

Thereupon we decided to utilize the difference between the laminar and turbulent C_f by artificially causing transition further upstream along the middle region. At this time the problem was discussed with Mr. Phillip Eisenberg of the David Taylor Model Basin.* In particular he indicated that single

---

* Currently at the Office of Naval Research (Head, Mechanics Branch)

roughness elements had been used successfully to promote transition on ship models, and he directed us to the literature on this work and referred us to the research that has been done by the David Taylor Model Basin. One advantage of single roughness elements, as he pointed out, is their small profile drag. In the channel they have an additional merit. The stream contracts as it passes over the tripper and the pressure gradient tends to become more favorable since Bernoulli's equation applies to the stream core. If the transition device is continuous, such as a wire, the favorable pressure gradient could be so large that the stream could conceivably reattack and remain laminar.

We discussed the problem with Mr. Marshall Tulin of the David Taylor Model Basin, and his experience with short cylinders normal to the surface was very helpful to us. Also the influence of Reynolds number (ref. 30) for other trippers could be interpreted to our case. Therefore we decided as the second plan to place a row of tacks on each wall at a distance of 3 1/4 in. from the inlet at the midplane and curving further downstream near the floor and ceiling. The initial results were surprisingly good. Following several hours running we discovered, quite by accident, that the dust formed on the surface in such a manner that when a light was placed nearly flat to the surface the laminar regions were dark and the turbulent regions light. * The dust patterns revealed that some of the tacks had not caused transition. We found these tacks did not protrude as far from the surface. They were pulled further out whereupon all the tacks had turbulent boundary layers in their wakes.

---

*

No explanation has been given, in fact one would expect the opposite to take place. When the surface was wiped it all became dark, so it is clear that dust had settled.

We then remeasured P_r at the outlet of the approach section; at the top and bottom it improved to 1.00 and 0.985 respectively. The two-dimensionality in the test section was also significantly better and the very low frequency fluctuations that interfered with velocity measurements were considerably reduced. A small Reynolds number effect and a difference when the number of fans were changed was observed. This was not traced further. Some effort was spent to raise the dynamic pressure at the floor but with little success. These values were therefore accepted. The characteristics of the downstream flow were measured in some detail, so they will now be examined.

Evaluation Of The Test Conditions

The purpose of this section is to determine how well the wind tunnel satisfied the assumptions made in the Preliminary Analysis. We will show how the integral equations derived in the Preliminary Analysis section, can be used to make definite numerical statements about the individual conditions.

In principle the plan will be to examine each term that was eliminated in the analysis by virtue of the assumptions and to determine whether it actually is as small as the analysis requires. This will eliminate the possibility of two cancelling affects.

The examination of the basic assumption concerning continuity, the Navier-Stokes equations, and the Reynolds postulate to obtain equations (1), (2), and (3) is more sophisticated than we are attempting here so we will proceed from these equations. In exparded form equations (1) and (2) are

$$\frac{\partial \bar{U}}{\partial x} + \frac{\partial \bar{V}}{\partial y} + \frac{\partial \bar{W}}{\partial z} = 0 \qquad (1')$$

$$\bar{U}\frac{\partial \bar{U}}{\partial x} + \bar{V}\frac{\partial \bar{U}}{\partial y} + W\frac{\partial \bar{U}}{\partial z} = -\frac{1}{\rho}\frac{\partial \bar{P}}{\partial x} + \nu\nabla^2\bar{U} - \left\{\frac{\partial \overline{u^2}}{\partial x} + \frac{\partial \overline{uv}}{\partial y} + \frac{\partial \overline{uw}}{\partial z}\right\} \qquad (2\text{-a}')$$

$$\bar{U}\frac{\partial \bar{V}}{\partial x} + \bar{V}\frac{\partial \bar{V}}{\partial y} + \bar{W}\frac{\partial \bar{V}}{\partial z} = -\frac{1}{\rho}\frac{\partial \bar{P}}{\partial y} + \nu\nabla^2\bar{V} - \left\{\frac{\partial \overline{uv}}{\partial x} + \frac{\partial \overline{v^2}}{\partial y} + \frac{\partial \overline{vw}}{\partial z}\right\} \qquad (2\text{-b}')$$

$$\bar{U}\frac{\partial \bar{W}}{\partial x} + \bar{V}\frac{\partial \bar{W}}{\partial y} + \bar{W}\frac{\partial \bar{W}}{\partial z} = -\frac{1}{\rho}\frac{\partial \bar{P}}{\partial z} + \nu\nabla^2\bar{W} - \left\{\frac{\partial \overline{uw}}{\partial x} + \frac{\partial \overline{vw}}{\partial y} + \frac{\partial \overline{w^2}}{\partial z}\right\} \qquad (2\text{-c}')$$

A complete discussion of turbulence assumption (d) and (e), and, more particularly, how they were used is quite involved and would divert attention from the more important assumptions. Also the main items were covered in the section on Preliminary Analysis. The question here is whether the flow satisfied the conditions: (a) $\bar{W}=0$, (b) $\frac{\partial(\,)}{\partial z}=0$ for all terms, the boundary-layer approximation, and longitudinal similarity.

From the boundary-layer approximation we deduced that $\bar{V} \ll \bar{U}$. Measurements at the midplane of station 5 with the x-meter showed this to be the case. Furthermore $\bar{W}$ was measured by the x-meter and claw probe at the same location and it was significantly smaller than $\bar{U}$, figure 33 But the derivatives $\frac{\partial \bar{V}}{\partial y}$, $\frac{\partial \bar{W}}{\partial z}$, and $\bar{W}\frac{\partial \bar{U}}{\partial z}$ must be carried since $\frac{\partial \bar{U}}{\partial x}$ is small. Since $\bar{W} \ll \bar{U}$, then each term in equation ($2\text{-}c^1$) is smaller than its counterpart in equation ($2\text{-}a^1$). But it is possible that in the aggregate they may interact through the pressure upon equation ($2\text{-}a^1$). It will be demonstrated later by measurements that $\frac{\partial P}{\partial z}$ was sufficiently small, so we will use this fact. Pressure interaction from equation ($2\text{-}b^1$) is not likely, except through $\overline{v^2}$ as mentioned in equation (5b), because $\bar{V}$ was less than one-fourth of $\bar{W}$. Therefore equations (1^1), ($2\text{-}a^1$), ($2\text{-}b^1$), and ($2\text{-}c^1$) reduce to

$$\frac{\partial \bar{U}}{\partial x} + \frac{\partial \bar{V}}{\partial y} + \frac{\partial \bar{W}}{\partial z} = 0 \qquad (1^1)$$

$$\bar{U}\frac{\partial \bar{U}}{\partial x} + \bar{V}\frac{\partial \bar{U}}{\partial y} + \bar{W}\frac{\partial \bar{U}}{\partial z} = -\frac{1}{\rho}\frac{dP^*}{dx} + \nu\frac{\partial^2 \bar{U}}{\partial y^2} - \frac{\partial \overline{uv}}{\partial y} \qquad (6^1)$$

Equation (1') can be substituted into equation (6') giving

$$\frac{\partial \bar{U}^2}{\partial x} + \frac{\partial(\bar{U}\bar{V})}{\partial y} + \frac{\partial(\bar{U}\bar{W})}{\partial z} = -\frac{1}{\rho}\frac{dP^*}{dx} + \nu\frac{\partial^2 \bar{U}}{\partial y^2} - \frac{\partial \overline{uv}}{\partial y}$$

This equation will now be put into the integral form to study the remaining assumptions. The second term drops out leaving

$$\int_0^b \frac{\partial \bar{U}^2}{\partial x}dy + \int_0^b \frac{\partial(\bar{U}\bar{W})}{\partial z}dy = -\frac{b}{\rho}\frac{dP^*}{dx} + \nu\left[\left(\frac{\partial \bar{U}}{\partial y}\right)_{y=b} - \left(\frac{\partial \bar{U}}{\partial y}\right)_{y=0}\right] + (\overline{uv})_{y=0}$$

The flow symmetry was checked and $\left(\frac{\partial \bar{U}}{\partial y}\right)_{y=0} \ll \left(\frac{\partial \bar{U}}{\partial y}\right)_{y=b}$ at station 5 in the midplane. Figure 13 shows that $(\overline{uv})_{y=0}$ was negligible, so the terms on the right-hand side of the equation reduce to the pressure term plus $\frac{1}{\rho}\tau_w$. The critical assumptions are wrapped up in the left-hand side. We will now expand these terms. The first term is

$$\int_0^b \frac{\partial \bar{U}^2}{\partial x}dy = \frac{\partial}{\partial x}\int_0^b \bar{U}^2 dy - \bar{U}_b^2\frac{db}{dx}$$

and since $\bar{U}_b = 0$ it can be further expanded to

$$= U_0^2\left[b\frac{\partial I_2}{\partial x} + 2\frac{I_2}{\bar{U}_0}\frac{\partial(bU_0)}{\partial x} - I_2\alpha\right]$$

or non-dimensionally, where $\xi(x) \equiv \int_0^x \frac{1}{b(x_1)}dx_1$

$$= U_0^2\left[\frac{\partial I_2}{\partial \xi} + \frac{2I_2}{R_b}\frac{\partial R_b}{\partial \xi} - I_2\alpha\right]$$

The second term on the left hand side is

$$\int_0^b \frac{\partial(\bar{U}\bar{W})}{\partial z}\,dy$$

or

$$U_o^2\left[\int_0^1 f^2 \frac{\partial\left(\frac{\bar{W}}{\bar{U}}\right)}{\partial\left(\frac{z}{b}\right)}d\eta + 2\int_0^1 \frac{\bar{W}}{\bar{U}} f \frac{\partial f}{\partial\left(\frac{z}{b}\right)}d\eta - \frac{1}{U_o^2}\frac{\partial U_o^2}{\partial\left(\frac{z}{b}\right)}\cdot\int_0^1 f^2\frac{\bar{W}}{\bar{U}}d\eta\right]$$

so the complete integral equation is

$$\underset{1^+}{\frac{\partial I_2}{\partial \xi}} + \underset{2^+}{\frac{2I_2}{R_b}\frac{\partial R_b}{\partial \xi}} + \underset{3^+}{\int_0^1 f^2 \frac{\partial\left(\frac{\bar{W}}{\bar{U}}\right)}{\partial\left(\frac{z}{b}\right)}d\eta} + \underset{4^+}{2\int_0^1 \frac{\bar{W}}{\bar{U}} f \frac{\partial f}{\partial\left(\frac{z}{b}\right)}d\eta} - \underset{5^+}{\frac{1}{U_o^2}\frac{\partial U_o^2}{\partial\left(\frac{z}{b}\right)}\int_0^1 f^2\frac{\bar{W}}{\bar{U}}d\eta} =$$

$$\underset{6^+}{-\frac{b}{\rho U_o^2}\frac{dP^*}{dx}} + \underset{7^+}{I_2\alpha} + \underset{8^+}{\frac{\tau_w}{\rho U_o^2}} \qquad (13')$$

which differs from equation (13) in the Preliminary Analysis by the terms on the left-hand side. These terms drop out if the assumptions are realized. The first term, 1^+, vanishes if the mean-velocity profiles satisfy longitudinal similarity. If the profiles are similar but fluid is fed into the plane then the second term, 2^+, is positive. Terms 3^+, 4^+ and 5^+ are the two-dimensionality effects. Term 3^+ is the removal of momentum due to a spreading of the stream surfaces above and below the plane; term 4^+ incorporates the two-dimensionality of the mean-velocity similarity term 5^+ accounts for a vertical change in the centerline dynamic pressure. At the midplane 4^+ and 5^+ would be expected to be zero by vertical symmetry. Terms 4^+ and 5^+ are sensitive to the deviation of the stream surface from planeness.

The separation of the longitudinal changes into the form of 1^+ and 2^+ and the vertical into 3^+, 4^+, and 5^+ was done to facilitate the experimental check. Analytically it might be preferable to use the mean velocity across a section instead of U_o ; then 1^+ would check longitudinal similarity, and 2^+, 3^+, 4^+, and 5^+ would check two-dimensionality.

In order to fulfill the assumptions of the analysis we would like to have $1^+, ---, 5^+$ individually smaller, by say a factor of 10, than any of the terms that remain, i. e. 6^+, 7^+, or 8^+. At α = 1 degree the pressure gradient, 6^+, and momentum gradient, 7^+, are nearly in balance and each is about 10 times larger than 8^+, which is 13×10^{-4}. Therefore the requirement is that $1^+, ---, 5^+ \ll 13 \times 10^{-4}$. In addition we should like to avoid local irregularities in the flow. The limit of integration in 1^+, 3^+, 4^+, and 5^+ is unity so we are on the conservative side if we ask that the integrand everywhere remain in the same bounds.

Term 1^+ between stations 2 and 3 was 1.7×10^{-4} so it is sufficiently small, thus satisfying longitudinal similarity. Let us examine the integrand in

$$\frac{\partial I_2}{\partial \xi} = 2 \int_0^{\eta'} f \frac{\partial f}{\partial \xi} \, d\eta$$

Between stations 2 and 3 the requirement would be that $f\Delta f < 35\,(10^{-4})$. Figure 8 shows this is about the duplication of the profiles.

Here is where a question arises in regard to Nikuradses' experiment (reference 13). His furthest downstream station was at $\xi = 34.7$ for $\alpha = 1$ degree. Results of pipe flow indicate that ξ values of 50 to 100 are required for uniform flow at the inlet to become fully developed. Nikuradse made additional velocity measurements at $\xi = 23.2$ to determine that the flow was fully developed. The above test would require $f\Delta f < 17 \times 10^{-4}$, or since f has a value of about unity the velocity profiles must duplicate to 0.2%. This is better than customary accuracy. Whether the profiles were this close is not known since Nikuradse did not report the upstream data.

In the present experiment term 1 between stations 2 and 5 was -1.7×10^{-4}. Again this is sufficiently small. For the integrand to be everywhere small we require $f\Delta f < 0.004$. Several points were larger, but the discrepancy did not appear serious. To measure 1^+ the precision manometer was needed as it corresponds over a large region of the channel to $\left(\frac{\Delta U}{U_0}\right)_{\eta = \text{const.}} < 0.004$ between the stations. The dynamic pressure at station 5 for U_0 is 0.06 in. of water, so the dynamic pressure should be resolved to 5×10^{-4} in. of water. The final manometer was more accurate than 10^{-4} in. of water, and is discussed in Appendix II. The accuracy of measuring f was tested by periodically measuring U_0 during each traverse and comparing it to the reference pressure. It had a probable error (0.675 x standard deviation) of 0.7×10^{-4} in. of water which is satisfactory.

The mean-velocity profile at stations 4 and 5 was slightly more peaked than at the upstream stations. This can be related to term 2. After the peaking was observed $\frac{dR_b}{dx}$ was measured and between stations 3 and 5 R_b increased 4 percent. But during each velocity traverse the wind-tunnel speed had been set so $R_b = 31,400$ at the particular station. Therefore when the downstream traverses' were made the upstream flow was at a lower R_b, and thus more peaked, than when the upstream traverse had been made. Laufer's data (ref. 5) would indicate that this would be a rise in f at $\eta = 0.2$

of about 0.005. This would account for roughly one-half of the change. This 4 percent rise in Reynolds number was confirmed by a corresponding increase in the dynamic pressure at the inlet to the parallel-wall approach section between the two runs. The latter method would indicate an R_b increase between stations 2 and 3 of 3.5 percent. The net result is that 2^+ between stations 2 and 5 was 21×10^{-4}, or roughly equal to the turbulence term, 8^+. It was only slightly balanced by 1^+.

Term 3 is believed to be the offender. Unfortunately it is very difficult to measure directly: for it to be smaller than $\frac{1}{10} \frac{\tau_w}{\rho U_0^2}$ at station 5 requires that the flow inclination differ by less than 0.04 degrees between the midplane and the traverse points 16 in. above or below the midplane. However, an estimate of its magnitude can be made from continuity of the flow. Integration of equation (1) across the channel using only the wall no-slip condition and $\overline{V} = 0$ at $y = 0$ gives

$$\underset{1^{++}}{\frac{dI_1}{d\xi}} + \underset{2^{++}}{\frac{I_1}{R_b}\frac{dR_b}{d\xi}} + \underset{3^{++}}{\int_0^1 \frac{d\left(\frac{\overline{W}}{\overline{U}}\right)}{d\left(\frac{z}{b}\right)} d\eta} + \underset{4^{++}}{\int_0^1 \frac{\overline{W}}{\overline{U}} \frac{df}{d\left(\frac{z}{b}\right)} d\eta} - \underset{5^{++}}{\frac{1}{U_0}\frac{dU_0}{d\left(\frac{z}{b}\right)} \int_0^1 f \frac{\overline{W}}{\overline{U}} d\eta} \qquad (12')$$

Terms 4^{++} and 5^{++} can be neglected, as before, by vertical symmetry. Between stations 2 and 5 term 1^{++} was -0.7×10^{-4} and term 2^{++} was 11.9×10^{-4}. Term 3^{++} is then -11.2×10^{-4} negative as expected. If $\frac{d\left(\frac{\overline{W}}{\overline{U}}\right)}{d\left(\frac{z}{b}\right)}$ is independent of η it would have the value of -13×10^{-4}. Then putting this back in equation (13') would indicate that term 3^+ is -10×10^{-4}.

The following table is a summary of the terms in equation (13′)

Term 1^+	=	-1.7×10^{-4}
" 2^+	=	21 "
" 3^+	=	- 10 "
" 5^+	=	negligible
Total		9×10^{-4}

Term 6^+	=	-100×10^{-4}
" 7^+	=	127 "
" 8^+	=	- 13 "
Total		14 "

Note: term 4 was not measured, but is believed to be small.

It is evident that terms 2^+ and 3^+ roughly account for the discrepancy of 13×10^{-4} in equation (13). The von Karman momentum equation for the turbulent boundary layer assumes terms equivalent to 3 , 4, and 5 are zero. In view of the present remarks it is not surprising that in the past the use of the von Karman equation to compute $\frac{\tau_w}{\rho \bar{U}_0^2}$ has led to apparent increases in the wall shear stress during a retardation, whereas a decrease is expected.

The net result is that longitudinal similarity existed, within the requirement set, but two-dimensionality of the mean flow deviated by an amount equal to the turbulence term in equation (13) $\frac{\tau_w}{\rho \bar{U}_0^2}$. The hope is that since this effect acts through the mean flow it would not appreciably disturb the turbulence. What it may amount to is a 10 percent reduction in the "effective" α . One is restrained, however, from concluding at this point that the assumption of longitudinal similarity for a fully two-dimensional channel is confirmed.

At this point consideration was given to diverging the floor and ceiling. However, this involves mechanical difficulties, and in view of the sensitivity of the flow to very small changes in this divergence angle, as indicated by term 3^+ in equation (13′) , the

decision was made to measure u' at two stations. If this were similar, as it turned out to be, then it would be considered sufficient evidence of flow similarity to proceed with further measurements.

The u' profile at station 2 is compared to the profile at station 5 in figure 10 . It compares very well. But again the statement can be made more precise, this time by means of the turbulent energy equation. A complete analysis including all of the assumptions, as was done for the momentum equation, will not be undertaken. But the similarity assumption will be carried out. This was done by rederiving equation (14) without making the assumption of similarity. The following additional term is obtained, $\frac{b}{2}\frac{dI_4}{dx}$. It can be expanded to

$$\frac{b}{2}\frac{dI_4}{dx} = \frac{1}{2}\int_0^1 f\frac{\partial h}{\partial \xi}d\eta + \frac{1}{2}\int_0^1 h\frac{\partial f}{\partial \xi}d\eta$$

For each of these terms to be negligible it must be small compared to the smaller of the terms that remain, which is $\frac{\nu}{U_0 b}\int_0^{\delta}\overline{\left(\frac{\partial u_i}{\partial x_k}\right)\left(\frac{\partial u_i}{\partial x_k}\right)}dy$. The latter term will be estimated by the isotropic relation

$$\overline{\left(\frac{\partial u_i}{\partial x_k}\right)\left(\frac{\partial u_i}{\partial x_k}\right)} = 5\frac{q^2}{\lambda^2}$$

where the values of $\frac{\lambda}{b}$ and $\frac{q^2}{U_0^2}$ at station 5 are used. Thus

$$\frac{5}{R_b}\left(\frac{b}{\lambda}\right)^2_{\eta=0}\int_0^1 \frac{q^2}{U_0^2}d\eta = \frac{5}{31{,}400}\left(\frac{3.860\ in}{0.25\ in}\right)^2(0.03) \approx 10^{-3}$$

If $\frac{1}{h}\frac{\partial h}{\partial \xi}$ and $\frac{1}{f}\frac{\partial f}{\partial \xi}$ are function of ξ only, then

$$\frac{b}{2}\frac{d\bar{I}_4}{dx} = \frac{1}{2}\bar{I}_4\left[\frac{1}{h}\frac{\partial h}{\partial \xi} + \frac{1}{f}\frac{\partial f}{\partial \xi}\right]$$

$$I_4 \approx 10^{-2};$$ so for

$$\frac{b}{2}\frac{d\bar{I}_4}{dx} < \frac{1}{10}\frac{\nu}{U_0^3 b}\int_0^b \overline{\left(\frac{\partial u_i}{\partial x_k}\right)\left(\frac{\partial u_i}{\partial x_k}\right)}\,dy$$

we require $\frac{1}{h}\frac{\partial h}{\partial \xi}$ and $\frac{1}{f}\frac{\partial f}{\partial \xi}$ to be less than 10^{-2}. Between stations 2 and 5 this means: $\frac{\Delta h}{h}, \frac{\Delta f}{f} < 0.5$ This was well satisfied.

There is one point to be cleared up. The statement was made that the interaction between equation (2 a′) and (2 c′) through the pressure is small. This will now be demonstrated. If equation (2-c′) is put in the integral form, similar to equation (13′), the pressure term is

$$\int_0^{\prime} \frac{b}{\rho U_0^2}\frac{\partial p}{\partial z}\,d\eta$$

The wall values of $\frac{\Delta p}{\Delta z}$ were measured between the midplane and 16 in. above and below the midplane to estimate this term. It is compared to term 6^+ of equation (13′) in figure 33 and it stays well below one-tenth of the latter term. To be assured that $\frac{dp}{dz}$ does not affect the turbulence one might like this integral to be even less than $\frac{1}{10}\frac{\tau_w}{\rho U_0^2}$. This is not quite satisfied downstream of about station 4, but the discrepancy is not believed to be serious.

APPENDIX II

PRECISION INCLINED MANOMETER

Introduction

In order to measure mean velocities with sufficient reliability to establish the existence of simple similarity, it is desirable to measure pressure with an accuracy of 0.0005 in. of water (this is justified in Appendix I.). The same is required to measure the mean velocity in the laminar sublayer and the static-pressure gradient in the direction of flow.

Several pressure measuring devices with greater sensitivities have been reported in literature, e.g. reference 31. But generally they are difficult to construct. Laufer in reference 6 stated that he obtained a sensitivity of 10^{-4} cm. of water with an inclined-tube manometer using Benzol, and a cathetometer to measure the meniscus displacement.

The inclined manometer is attractive because of its simplicity. The measurement is reduced to a simple determination of length to normal engineering accuracy. Its accuracy is limited by complications associated with the capillary force on the meniscus.

A cursory literature search did not uncover an analysis of either the static or dynamic response of the reservoir-type inclined manometer. Therefore a preliminary analysis was made. The result was that the static problem appeared to hinge upon the reproducibility of the capillary rise, e.g., surface cleanliness, temperature, etc.

A pilot-model manometer was assembled and it was found that the above difficulties were tractable. Therefore a final manometer was constructed and this is shown in figure 34.

The basis of the liquid-type manometers is the pressure-head relation

$$\Delta p = (\gamma_1 - \gamma_2)\, h \qquad (15)$$

where one column of fluid has the density γ_1 for a height h, the other has the density γ_2 for the same height, and over the remaining height of the two columns from the point of inter-connection to the (assumed) common elevation where Δp is measured the density is the same in each column. Obviously this could be generalized to include variable densities in the columns if one of the fluids is compressible, such as a gas. And, indeed these effects may not be negligible, but are generally easily computed and will not be discussed here.

The vertical U-tube manometer is the simplest but h is difficult to measure to the accuracy desired. The differential manometer makes the term $(\gamma_1 - \gamma_2)$ small to enlarge h but difficulties have been encountered with the meniscus interface. The inclined manometer attains its accuracy by making the actual length measured many times larger than h. It appeared to be the most probable for success, so it was selected.

Distilled water was used in this experiment because of the ease of maintaining constant density. Alcohol, for example, is significantly hydroscopic. Furthermore the thermal expansion of water is about one-fifth that of other liquids. The disadvantage of water is its high surface tension. This was reduced from 73 to 30 dynes per cm., a value typical of many liquids, by adding a wetting agent (The Meriam Instrument Company, D-2930) which does not change the density.

The chief question concerning the inclined manometer is whether the capillary rise is repeatable and constant over the length of the tube. Therefore this will be pursued. The following variables determine the capillary rise: the diameter and inclination of the tube, the liquid, and the angle of contact between the liquid and the tube. We would now like to find how each of these affects the capillary rise.

Intuitively it seems that there is an optimum meniscus shape (the rise of each point on the surface beyond the zero-capillarity position) to minimize capillary effects, i.e. to have a minimum sensitivity to surface wetness, slight changes in angle or surface tension, or whatever else may change the position of the meniscus minimum. For example, as the tube inclination is increased the meniscus spreads out further and consequently it would appear to be more sensitive to the way the contact is made at the glass. But at the same time the sensitivity to pressure, which is what we are looking for, increases. The ideal procedure would be to obtain an analytical expression for the meniscus shape then proceed to optimize. Unfortunately this cannot be done by a membrane analysis because the angle of contact between most liquids, including water, and clean, wetted glass in the presence of air is reported to be O degrees, reference 32 . In the present case the meniscus shape and tube inclination were selected by inclining several tubes at about a 20:1 slope and then taking the one with the largest tube diameter that did not have an unduly long meniscus. Obviously some study could be given to selecting an optimum meniscus shape and tube inclination.

However, having selected a meniscus shape and tube inclination we now wish to keep them fixed while we examine the effect of the other variables. We can do this by obtaining a similarity parameter. The forces involved are the gravitational force and capillary force, so we shall call their ratio M. This parameter was not found in the literature but it can be obtained from the ratio of the Weber number to the Froude number

$$\left[\frac{\text{Weber No.}}{\text{Froude No.}}\right]^2 = \frac{\frac{U^2 \gamma r}{Sg}}{\frac{U^2}{gr}} = \frac{\gamma r^2}{S} \equiv M$$

where r is the tube inside radius, g is the local gravitational acceleration, and S is the surface tension. M would then be a constant for one meniscus shape, one angle of contact between the meniscus and glass, and one tube inclination. Henceforth we will keep M fixed.

As mentioned, an equation for the meniscus shape is not available from which we can compute the position of the meniscus minimum. But we can determine the "average" height of the meniscus due to capillarity, h_c . Define h_c as the product of the volume of fluid raised by the capillary effect times the sine of the angle of elevation of the tube, β , divided by the cross-sectional area of the tube. figure 35 . For a vertical tube (i.e $\beta = 90$ degrees) h_c can be computed from a balance of capillary forces and gravity for a O degree contact angle

$$h_c = \frac{2S}{\gamma r} \qquad (16)$$

A 7 mm. I. D. tube was chosen for the water-wetting agent combination in the present case. In the vertical position the measured rise of the meniscus minimum was 0.045 in. By equation 16 this tube size and fluid would give $h_c = 0.068$ in. This warrants the use of equation (16) for the order-of-magnitude considerations that will be made below. (The approximation is actually somewhat better than appears since h_c is the mean height somewhere between the meniscus minimum and maximum.)

Before going through the analysis with equation (16) let us show how this equation can also be used to obtain the capillary rise in an inclined tube. This will be carried out by reference to figure 36 . The top sketch represents a sectional view through the plane containing the axis of the tube. An element of the glass surface containing the line of contact of the meniscus is shown in

the lower diagram. Since the angle of contact is 0°, the resultant force, dT, on the element of the meniscus perimeter, ds, is in the plane of the glass and proportional to ds.

$$dT = S\,ds$$

The component in the direction of the axis, dT_z, is

$$dT_z = \frac{r\,d\theta}{ds}\,dT$$

in polar-cylindrical coordinates about the tube axis. The total force in the axial direction, T_z, is

$$T_z = \int_{\substack{\text{around} \\ \text{the meniscus} \\ \text{perimeter}}} S\,\frac{r\,d\theta}{ds}\,ds = Sr\int_0^{2\pi} d\theta = 2\pi r S$$

Therefore, T_z is independent of the tube inclination. The capillary force balances the gravity force so that the volume raised, V_c, is related by the angle of elevation β,

$$T_z = \gamma V_c \cdot \sin\beta$$

and by definition of h_t

$$V_t = \frac{\pi r^2 L h_c}{\sin \beta}$$

then combining

$$T_z = \pi r^2 h_c \gamma$$

so h_c is independent of the tube slope (as was h). Of course, the rise of the meniscus minimum in a vertical tube is somewhat less than h_c--- the two becoming equal as r approaches O. But within this difference, the rise of the meniscus minimum in an inclined tube can be approximated by the rise in a vertical tube. This will be done in the following analysis.

Let us now select the liquid. Introducing M into equation (16)

$$h_t = 2 \left[\frac{S}{M \gamma} \right]^{\frac{1}{2}}$$

M is fixed, so one chooses a fluid with the smallest value of $\frac{S}{\gamma}$ to give the least capillary rise. A survey of a large number of liquids revealed that Methanol has the lowest value, and this is only four percent below the water-wetting agent combination.

The uniformity requirement for the tube diameter can be established by putting equation (16) in the form

$$\frac{\partial h_c}{\partial r} = - \frac{2S}{\gamma r^2} = - \frac{2}{M}$$

One sees that all liquids under similar (which could mean optimum) conditions have the same sensitivity to absolute variations in radius. With the present combination a $\Delta r = 0.0003$ in. gives $\Delta h_c = 0.0001$ in. Normal precision tube tolerance is +0.0004 in. from the nominal size, and because of the method of manufacture the uniformity along one tube is significantly better. Similarly, the reservoir accuracy was established and turned out to be easily fulfilled.

Temperature, Θ, enters in three principal ways: (1) volumetric change of the container, (2) expansion of the liquid, and (3) variation in capillarity. These will now be discussed.

(1) Consider a thin-wall cylindrical glass reservoir of circular cross-section resting on its base. The volume of liquid enclosed equals the depth x (circumference)$^2/4\pi$. If the liquid volume is constant then for a thin-wall reservoir a one per cent change in circumference corresponds to a two per cent change in depth. The thermal coefficient of linear expansion of glass is nearly 5×10^{-6}/°F (reference 33). Therefore, if the depth is about one inch, a temperature rise of 1°F corresponds to a decrease in depth (zero-level) of 10^{-5} in. of water, which is negligible. The changes in the glass tube affect the level even less if its portion of the enclosed volume of liquid is significantly smaller than that in the reservoir, as it was in the present manometer.

(2) The thermal coefficient of volumetric expansion of water is 0.0001/°F (reference 33). (For most other liquids it is about five times larger.) Thus the zero level in a one-inch deep reservoir would rise 10^{-4} in. per degree F. This is the accuracy desired so the temperature must be controlled within this limit.

The above considerations are all connected with the change in zero level. These effects can be reduced by periodically taking zero readings. This procedure has been adopted during tests. However, there is another effect due to the thermal expansion of the liquid; namely, h is inversely proportional to γ in the pressure-head relation. This causes a percentage error, namely $\frac{1}{h}\frac{\partial h}{\partial \theta} = 0.0001/F°$.

(3) The temperature effect on the capillary rise is computable by putting equation (2) in the form

$$\frac{1}{h_c}\frac{\partial h_c}{\partial \theta} = \frac{1}{S}\frac{\partial S}{\partial \theta} - \frac{2}{\gamma}\frac{\partial \gamma}{\partial \theta}$$

The first term represents the change due to surface tension and the other is the density change within the capillary-rise portion. For the water-wetting agent combination $\frac{1}{h_c}\frac{\partial h_c}{\partial \theta}$ = 0.0011/F°. A slight drop in the zero level was observed after turning on the light illuminating the meniscus. However, within one hour this effect tended to reach equilibrium. Actually, it was very easy to shield the manometer against all thermal effects by enclosing it in a plastic bag.

A side point could be mentioned. It is conceivable that the manometer could be designed so that the thermal expansion effect of the liquid could be nullified by the surface tension recession and expansion of the reservoir.

The manometer, figure 34 was constructed as follows. The inclined tube is 7 mm. I.D. the reservoir is 100 mm. I.D., and the tube inclination is 20:1. The microscope is mounted in the vertical plane so that light rays pass through normal to the glass. The meniscus appears symmetrical and nearly flat over a wide region, and is sharp and clearly identifiable to 1/10 of the smallest reading desired. A dial indicator graduated in 10^{-3}in. indicates the microscope travel: 0.002 in. represents a pressure of 10^{-4} in. of water. An internal scale within the microscope has graduations equivalent to a pressure of 10^{-4} in. of water which facilitates averaging pressure fluctuations.

It was found important in the experimental technique to wet the surface ahead of the meniscus. (Reference 32 states that the contact angle of a non-wetted surface is different). The tubes were first thoroughly cleaned with a standard acid cleaner. Then they were flushed with tap water and finally distilled water. Nevertheless,

the readings could be in error by as much as 0.0004 in. of water unless the meniscus was displaced far enough ahead to wet the glass. With the wetting technique, the meniscus would return to the same position with the probable error of a small fraction of 10^{-4} in. of water. In this connection, one must be careful to avoid foreign matter since it generally tends to accumulate at the surface.

Evaporation effects can enter. The zero level with the reservoir open was observed to drop by 10^{-4} in. in a five-minute period. Therefore, a constriction was found necessary. The constriction should be small enough to prevent evaporation from changing the zero level, and large enough so the vapor pressure does not differ appreciably from the ambient. For example, the zero level consistently rose 0.0002 in. when the reservoir connection was switched from a 1/4 in. I.D. tube open to the atmosphere to an identical tube with a 0.020 in. diameter hole forming a constriction to the atmosphere. This is the pressure difference due to the flow of vapor. A slightly larger opening gives no effect.

Three calibration tests were made:

(1) Zero reading - A number of zero readings were taken and the spread was always within 10^{-4} in. of water so long as the fluid was sufficiently clean. Following several weeks use, the fluid would become dirty which always manifested itself by not duplicating zero readings.

(2) Hysteresis - Small quantities of liquid were added in the reservoir and the rise was measured in the tube. Then the quantities were successively removed. No hysteresis effect was observable.

(3) Accuracy - The final calibration was made by adding measured volumes of liquid in the reservoir by a precision burette. The probable error over a range equivalent to 0.2 in. of water pressure was 0.00007 in. of water.

APPENDIX III

CORRECTION OF THE HOT-WIRE SENSITIVITY DUE TO THE TEMPERATURE DEPENDENCE OF KING'S CONSTANT, A

As mentioned on page 23, the so-called constant, A, in King's equation (ref. 22) is actually a function of the wire temperature. This was originally observed by King, but evidently has been overlooked in a nember of intervening investigations. Therefore a correction must be made when the hot-wire is calibrated at constant resistance (constant temperature) and used at constant current. In the present experiment this correction (a monotonic function of overheat ratio) increased the computed values of all $\frac{u'}{U}$ by 16 to 24 percent. Therefore the correction will be derived below.

King's equation for the heat loss, I^2R, of an infinite circular cylinder with axis normal to the stream direction is

$$I^2R = \left[A(\vartheta) + B\sqrt{U}\right](\vartheta - \vartheta_e) \qquad (17)$$

where U is the air speed, constant and low, ϑ is the wire temperature, and ϑ_e is the ambient air temperature. $A(\vartheta)$ is the term under examination, but for some operating conditions the temperature dependence of R is equally important so it will be included. King's result that B is only slightly temperature sensitive has been verified, so it will be assumed constant.

To apply equation (17) to turbulence measurement the usual assumption of a quasi-equilibrium state of the flow field will be admitted. The justification will not be undertaken here. So for constant-current operation of the hot-wire in a constant ϑ_e stream the functional form of equation (17) is

$$R = R\left[A(\vartheta), \vartheta, U\right]$$

ϑ is independently related to R by the thermal resistivity, so neglecting second-order and higher terms in a Taylor's expansion

$$\Delta R = \left[\frac{\partial R}{\partial A}\frac{dA}{d\vartheta} + \frac{\partial R}{\partial \vartheta}\right]\frac{d\vartheta}{dR}\Delta R + \frac{\partial R}{\partial U}\Delta U$$

or

$$\Delta R = \frac{\frac{\partial R}{\partial U}}{1 - \frac{\partial R}{\partial \vartheta}\frac{d\vartheta}{dR} + \Phi}\Delta U \qquad (18)$$

where $$\Phi \equiv -\frac{\partial R}{\partial A}\frac{dA}{d\vartheta}\frac{d\vartheta}{dR}$$

The term Φ embodies the correction, and usually has been neglected without explicit mention.

The terms $\frac{\partial R}{\partial U}$, $\frac{\partial R}{\partial A}$, and $\frac{\partial R}{\partial \vartheta}$ are easily obtained from equation (17) by differentiation. For $A(\vartheta)$ we will use the relation defined by King

$$A = A_e\left[1 + c(\vartheta - \vartheta_e)\right] \qquad (19)$$

which gives

$$\frac{dA}{d\vartheta} = \frac{Ac}{1 + c(\vartheta - \vartheta_e)}$$

The evaluation of c will be discussed later. The remaining term, $\frac{dR}{d\vartheta}$, is obtained from the customary expansion

$$R = R_f\left[1 + \alpha(\vartheta - \vartheta_f) + \beta(\vartheta - \vartheta_f)^2\right]$$

where ϑ_f is the reference temperature for R, usually different from ϑ_e.

Substituting these expressions into equation (18) gives

$$\frac{\Delta R}{R} = \frac{B}{(A + B\sqrt{U})}\frac{\Delta U}{2\sqrt{U}}\Bigg/\left\{1 - \left[\frac{A + B\sqrt{U}}{I^2}\right.\right.$$

$$\left.\left. + \frac{R}{A + B\sqrt{U}}\frac{Ac}{1 + c(\vartheta - \vartheta_e)}\right]\frac{1 + (\vartheta - \vartheta_f)\alpha + \beta(\vartheta - \vartheta_f)^2}{[\alpha + 2\beta(\vartheta - \vartheta_f)]R}\right\} \quad (20)$$

We will now evaluate A/B from a calibration of the hot-wire at a constant resistance, figure 37. The value of the resistance in curve I corresponds to the mean operating resistance. This curve will be used for the present calculation. We will adopt several convenient definitions from reference 21.

$$z \equiv \frac{\sqrt{U}}{\sqrt{U_h} + \sqrt{U}}, \quad \sqrt{U_h} \equiv \frac{A}{B}$$

where $\sqrt{U_h}$ corresponds to the abcissa-intercept of curve I. Equation (20) becomes

$$\frac{\Delta R}{R} = \frac{z}{2}\frac{\Delta U}{U}\Bigg/\left\{1 - \left[\frac{1}{\vartheta - \vartheta_e}\right.\right.$$

$$+ (1-z)\frac{c}{1+c(\vartheta-\vartheta_e)}\Bigg]\frac{1+(\vartheta-\vartheta_f)\alpha+\beta(\vartheta-\vartheta_f)^2}{\alpha+2\beta(\vartheta-\vartheta_f)}\Bigg\}$$

or

$$\frac{\Delta R}{R} = \frac{z}{2}\frac{\Delta U}{U}\Bigg/\Bigg\{\frac{\beta(\vartheta-\vartheta_e)}{\alpha+2\beta(\vartheta-\vartheta_f)}$$

$$-\frac{1+\alpha(\vartheta_e-\vartheta_f)+\beta(\vartheta_e-\vartheta_f)^2}{(\vartheta-\vartheta_e)[\alpha+2\beta(\vartheta-\vartheta_f)]}-\frac{(1-z)[1+\alpha(\vartheta-\vartheta_f)+\beta(\vartheta-\vartheta_f)^2]c}{[\alpha+2\beta(\vartheta-\vartheta_f)][1+c(\vartheta-\vartheta_e)]}\Bigg\}$$

Using the following definitions of "overheats"

$$a_w \equiv \frac{R-R_f}{R_f} = \alpha(\vartheta-\vartheta_f)+\beta(\vartheta-\vartheta_f)^2$$

$$a_e \equiv \frac{R_e-R_f}{R_f} = \alpha(\vartheta_e-\vartheta_f)+\beta(\vartheta_e-\vartheta_f)^2$$

$$a'_w \equiv \frac{R-R_e}{R_e} = \frac{1+\alpha(\vartheta-\vartheta_f)+\beta(\vartheta-\vartheta_f)^2}{1+\alpha(\vartheta_e-\vartheta_f)+\beta(\vartheta_e-\vartheta_f)^2}-1$$

and Ohm's law, we obtain for constant current

$$\frac{\Delta E}{E} = -\frac{a'_w z}{2(1+\Phi)}\frac{\Delta U}{U} \qquad (21)$$

where E is the voltage drop across the hot-wire and

$$1 + \bar{\phi} = \left[a_w - a_e + (1 - z)(1 + a_w) \frac{a'_w}{\frac{1}{c(\vartheta - \vartheta_e)} + 1} \right.$$

$$\left. - \beta(\vartheta - \vartheta_e)^2 a'_w \right] \Big/ \left[a_w - a_e + \beta(\vartheta - \vartheta_e)^2 \right]$$

By the following approximations,

$$\frac{1}{1 + \frac{\beta(\vartheta - \vartheta_e)^2}{a_w - a_e}} \approx 1 - \frac{\beta(\vartheta - \vartheta_e)^2}{a_w - a_e}$$

$$\frac{1}{c(\vartheta - \vartheta_e)} = \frac{\alpha}{c} \left\{ \frac{1}{a_w - a_e - \beta\left[(\vartheta - \vartheta_f)^2 - (\vartheta_e - \vartheta_f)^2\right]} \right\}$$

$$\approx \frac{\alpha}{c} \frac{1}{a_w - a_e}$$

$$(\vartheta - \vartheta_e)^2 = \frac{1}{\alpha^2}(a_w - a_e)\left\{1 - \beta\left[(\vartheta - \vartheta_f)^2 - (\vartheta_e - \vartheta_f)^2\right]\right\}^2$$

$$\approx \frac{a_w - a_e}{\alpha^2}$$

The expression for $\bar{\phi}$ reduces to

$$\bar{\phi} = a'_w(1 + a_w)\left[\frac{1 - z}{\frac{\alpha}{c} + a_w - a_e} - \frac{\beta}{\alpha^2} \right] \qquad (22)$$

Equations (21) [with (22)] expresses the hot-wire response at a constant current to velocity fluctuations. Equation (21) is identical to equation (12) of reference 21 when $\Phi_I = 0$.

The effect of Φ_I upon the hot-wire response is shown in figure 37. (1) For A = constant the straight lines I, II, and III would represent three typical constant-resistance responses $R_{II} > R_I > R_{III}$ of a hot-wire following King's equation. The constant-current response of the same hot wire would be represented by the dashed line, h, between curves II and III. (2) In the actual case where $A = A(\vartheta)$ the straight lines I, II', and III' represent the constant-resistance response, and the constant-current operation would follow the dashed line, j, between II' and III'. Obviously since $R_{II} > R_{II'}$ and $R_{III} < R_{III'}$ the hot-wire signal is reduced. Or, in other words, for a given signal from a hot wire in a fluctuating velocity field the true velocity fluctuation is greater than would be computed by assuming $\Phi_I = 0$.

King found empirically that with a wire perpendicular to the flow, c = 0.00114 Cent. degrees $^{-1}$ for air based upon $\vartheta_e = 17$ deg. Cent. This value was verified in the present experiment with a 0.00015 in. dia. platinum wire 0.040 in. long in a non-turbulent air stream at 15 to 35 feet per second. The wire was oriented in two positions relative to the flow, (1) normal, and (2) inclined 50 degrees from the normal. The procedure was to calibrate the wire at $a'_w = 0.4$, 0.7, and 1.0 in each of the two positions. The value of A was computed by assuming B was independent of ϑ. The comparison of c to King's value is made in figure 38. Case 1 is in agreement with King's value. The trend in case 2 may represent experimental error. This warrants further investigation.

The values of α and β for platinum and tungsten were taken from reference 32 (Vol. VI, page 136) and are tabulated below in the form in which they appear in equation (22).

	Pt.	W
$\frac{\alpha}{c}$	3.09	4.59
$\frac{\beta}{\alpha^2}$	− 0.044	0.026

c = 0.00114 Cent. deg. $^{-1}$

ϑ_f = 0 deg. Cent.

The following remarks pertain to equation (22).

1. $\frac{\alpha}{c}$ dominates the denominator of the first term.

This is the A(ϑ) effect. Therefore the values of Φ are generally larger for platinum than for tungsten. ($\mathcal{Z}$ is a function of aerodynamic properties and wire geometry, and is independent of the wire material.)

2. $\frac{\beta}{\alpha^2}$ is negative for platinum and therefore increases Φ, whereas for tungsten this term is positive and tends to reduce Φ. In the present experiment $\frac{\beta}{\alpha^2}$ contributed about 20 percent to the value of Φ, or 4 percent to the value of $\frac{u'}{U}$.

3. For values of $a'_w < 0.5$, Φ is roughly proportional to the overheat, a'_w. Of course the signal is also roughly proportional to a'_w so it is not necessarily feasible to reduce a'_w in order to reduce Φ.

In figure 39 the Φ correction has been plotted for both platinum and tungsten as a function of the velocity term, $\mathcal{Z}$, with a'_w as a parameter. The difference between platinum and tungsten is evident. In the present experiment tungsten wires would have reduced the values of Φ by a factor of 2.

A few remarks should be made concerning the hot-wire end effect on Φ. Equation (17) presumes an infinitely long circular cylinder. The finite-length hot wire does not have a uniform temperature distribution. But simple considerations would indicate that the average (spatial) ϑ corresponding to the average (spatial) R is probably satisfactory for equation (17) with the usual hot-wires. But the heat conducted out the end of the wire to the holder, a length effect, is not of the form of equation (17). Presuming a fixed temperature of the holder at ϑ_e, and estimating the heat conducted out of the end of the wire, Q_E, to be

$$Q_E \sim k(\vartheta - \vartheta_e)$$

and taking first order temperature changes in k

$$k = k_e[1 + c_k(\vartheta - \vartheta_e)]$$

it is evident that the problem is to compare c to c_k. Reference 32 (Vol. V, p. 221) gives the following values

	Pt.	W
c_k	0.00053	- 0.00010
(Cent. deg.$^{-1}$)	0.0018	

($0 < \vartheta < 100$)

Since for platinum c_k and c are of the same order, and in addition the end losses are probably small for most hot-wires, the end losses could be included in A. For very short hot-wires this should be reexamined. But for tungsten the correction is of the opposite sign. Therefore for tungsten the end losses should be either isolated in equation (17), or be shown to be negligible.

APPENDIX IV

Remarks on the Calibration of the X-meter

The X-meter was used to measure v', $\cdot'$, $\overline{uv}$ and incidentally, u'. It turns out that these measurements are subject to appreciable instrument errors under ordinary precisions of manufacture and operation. In particular the measured $\overline{uv}$ is very sensitive to a small error in the probe alignment. Therefore (1) an analysis will be made of the effect of a first-order difference between the wires in the sensitivity to u and v (fluctuations) in the light of existing data. (2) A procedure to nullify the effect of the differences will be out-lined. The "black box" technique of calibrating the X-meter described below is similar to the procedure described in reference 23. The present report extends this work by items (1) and(2) above.

The X-meter, figure 40, consists of two fairly-well matched wires oriented in an "x" somewhat symmetrically about the mean stream direction, i.e. $\varphi_1 \approx \varphi_2$. For small fluctuations, the conventional linearized hot-wire analysis permits writing the voltage sensitivity of wires no. 1 and no. 2 to fluctuations u and v in the form

$$e_1 = a_1 u + b_1 v$$

$$e_2 = a_2 u - b_2 v \qquad (23)$$

where the sensitivity coefficients are in general not equal. Define the differences

$$\Delta a = a_2 - a_1 \qquad a = \frac{a_1 + a_2}{2}$$

$$\Delta b = b_2 - b_1 \qquad b = \frac{b_1 + b_2}{2}$$

where the non-zero values of Δa and Δb represent the inevitable physical and geometrical differences between the two wires.

In order to compute the turbulence terms from the voltage measurements we will assume Δa a and b, and neglect second-order terms (e.g. $\frac{\Delta a \Delta b}{a b}$), obtaining

$$(e_1 + e_2)^2 = 4a^2\left[1 - \frac{\Delta b}{a}\frac{\overline{uv}}{u^2}\right]\overline{u^2} \tag{24}$$

$$(e_2 - e_1)^2 = 4b^2\left[1 - \frac{\Delta a}{b}\frac{\overline{uv}}{v^2}\right]\overline{v^2} \tag{25}$$

$$\overline{e_1^2} - \overline{e_2^2} = 4ab\left[1 - \frac{1}{2}\left(\frac{\Delta a}{b}\frac{\overline{u^2}}{\overline{uv}} + \frac{\Delta b}{a}\frac{\overline{v^2}}{\overline{uv}}\right)\right]\overline{uv} \tag{26}$$

In order to compute the turbulence quantities we must determine a, b, Δa, and Δb. We will discuss the first two later. Two alternative procedures are available in connection with Δa and Δb. (1) Δa and Δb could be measured at what ever value they happen to have and equations (24), (25), and (26) would then be solved simultaneously for the unknowns u, v and uv. (2) The probe could be reoriented, etc. to make $\Delta a = 0$ and $\Delta b = 0$ and then the equations would each have only one unknown. Our experience has been that it is more expedient to use method (2), without sacrificing accuracy, than to measure the original values. Therefore the second procedure has been used, and we will focus our attention on examining the effect of the error involved in ascertaining that Δa and Δb are indeed zero.

The three conditions that the final X-meter will satisfy are:

$$\left.\begin{array}{ll} (1) & \Delta a = 0 \\ (2) & \Delta b = 0 \\ (3) & M_1 = M_2 \end{array}\right\} \tag{27}$$

where M_1 is the time constant of wire no. 1.

In order to satisfy condition (3) we will overheat the wires equally, i.e. $a'_{w_1} = a'_{w_2}$. The overheat condition does not have to be satisfied as exactly as conditions (1) and (2). We have three adjustable quantities available to fulfill these requirements:

(1) the probe orientation, φ,
(2) a voltage divider across the out put from one wire
(3) the current into each wire (by a resistance in series with one hot wire if it is in a bridge.)

Arbitrarily we will place the voltage divider across hot wire no. 2 so that its measured voltage is $k e_2$. Henceforth the notation will be changed so that $\Delta a = ka - a$ and $\Delta b = kb - b$.

We will now estimate the effect of an angle change on the a's and b's. The assumption will be made that if a stream approaches a wire obliquely it is the component normal to the wire that does the cooling. This is not accurately borne out by experiment, but it is close enough for a good estimate. We will not use it to evaluate the coefficients, but only to estimate the order of their change. King's equation for this inclined wire, figure 40, becomes

$$\frac{I_i^2 R_i}{R_i - R_{e_i}} = A_i + B_i \sqrt{\cos \varphi_i}\, y \qquad i = 1, 2 \tag{28}$$

$$= (y_{o_i} + \Theta_i y)\, B_i$$

where $y \equiv \sqrt{U}$, $\Theta_i \equiv \sqrt{\cos \varphi_i}$, $y_{o_i} \equiv \frac{A_i}{B_i}$, and the second-order resistance coefficient β is neglected so A_i and B_i include only the first-order resistance coefficient α (in contrast to Appendix III). (Note: the subscript i will be suppressed through the remainder of this paragraph) After several algebraic steps equation (28) becomes

$$E = \frac{(y_o + \Theta y)\, B R_e I}{(y_o + \Theta y) B - I^2}$$

where E is the voltage across the wire. Define

$$a'_w \equiv \frac{R - R_e}{R_e} \qquad z \equiv \frac{y}{y_o + y} \qquad \psi \equiv \frac{y_o + y}{y_o + \Theta y}$$

Then the coefficients a and b (for the single wire) are for constant current operation

$$a \equiv \left(\frac{\partial \epsilon}{\partial U}\right)_I = \frac{1}{2y}\left(\frac{\partial \epsilon}{\partial y}\right)_I = -\frac{a'_w z}{2}\,\frac{\epsilon}{U}\,\psi\,\Theta$$

$$b \equiv \left(\frac{\partial \epsilon}{\partial V}\right)_I = \left(\frac{\partial \epsilon}{\partial \varphi}\right)_I \frac{d\varphi}{V} = -\frac{a'_w z}{2}\,\frac{\epsilon}{U}\,\psi\,\frac{\sin\varphi}{\Theta} \qquad (29)$$

The probe is rotated by $\Delta\gamma$ to a new position. At the new position a'_w is made the same by changing the current (although, of course, once in the new position the X-meter operates at constant current). Express E as

$$E = R\sqrt{\frac{a'_w}{1+a'_w}\,(y_0 + \Theta y)\,B}$$

The indicated steps give

$$\left(\frac{\partial a}{\partial \gamma}\right)_{a'_w} = -\frac{d\varphi}{d\gamma}\left[\tan\varphi - \frac{z\psi\,\sin\varphi}{2\Theta}\right]\frac{a}{2}$$

$$\left(\frac{\partial b}{\partial \gamma}\right)_{a'_w} = \frac{d\varphi}{d\gamma}\left[\tan\varphi + \frac{z\psi\,\sin\varphi}{2\Theta} + \frac{2}{\tan\varphi}\right]\frac{b}{2} \qquad (30)$$

and at φ = 45 degrees and $\psi \approx 1$

$$\left(\frac{\partial a}{\partial \gamma}\right)_{a'_w} \approx -\frac{d\varphi}{d\gamma}\left(2 - \frac{z}{\Theta}\right)\frac{a}{4}$$

$$\left(\frac{\partial b}{\partial \gamma}\right)_{a'_w} \approx \frac{d\varphi}{d\gamma}\left(6 + \frac{z}{\Theta}\right)\frac{b}{4} \qquad (30')$$

Note that $0 < z < 1$ and $\frac{d\varphi}{d\gamma} = \pm 1$ so

$$\left| \frac{1}{a}\left(\frac{da}{d\gamma}\right)_{a_{sw}} \right| \approx \frac{1}{2}, \quad \text{if} \quad z = 0$$

$$\approx \frac{1}{4}, \quad \text{if} \quad z = 1$$

$$\left| \frac{1}{b}\left(\frac{db}{d\gamma}\right)_{a_{sw}} \right| \approx \frac{3}{2}, \quad \text{if} \quad z = 0$$

$$\approx \frac{7}{4}, \quad \text{if} \quad z = 1$$

At the wall where $U \to 0$, $\bar{z} \to 0$; as $U \to \infty$, $\bar{z} \to 1$. Roughly b is 3 to 7 times as sensitive to the probe orientation as a. At 45°, equations (29) give a = b.

We now have sufficient equations to evaluate the effect of an angle change of the probe on the turbulence measurement. For simplicity the two wires will be oriented at $\varphi_1 = \varphi_2 = 45$ degrees and $\gamma = 0$ degrees. (However, the equations are general and the extension is obvious.) The angle change, $\Delta\gamma$, affects the turbulence terms through Δa and Δb in equations (24), (25), and (26). From equations (30′)

$$\left[\frac{d(\Delta a)}{d\gamma}\right]_{a_{sw}} \approx \frac{d\varphi_1}{d\gamma}(2 - z_1)\frac{a_1}{4} - \frac{d\varphi_2}{d\gamma}(2 - z_2)\frac{a_2}{4}$$

$$\left[\frac{d(\Delta b)}{d\gamma}\right]_{a_{sw}} \approx \frac{d\varphi_2}{d\gamma}(6 + z_2)\frac{b_2}{4} - \frac{d\varphi_1}{d\gamma}(6 + z_1)\frac{b_1}{4}$$

and within this approximation

$$\left[\frac{d}{d\gamma}\left(\frac{\Delta a}{b}\right)\right]_{a_{sw}} \approx \frac{2 - z}{2} \to 1 \quad \text{near wall}$$

$$\left[\frac{d}{d\gamma}\left(\frac{\Delta b}{a}\right)\right]_{a_{sw}} \approx -\frac{6 + z}{2} \to -3 \quad \text{near wall}$$

since $\frac{d\varphi_1}{d\gamma} = 1$ and $\frac{d\varphi_2}{d\gamma} = -1$, figure 40. Therefore near the wall a 1 degree error in γ corresponds to a 1.7 percent error in $\frac{\Delta a}{\bar{u}}$ and a 5 percent error in $\frac{\Delta b}{\bar{u}}$. In this region the effect on $\overline{u^2}$ is small since $\frac{\overline{uv}}{\overline{u^2}} \ll 1$; on $\overline{v^2}$ also small as $\frac{\overline{uv}}{\overline{v^2}} \approx 1$; but $\frac{\overline{u^2}}{\overline{uv}} > 20$ near the laminar sublayer (figure 30 and reference 6) so a one degree error would give an error in $\overline{uv}$ of 15 percent. At $y_* = 100$, $\frac{\overline{u^2}}{\overline{uv}} \doteq 6$ and $\frac{\overline{v^2}}{\overline{uv}} \doteq 1.5$, the error in $\overline{uv}$ for a one degree error would be approximately 2 percent.

A method of adjusting the probe to satisfy equations (27) and measure a and b will now be presented. Two general methods (of unequal accuracy) are obviously available

(1) "Cosine-law" method, for approximate measurements: each wire is calibrated separately normal to the air stream in the usual constant-resistance way. Then, by finding the $\varphi_{1,2} = 0$ positions and using equation (28) the terms in equations (29) are computed, giving $a_{1,2}$ and $b_{1,2}$ and thus determining the position which satisfies equations (27). In addition to inaccuracy of the "Cosine law", equation(28), a weakness of this method arises in the error of determining the $\varphi_{1,2} = 0$ position for each wire. (The effect of wire differences has been analyzed by reference 3 where the wire sensitivities are determined by the "Cosine-law" method.)

(2) "Black-box" technique for more accurate measurements: Pragmatically consider the X-meter as an electrical device which simply responds to U and V in some unknown way. (u, v, and e are increments). Keeping only the first-order terms in a Taylor series expansion, we obtain equation (23), as before. But this time we will find the sensitivity coefficients empirically, by installing the X-meter in a stream where u and v are varied independently. During the calibration we measure only $e_1 + e_2$ and $e_2 - e_1$.

To first satisfy equations (27) the following procedure is employed. Place the probe in a calibration duct at roughly the "neutral angle" (where $\Delta a = \Delta b = 0$) with the correct a'_{uv}. Note that

$$\Delta a = \frac{d(e_2 - e_1)}{d u}$$

$$\Delta b = -\frac{d(e_1 + e_2)}{d v}$$

$$\doteq -\frac{1}{U}\frac{d(e_1+e_2)}{d\gamma} \qquad \text{if } \gamma \ll 1$$

The obvious procedure is to keep the probe fixed and vary the air speed (at "constant current" *), then to fix the air speed and rotate the probe. (Actually it will be apparent that the process is hastened by measuring Δb first.) Typical curves are shown in figure 41.

To satisfy equations (27) we can change γ, and utilize the voltage divider measuring ke_2 (or ke_1) where the first measurement was then at $k = 1$. The value of a'_{air} is the same. Indicate the second measurements by a prime ('). Using a Taylor series expansion to first order terms only

$$\Delta a' \equiv k'a_2' - a_1' = ka_2 + k\left(\frac{\partial a_2}{\partial \gamma}\right)_{a_{air}'}(\gamma'-\gamma) + a_2(k'-k)$$

$$- a_1 - \left(\frac{\partial a_1}{\partial \gamma}\right)_{a_{air}'}(\gamma'-\gamma)$$

$$\Delta b' \equiv k'b_2' - b_1' = kb_2 + k\left(\frac{\partial b_2}{\partial \gamma}\right)_{a_{air}'}(\gamma'-\gamma) + b_2(k'-k)$$

$$- b_1 - \left(\frac{\partial b_1}{\partial \gamma}\right)_{a_{air}'}(\gamma'-\gamma)$$

This is solved for $\Delta\gamma$ and Δk with $\Delta a' = \Delta b' = 0$.

$$0 = (ka_2 - a_1) + \left[k\left(\frac{\partial a_2}{\partial \gamma}\right)_{a_{air}'} - \left(\frac{\partial a_1}{\partial \gamma}\right)_{a_{air}'}\right]\Delta\gamma + ka_2\frac{\Delta k}{k}$$

$$0 = (kb_2 - b_1) + \left[k\left(\frac{\partial b_2}{\partial \gamma}\right)_{a_{air}'} - \left(\frac{\partial b_1}{\partial \gamma}\right)_{a_{air}'}\right]\Delta\gamma + kb_2\frac{\Delta k}{k}$$

---

* Simulating operation, i.e. without adjusting electronic equipment.

The coefficients of the second terms on the right hand side are evaluated by equations (30). Generally the approximate values of equations (30′) will suffice. Equations (30) give for the X-meter of figure 40

$$0 = (k e_2 - e_1) + (k a_2 + a_1)\left(\frac{2-z}{4}\right)\Delta\gamma + k a_2 \frac{\Delta k}{k}$$

$$0 = (k b_2 - b_1) - (k b_2 + b_1)\left(\frac{6+z}{4}\right)\Delta\gamma + k b_2 \frac{\Delta k}{k}$$

The new values, $(k\,a_2 - a_1)'$ and $(k\,b_2 - b_1)'$, should be measured by repeating the foregoing procedure, to verify that equations (27) are indeed satisfied, and the process could be repeated again although generally it was not found necessary.

The next step in method (2) is to measure a and b. The method is obvious following the procedure for Δa and Δb since

$$a = \frac{1}{2}\frac{d}{du}(k e_2 + e_1)$$

$$b = -\frac{1}{2}\frac{d}{dv}(k e_2 - e_1)$$

The accuracy in determining a and b is very good, and there can be little doubt as to the correctness since the probe is calibrated in the manner in which it is used. In principle this calibration should be repeated over the range of mean velocities required. However U enters through z and ψ of equations (29). Calibrating the hot-wire at constant R and treating the two wires as one gives y_0, and thus z and ψ can be computed.

In practice it was noted that the calibration is limited in accuracy by the determination of Δb, The velocity is fixed, the probe rotated, and $e_1 + k e_2$ is measured. But since the coefficient a is relatively large, $e_1 + k e_2$ is sensitive to small variations in the air speed of the calibration stream. This is not a

weakness singular to method (2) but also occurs in method (1) in the determination of $\varphi = 0$ and A and B in King's equation. This kind of difficulty is less troublesome in the measurement of Δa since the direction of the calibration stream is generally more constant. The difficulty in determining Δb is indicated in figure 41. The spread of the points indicates perhaps an uncertainty in determining the "neutral position" of about $\pm$ 1-2 degrees.

Once a value of φ had been selected the X-meter was oriented in the wind tunnel by measuring $k e_2 - e_1$, see figure 41, and rotating the probe to the appropriate value. This could be achieved within $\pm$ 1/2 degree. Therefore it is evident that the problem in the present case was not resetting the probe to the same angle, but finding out what angle is the correct one for satisfying equation (27).

Incidently, in a boundary-layer type flow, if the probe is simply translated "laterally" a realignment may be necessary near the surface since the streamlines are not paralliel.

APPENDIX V

EQUATIONS OF MOTION IN CYLINDRICAL-POLAR COORDINATES FOR FLOW IN A TWO-DIMENSIONAL CONVERGING OR DIVERGING CHANNEL

Introduction

For the steady-state two-dimensional laminar flow between converging or diverging plane walls a general solution has been obtained by Rosenhead * by applying the restriction of radial flow. Rosenhead discussed in detail the effect of the Reynolds number and the angle between the walls for both the inflow and outflow cases.

In view of the success achieved for the laminar case an analysis was undertaken at the outset of the present turbulent flow investigation to learn whether the restriction of radial flow applied to the mean motion might yield additional information, perhaps permitting one integration of the resulting ordinary differential equation. Since purely radial mean flow is presumably possible only with full dynamical similarity, it is implied that all appropriately dimensionless statistical properties of the turbulence must also be functions of the angle only. Unfortunately the final equation contained four unknowns in the general case which could still be reduced only to two unknowns by the additional assumption of low turbulence level. In the absence of an independent relation this approach was temporarily abandoned.

The next attempt was through the integral relations. The differential equations in cylindrical-polar coordinates were integrated from the centerline to the wall along a constant radius arc similar to the Cartesian case (p. 8). The final equation was not different from the Cartesian integral equations for a small angle so this was not pursued further.

It was only near the end of the present investigation that a pragmatic advantage of cylindrical-polar coordinates in the divergent channel was realized: The Cartesian coordinates had been oriented on the centerline of the channel in order to simplify the integral equations (by incorporating symmetry). But the disadvantage was that at the wall these coordinates are not parallel to the surface, so

---

* Rosenhead, L.: The Steady Two-dimensional Radial Flow of Viscous Fluid Between Two Inclined Plane Walls. Proc. Royal Soc., Ser. A, v. 175, 1940, p. 436-67.

comparison to the pipe, channel, and boundary layer data could not be made in this region: in particular $\overline{uv}$ is quite sensitive to a rotation of the coordinates (p.29), as are also two of the production of turbulent energy terms (footnote, p. 7, and p. 29). Cylindrical-polar coordinates eliminate this problem since they are aligned with both the centerline as well as the wall. There was insufficient time available when this was discovered to rework the whole paper. Therefore the differential equations in cylindrical-polar coordinates are presented in this appendix. In addition the ordinary differential equation for radial flow described above will be deduced.

Equations of Motion in Cylindrical-Polar Coordinates

Consider the cylindrical-polar coordinates r, ω, and z where $\omega = 0$ is the centerline between the walls and $r = 0$ is at their intersection; U, V, and W are the instantaneous velocities in the respective directions. Again the time (or ensemble) average will be indicated by a bar, etc., so

$$U(r, \omega, z, t) = \bar{U}(r, \omega, z) + u(r, \omega, z, t)$$

etc.

$$P(r, \omega, z, t) = \bar{P}(r, \omega, z) + p(r, \omega, z, t)$$

The Reynolds equations and turbulent kinetic-energy equations in cylindrical-polar coordinates have been written out independently by Wislicenus and Yeh (ref. 34) so they will be presented here merely in their final form.

The continuity equation (31), Reynolds equations (32), (33), and (34) and turbulent kinetic-energy equation (35) are

$$\frac{1}{r}\frac{\partial}{\partial r}(r\bar{U}) + \frac{1}{r}\frac{\partial \bar{V}}{\partial \omega} + \frac{\partial \bar{W}}{\partial z} = 0 \qquad (31)$$

$$\bar{U}\frac{\partial \bar{U}}{\partial r} + \frac{\bar{V}}{r}\frac{\partial \bar{U}}{\partial \omega} + \bar{W}\frac{\partial \bar{U}}{\partial z} - \frac{\bar{V}^2}{r} = -\frac{1}{\rho}\frac{\partial \bar{P}}{\partial r} + \nu\left\{\nabla^2\bar{U} - \frac{\bar{U}}{r^2} - \frac{2}{r^2}\frac{\partial \bar{V}}{\partial \omega}\right\}$$

$$-\frac{\partial \overline{u^2}}{\partial r} - \frac{1}{r}\frac{\partial \overline{uv}}{\partial \omega} - \frac{\partial \overline{uw}}{\partial z} - \frac{\overline{u^2}}{r} + \frac{\overline{v^2}}{r} \qquad (32)$$

$$\bar{U}\frac{\partial \bar{V}}{\partial r} + \frac{\bar{V}}{r}\frac{\partial \bar{V}}{\partial \omega} + \bar{W}\frac{\partial \bar{V}}{\partial z} + \frac{\bar{U}\bar{V}}{r} = -\frac{1}{\rho r}\frac{\partial \bar{P}}{\partial \omega} + \nu\left\{\nabla^2\bar{V} - \frac{\bar{V}}{r^2} + \frac{2}{r^2}\frac{\partial \bar{U}}{\partial \omega}\right\}$$

$$-\frac{\partial \overline{uv}}{\partial r} - \frac{1}{r}\frac{\partial \overline{v^2}}{\partial \omega} - \frac{\partial \overline{vw}}{\partial z} - \frac{2\overline{uv}}{r} \qquad (33)$$

$$\bar{U}\frac{\partial \bar{W}}{\partial r} + \frac{\bar{V}}{r}\frac{\partial \bar{W}}{\partial \omega} + \bar{W}\frac{\partial \bar{W}}{\partial z} = -\frac{1}{\rho}\frac{\partial \bar{P}}{\partial z} + \nu\nabla^2\bar{W}$$

$$-\frac{\partial \overline{uw}}{\partial r} - \frac{1}{r}\frac{\partial \overline{v}\overline{w}}{\partial \omega} - \frac{\partial \overline{w^2}}{\partial z} - \frac{\overline{uw}}{r} \qquad (34)$$

$$
\begin{aligned}
&\frac{\partial^2 p}{\partial \bar{p}}\,\overline{m'\lambda'} + \frac{m'p}{\partial p}\,\frac{v'}{1}\,\overline{\lambda'^2} + \frac{v'p}{\partial p}\,\overline{\lambda' v'} + \frac{\partial^2 p}{\partial p}\,\overline{m'v'} + \frac{m'p}{\partial p}\,\overline{\lambda' v'} + \frac{v'p}{\partial p}\,\overline{v'^2}\Big\}\omega \\
&\qquad \overline{m'\lambda'}\,\frac{\partial^2 p}{\partial \bar{p}} + \overline{\lambda'^2}\,\frac{\partial^2 p}{\partial \bar{p}} + \frac{m'p}{\partial p}\,\frac{v'}{1}\,\overline{m'\lambda'} + \frac{v'p}{\partial p}\,\overline{m'^2} \\
&\qquad \left.\overline{\lambda' v'}\,\frac{v'}{\lambda}\right\} = \\
&\left\{\bar{\rho}\,\frac{v'p}{\partial \bar{p}} + \frac{\bar{v}}{\lambda}\,\frac{m'p}{\partial p} + \frac{\partial^2 p}{\partial \bar{p}}\,\overline{m'}\right\} + \left\{\frac{v'p}{\partial \bar{p}}\,\overline{m'(e+\phi)} + \frac{v'}{1}\,\frac{m'p}{\partial p}\,\overline{\lambda'(e+\phi)}, \frac{\partial^2 p}{\partial \bar{p}}\,\overline{m'(e+\phi)}\right\} \\
&-\mu\left\{\frac{v'}{1}\,\nabla^2\bar{e} + \overline{\left(\frac{v'}{m'p}\right)^2} + \overline{\left(\frac{v'}{1}\,\frac{m'p}{\lambda' p} + \frac{v'}{m'}\right)^2} + \overline{\left(\frac{\partial^2 p}{\partial p}\right)^2} - 2\,\frac{v'p}{\lambda' p}\,\frac{v'}{\lambda}\,\overline{\lambda'^2}\right. \\
&\qquad \left. + 2\,\frac{v'p}{\partial p}\,\frac{\partial^2 p}{m'p}\,\overline{m'v'} + \frac{v'}{2}\,\frac{v'p}{\lambda' p}\,\frac{m'p}{m'p}\,\overline{\lambda' m'} + \frac{v'}{2}\,\frac{\partial^2 p}{\partial p}\,\frac{m'p}{m'p}\,\overline{\lambda' m'}\right\} \\
&+\mu\left\{2\,\overline{\left(\frac{v'p}{m'p}\right)^2} + 2\,\overline{\left(\frac{v'}{1}\,\frac{m'p}{\lambda' p} + \frac{v'}{m'}\right)^2} + 2\,\overline{\left(\frac{\partial^2 p}{\partial p}\right)^2} - 2\,\frac{v'p}{\lambda' p}\,\frac{v'}{\lambda}\,\overline{\lambda' v'}\right. \\
&\qquad \left. + 2\,\frac{\partial^2 p}{\partial p}\,\frac{m'p}{m'p}\,\overline{m'v'} + \frac{v'}{2}\,\frac{m'p}{m'p}\,\frac{v'p}{\lambda' p}\,\overline{\lambda' m'} + \frac{v'}{2}\,\frac{m'p}{\lambda' p}\,\frac{\partial^2 p}{\partial p}\,\overline{\lambda' m'}\right\} \qquad (35)
\end{aligned}
$$

where

$$\nabla^2(\ ) \equiv \frac{\partial^2(\ )}{\partial r^2} + \frac{1}{r}\,\frac{\partial(\ )}{\partial r} + \frac{1}{r^2}\,\frac{\partial^2(\ )}{\partial \omega^2} + \frac{\partial^2(\ )}{\partial z^2}$$

$$e \equiv \tfrac{1}{2}\rho\left(u^2 + v^2 + w^2\right)$$

The first three groups of terms in equation (35) were identified essentially as in reference 34: Group I represents the production of turbulent energy from the mean motion, where the last two terms are associated with the turbulent centrifugal and coriolis forces; Group II represents the convectio.. of turbulent energy by the mean flow; and Group III represents the convection of energy by the turbulent motion plus the transfer of energy by the work of fluctuating pressure gradients. The following identification is given to the remaining terms: Group IV represents the diffusion of turbulent energy by viscous forces (i.e. viscous work terms); and Group V represents the dissipation of turbulent energy to heat. Group V was identified independently following the method of Goldstein, et al.* extended to the turbulent motion.

Radial Flow

The mean flow will now be assumed to be radial, and all mean values of velocity terms will be assumed to be two-dimensional. Specifically

$$\bar{V} = \bar{W} = \frac{d\bar{\xi}}{dz} = 0 \qquad \text{where } \xi \text{ is any velocity term}$$

The continuity equation (31) reduces to

$$\frac{1}{r}\frac{d(r\bar{U})}{dr} = 0$$

So define Ω_1

$$\Omega_1(w) \equiv r\bar{U} \tag{36}$$

It is evident that

$$\frac{d^n\bar{U}}{dw^n} = \frac{\Omega_1^{(n)}(w)}{r}$$

---

* Goldstein, S., editor: Modern Developments in Fluid Dynamics, Vol. I, First Edit., 1938, p. 98.

Furthermore,

$$r^2\overline{u^2} = \Omega_1(\omega) \qquad r^2\overline{uw} = \Omega_5(\omega)$$

$$r^2\overline{v^2} = \Omega_3(\omega) \qquad r^2\overline{vw} = \Omega_6(\omega)$$

$$r^2\overline{uv} = \Omega_4(\omega)$$

These are equivalent to the assumption of longitudinal similarity for turbulent terms in the Cartesian case (p. 11), since $\frac{\overline{u^2}}{U_2^2}$, $\frac{\overline{v^2}}{U_2^2}$, etc. are functions of ω only. Equations (32), (33), and (34) reduce respectively to

$$\Omega_1^2 + \nu\Omega_1'' = \frac{r^3}{\rho}\frac{d\bar{p}}{dr} - \Omega_2 - \Omega_3 + \Omega_4' \tag{37}$$

$$\nu\Omega_1' = \frac{r^2}{\rho}\frac{d\bar{p}}{d\omega} + \Omega_3' \tag{38}$$

$$0 = \frac{r^3}{\rho}\frac{d\bar{p}}{dz} + \Omega_5 - \Omega_6' \tag{39}$$

The integration of equation (38) gives

$$\bar{p} = \frac{2\mu}{r^2}\Omega_1 + \frac{\rho\Omega_3}{r^2} + F(r) \tag{40}$$

Differentiating equation (40) with respect to z and equating with equation (39) gives

$$\frac{d\bar{p}}{dz} = 0$$

$$\Omega_5 = \Omega_6'$$

Differentiating equation (40) with respect to r we obtain

$$\frac{r^3}{\rho}\frac{d\bar{P}}{dr} = -4\nu\Omega_1 + 2\Omega_3 + \frac{r^3}{\rho}F'(r) \qquad (41)$$

Equating with equation (37) gives

$$\frac{r^3}{\rho}F'(r) = \Omega_1^2 + \nu(\Omega_1'' + 4\Omega_1) + \Omega_2 - \Omega_3 - \Omega_4' \qquad (42)$$

and since the right-hand side is a function of ω alone define

$$\frac{r^3}{\rho}F'(r) \equiv k\nu, \quad \text{a constant}$$

The constant, k, can be evaluated from the radial pressure gradient at the wall by equation (41) since

$$\Omega_1(\pm\alpha) = \Omega_3(\pm\alpha) = 0$$

where α is again the half-angle between the walls.
Therefore

$$k = \frac{r^3}{\mu}\left(\frac{d\bar{P}}{dr}\right)_{\omega = \pm\alpha}$$

Equation (42) is

$$\Omega_1'' + 4\Omega_1 + \frac{1}{\mu}\left(\Omega_1^2 + \Omega_2 - \Omega_3 - \Omega_4'\right) = h_2 \qquad (43)$$

Equation (43) is the primary differential equation for the flow field. Its counterpart in the Cartesian coordinates is equation (6), except that equation (43) applies without restriction on α or turbulence level. Unfortunately there are four unknowns. The corresponding equation for parallel-wall channel flow (equation (3a) of reference 5) can be integrated once directly.

Equation (43) reduces to two unknowns where the turbulence level is sufficiently small that

$$\frac{\Omega_2}{\Omega_1^2}, \frac{\Omega_3}{\Omega_1^2} << 1$$

in which case

$$\Omega_1'' + 4\Omega_1 + \frac{1}{\mu}\left(\Omega_1^2 - \Omega_4'\right) = h_2 \qquad (44)$$

Equation (44) is identical to the laminar case when $\Omega_4' = 0$. Since two unknowns remain in the equation an independent relation is required for its solution. This was not available so the analysis was terminated.

The turbulent energy equation (35) is not significantly simplified in radial flow. The eleven production terms reduce to three, the three convection terms to one, but only two of the remaining terms in III, IV, and V are eliminated. Therefore the turbulent energy equation will not be presented.

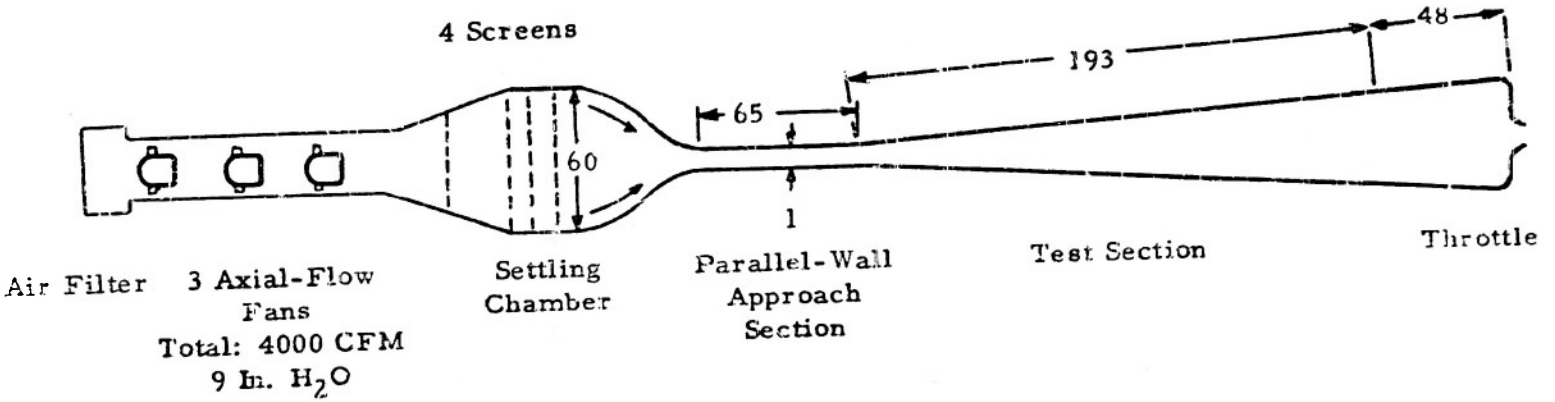

Plan View

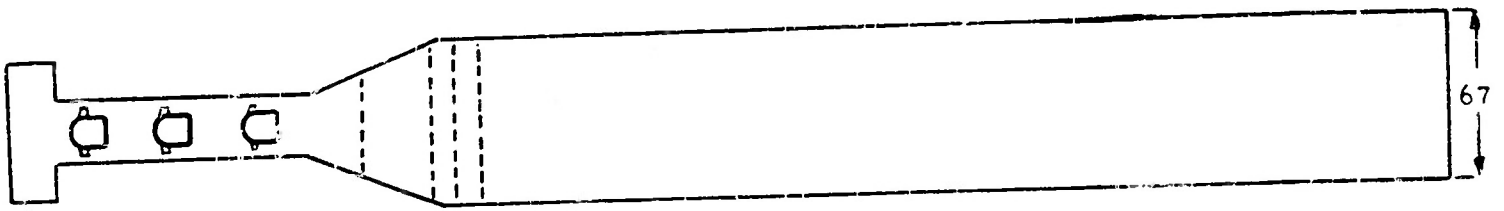

Elevation View

Figure 1. - Diagram of two-dimensional channel.

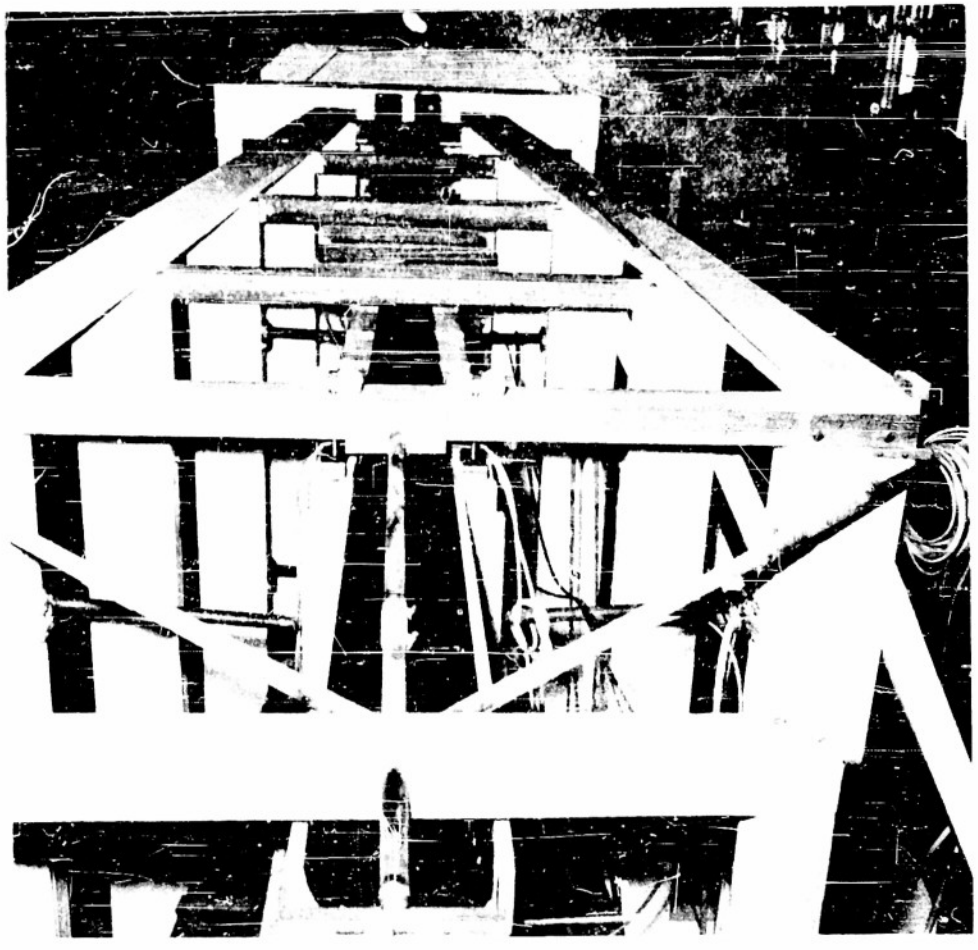

Figure 2.- Downstream portion of diffuser.

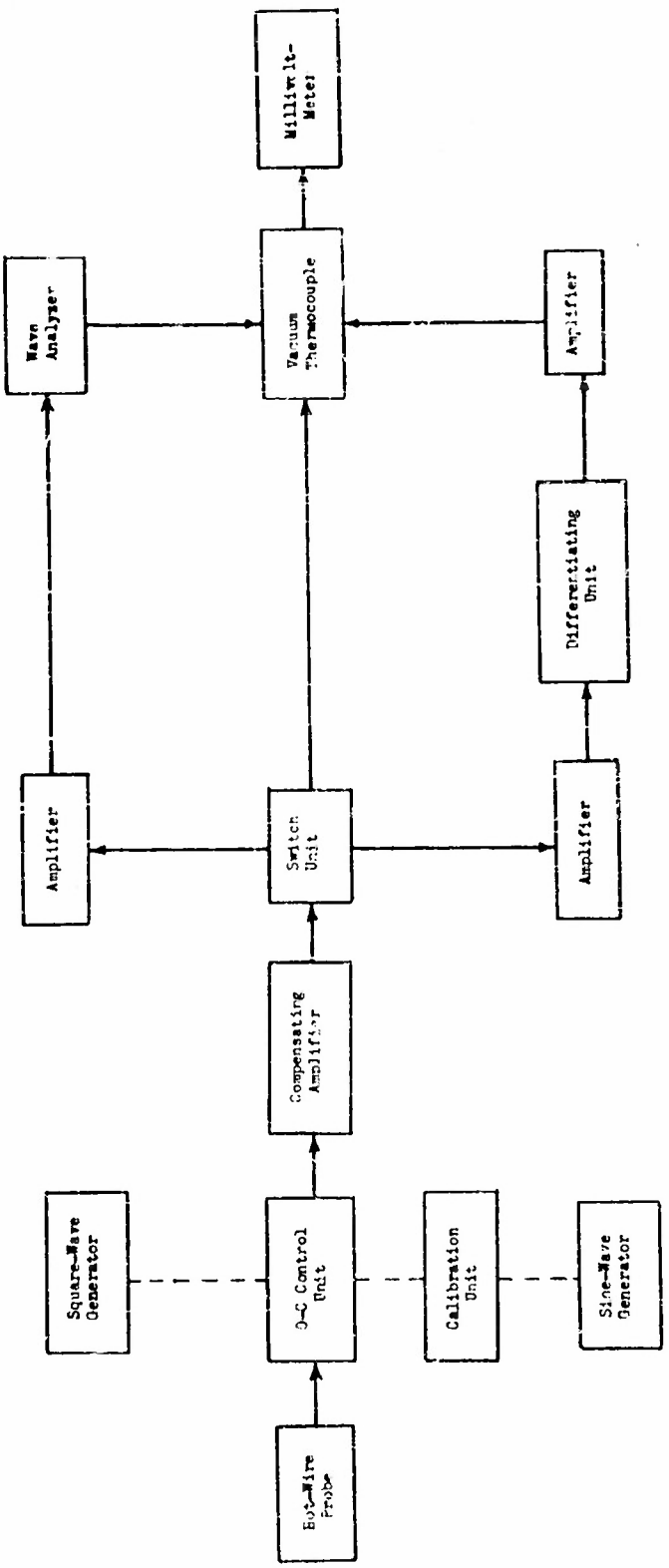

Figure 4.- Block diagram of turbulence measuring equipment.

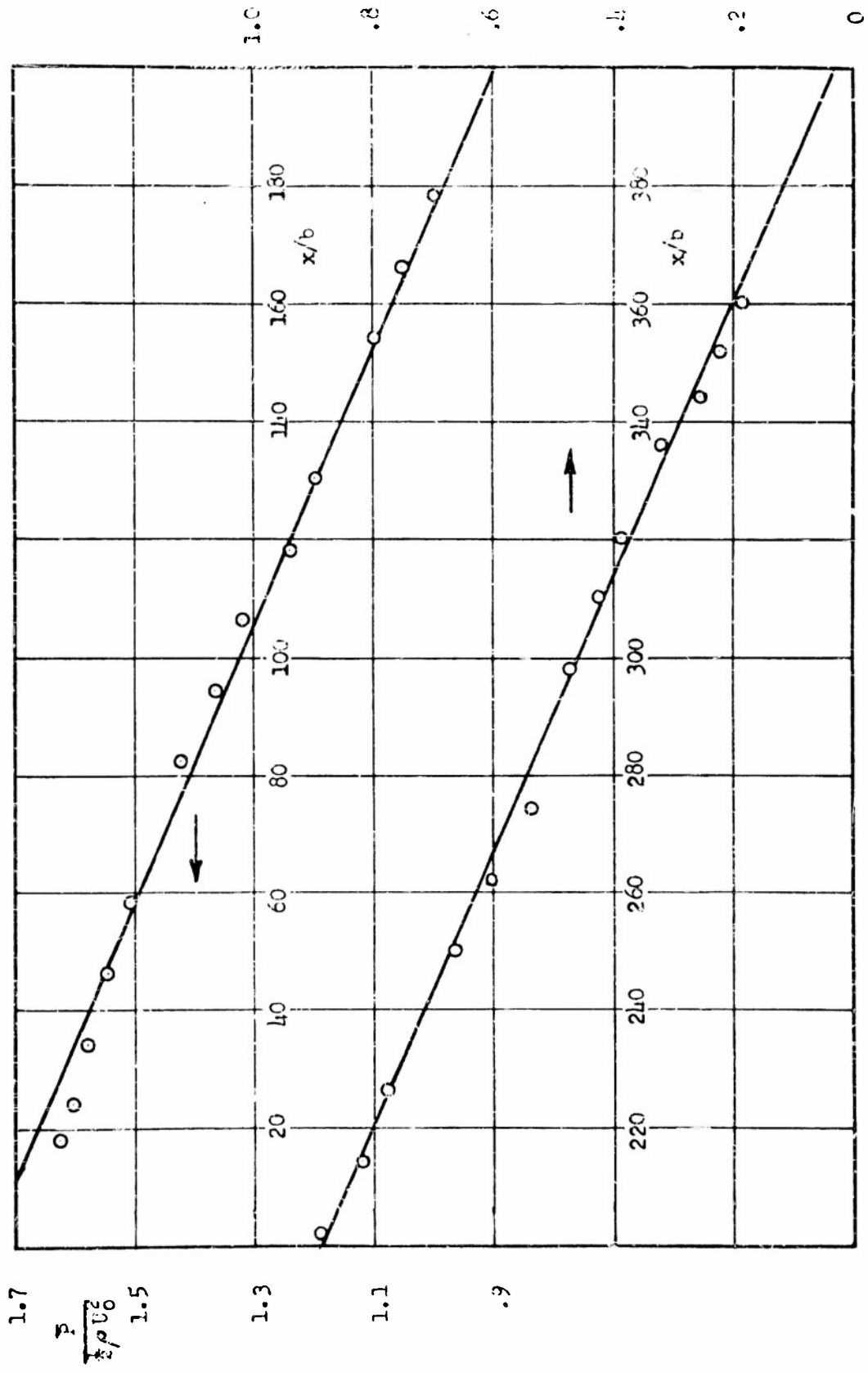

Figure 5.- Pressure distribution along diffuser wall. α = 0 deg., b = 0.5 in., R_b = 12,200.

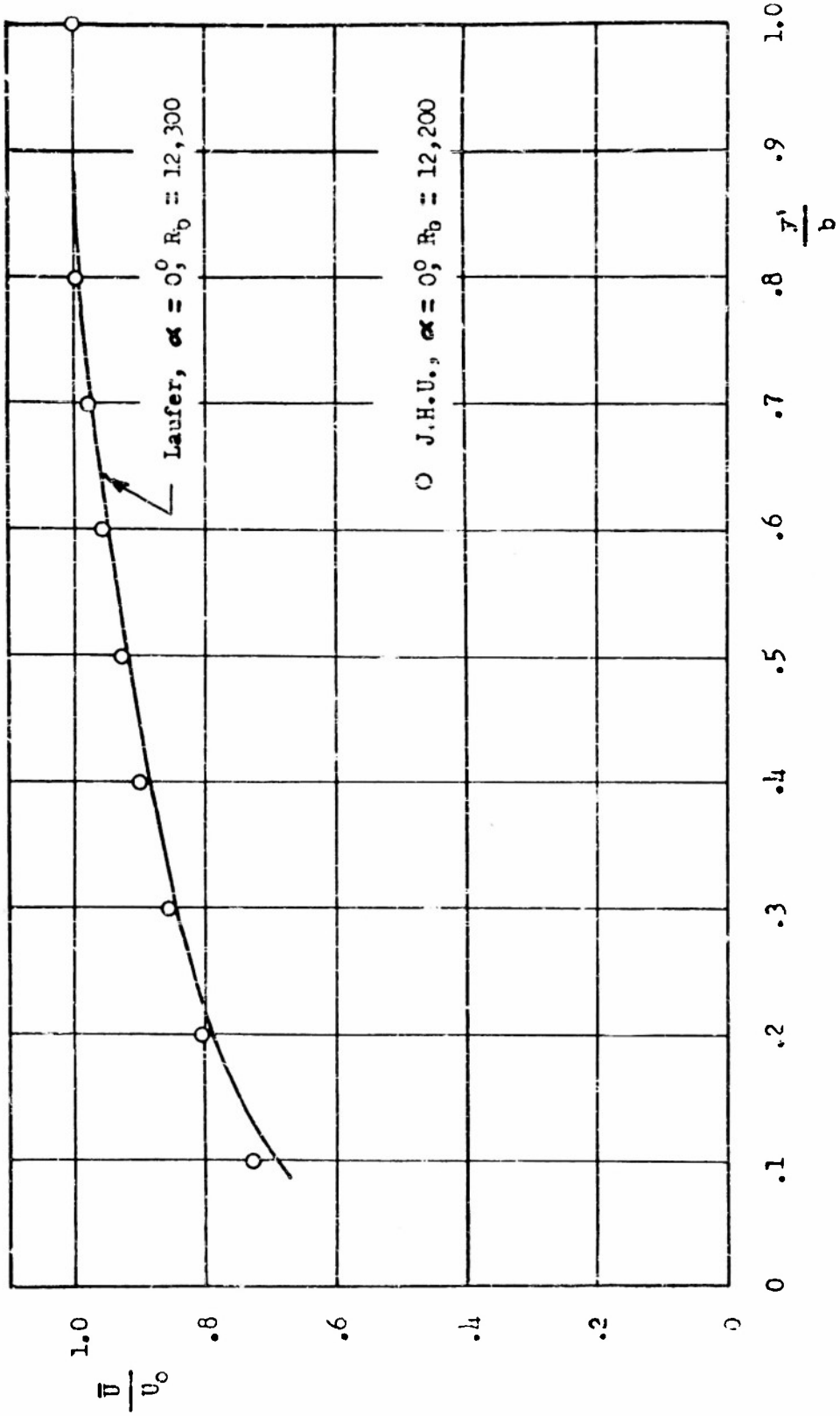

Figure 6.- Mean-velocity distribution in 1 in. channel.

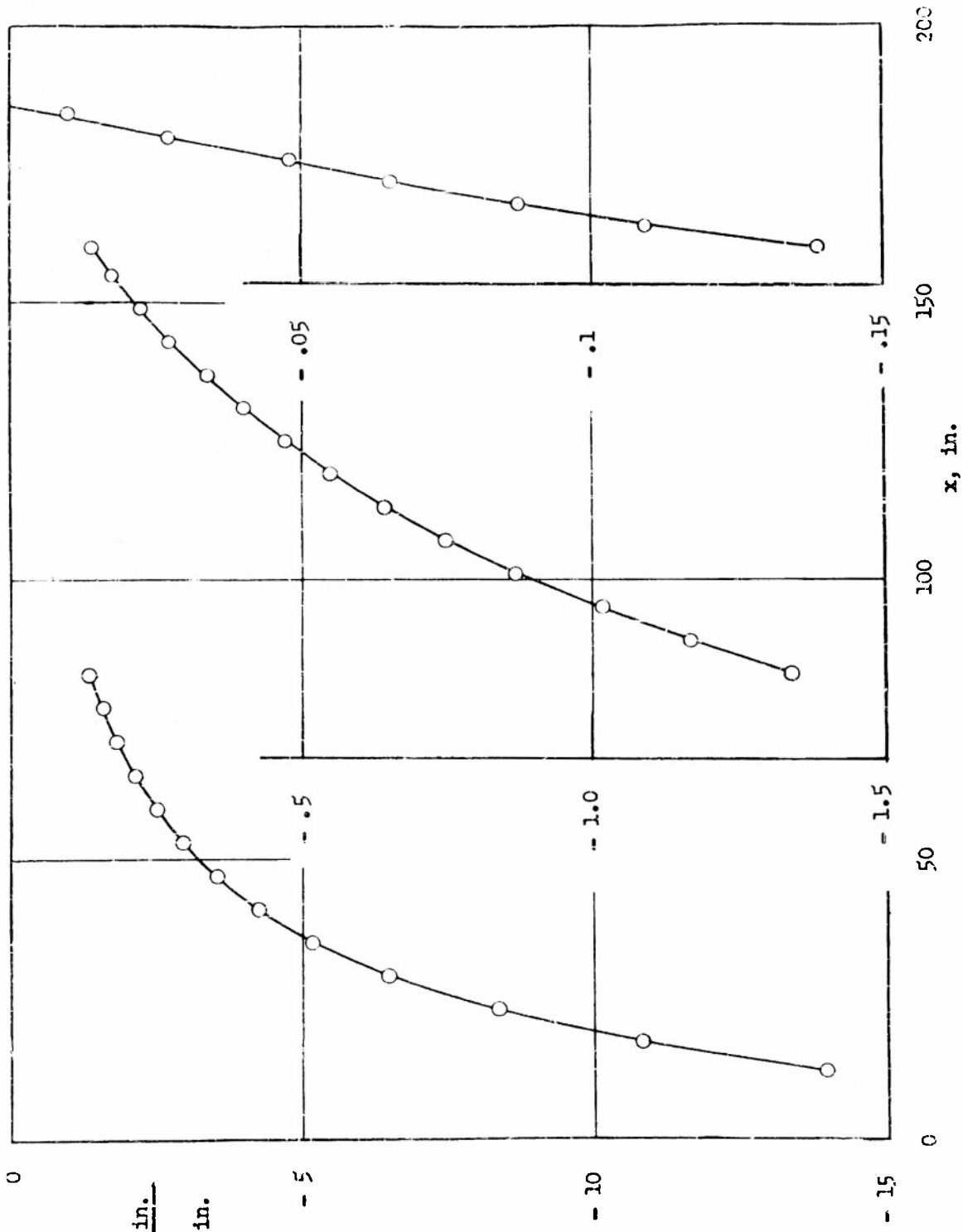

Figure 7.- Mean-pressure distribution along diffuser wall.

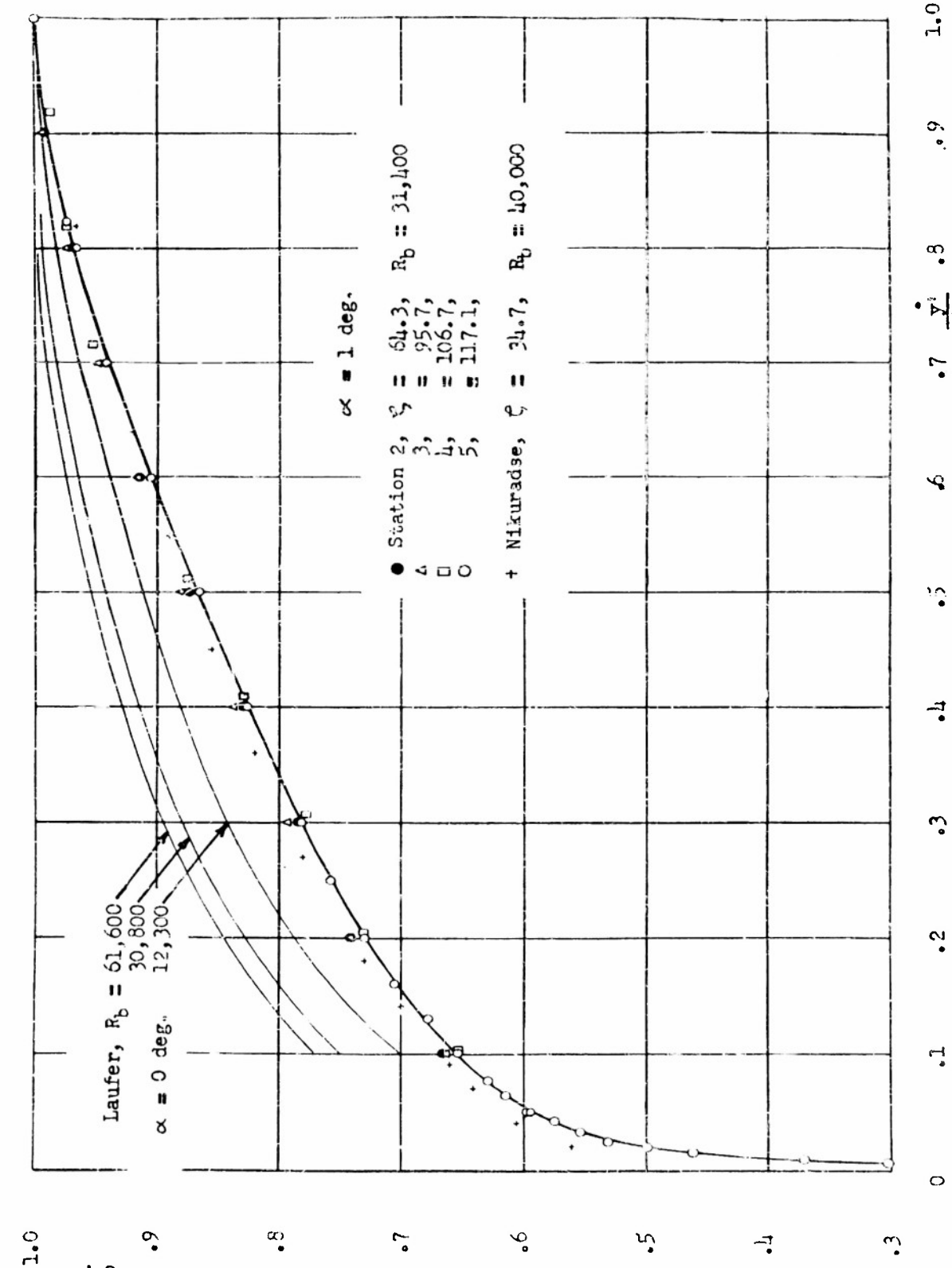

Figure 3.- Rear-velocity distribution.

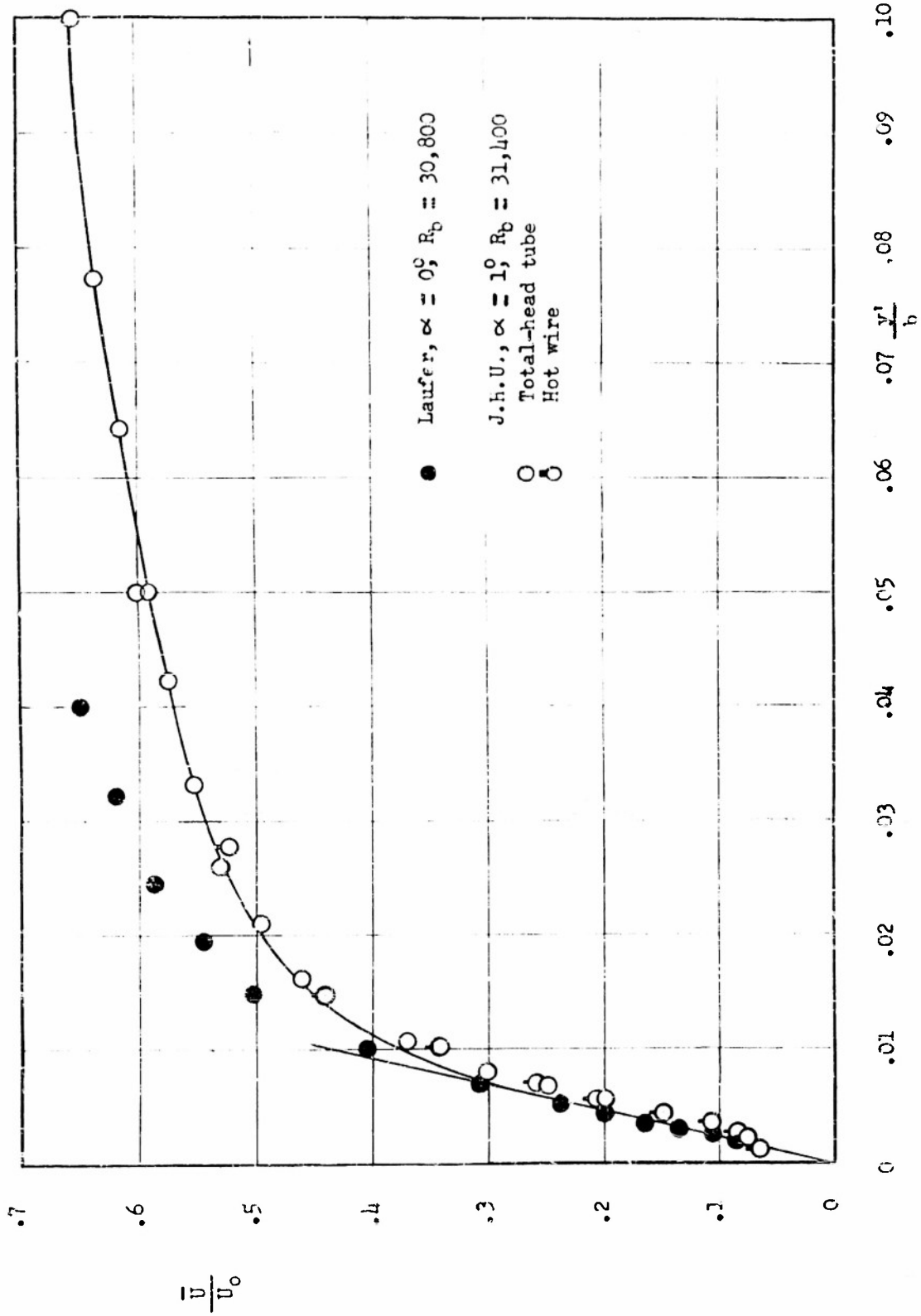

Figure 9.-- Mean-velocity distribution near wall.

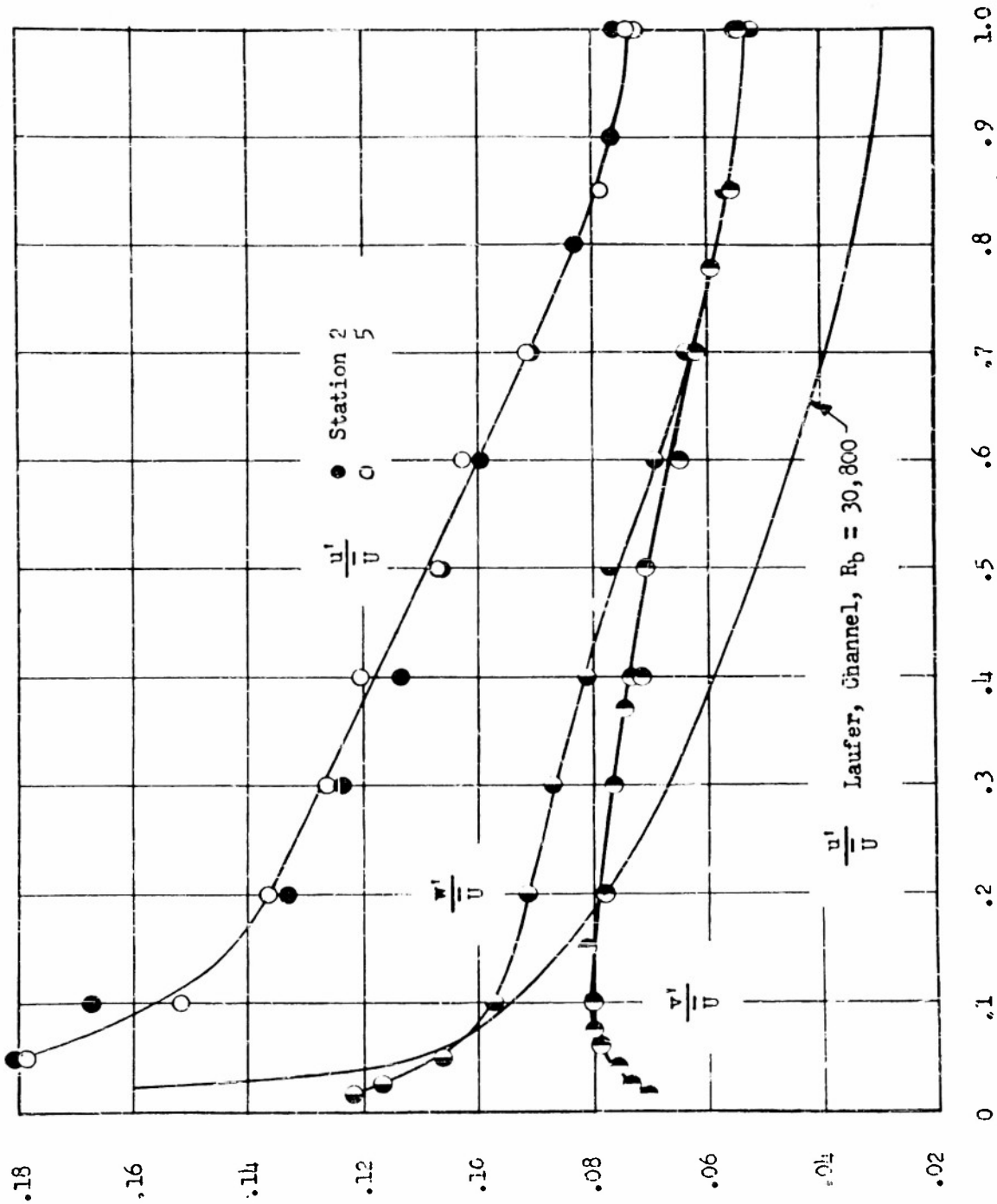

Figure 10.- Distribution of u', v', and w' relative to $\bar{U}$.

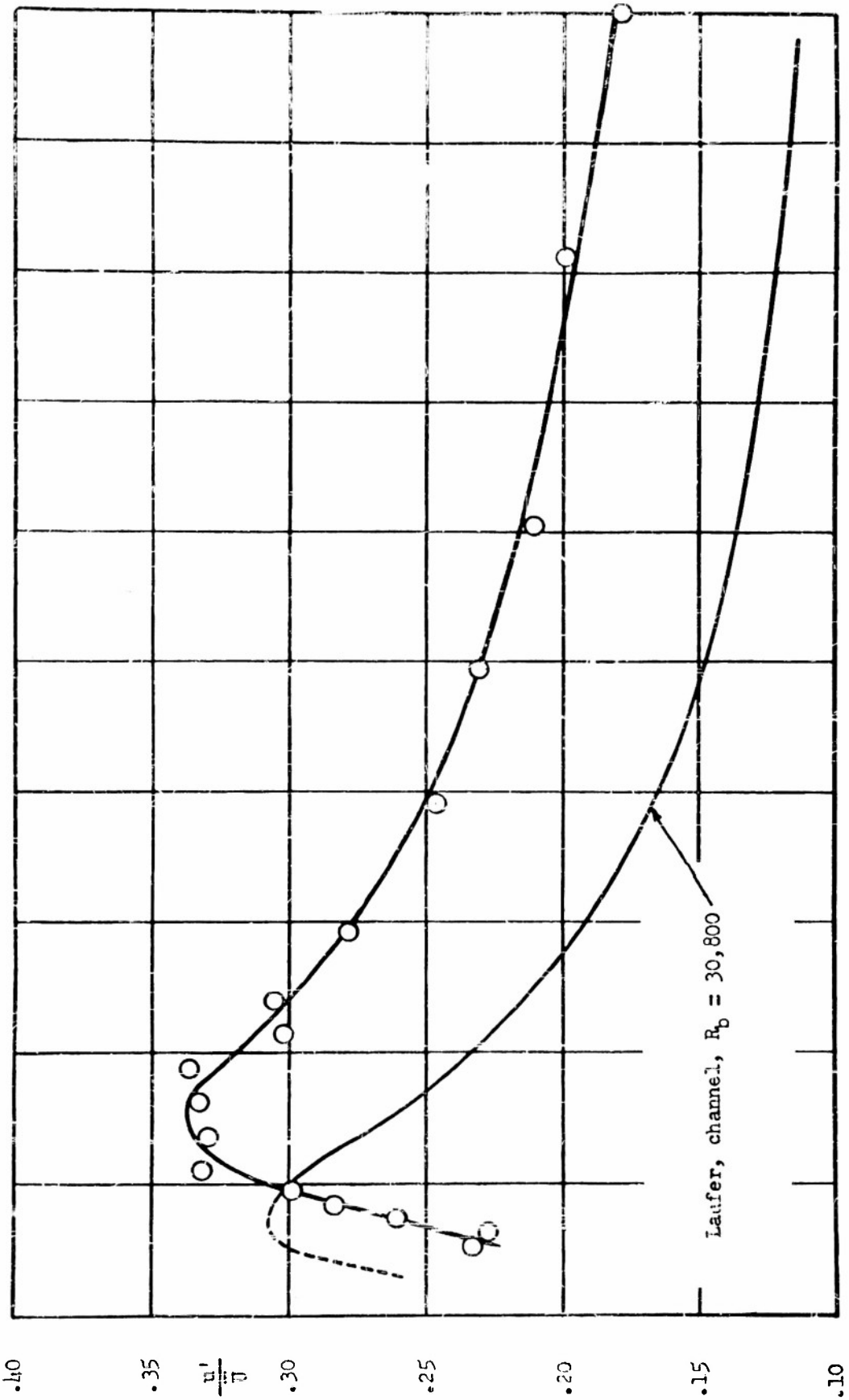

Figure 11.- Distribution of u' relative to $\bar{U}$ near wall.

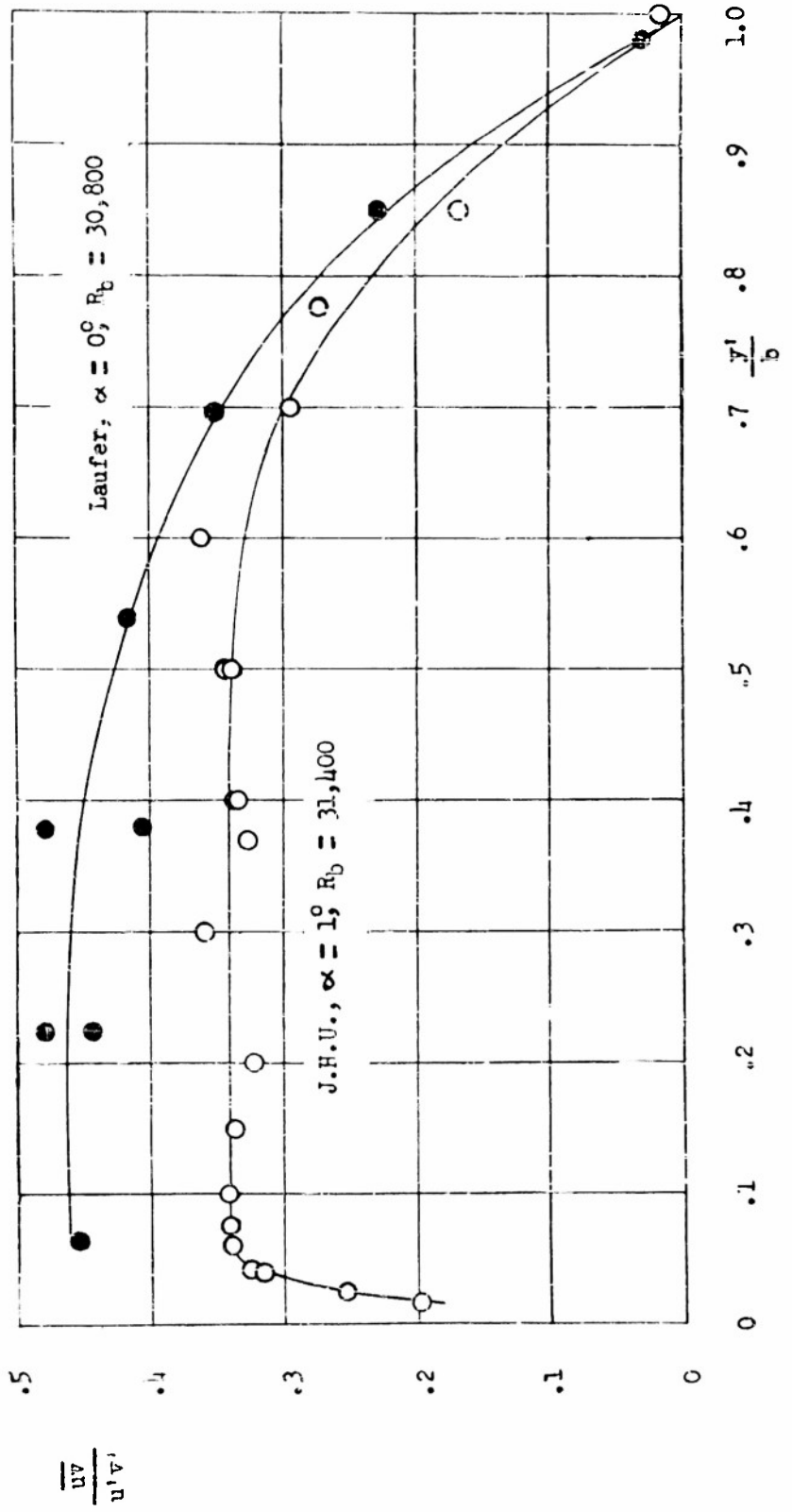

Figure 12.- Correlation-coefficient distribution.

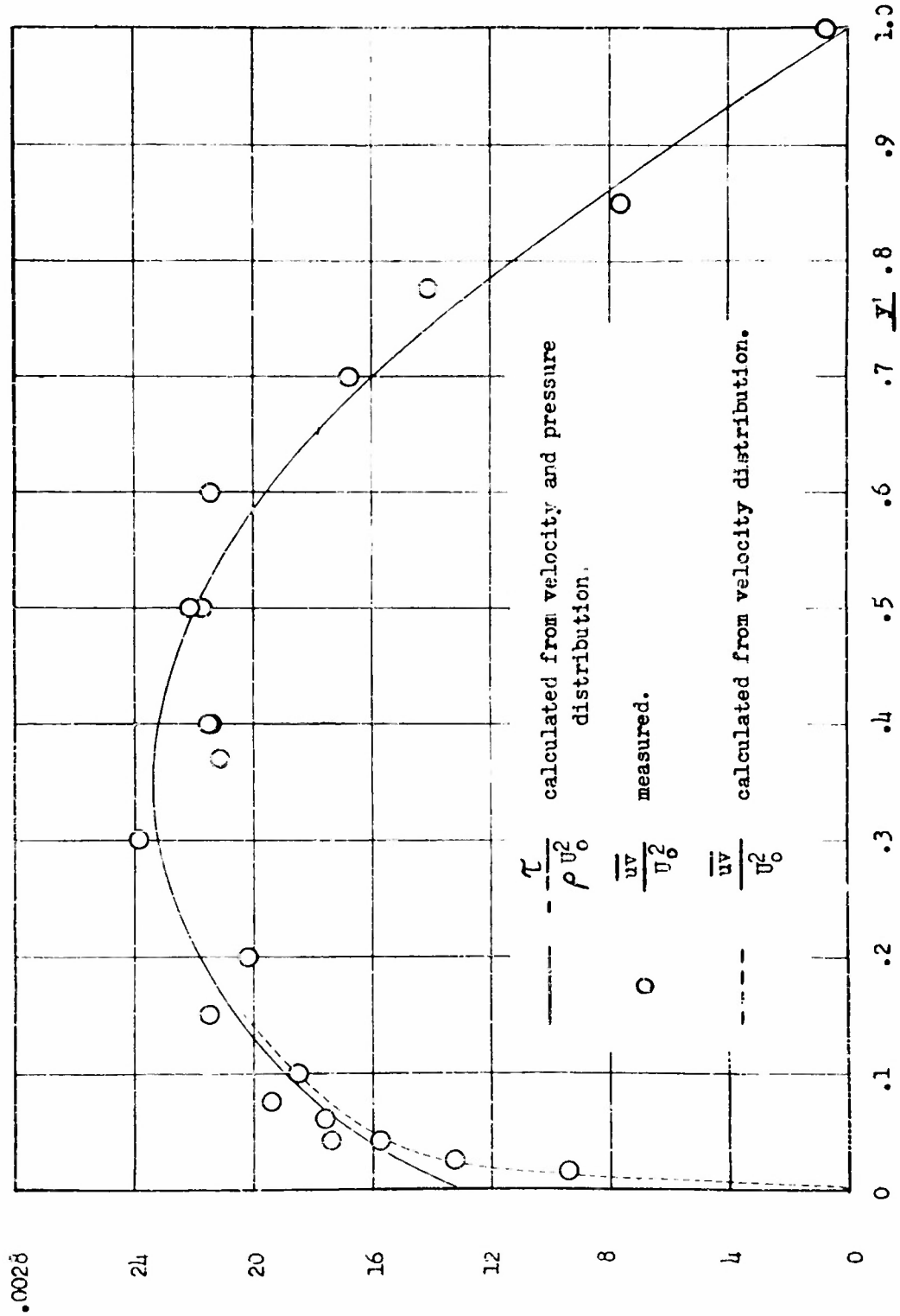

Figure 13.- Shear-stress distribution.

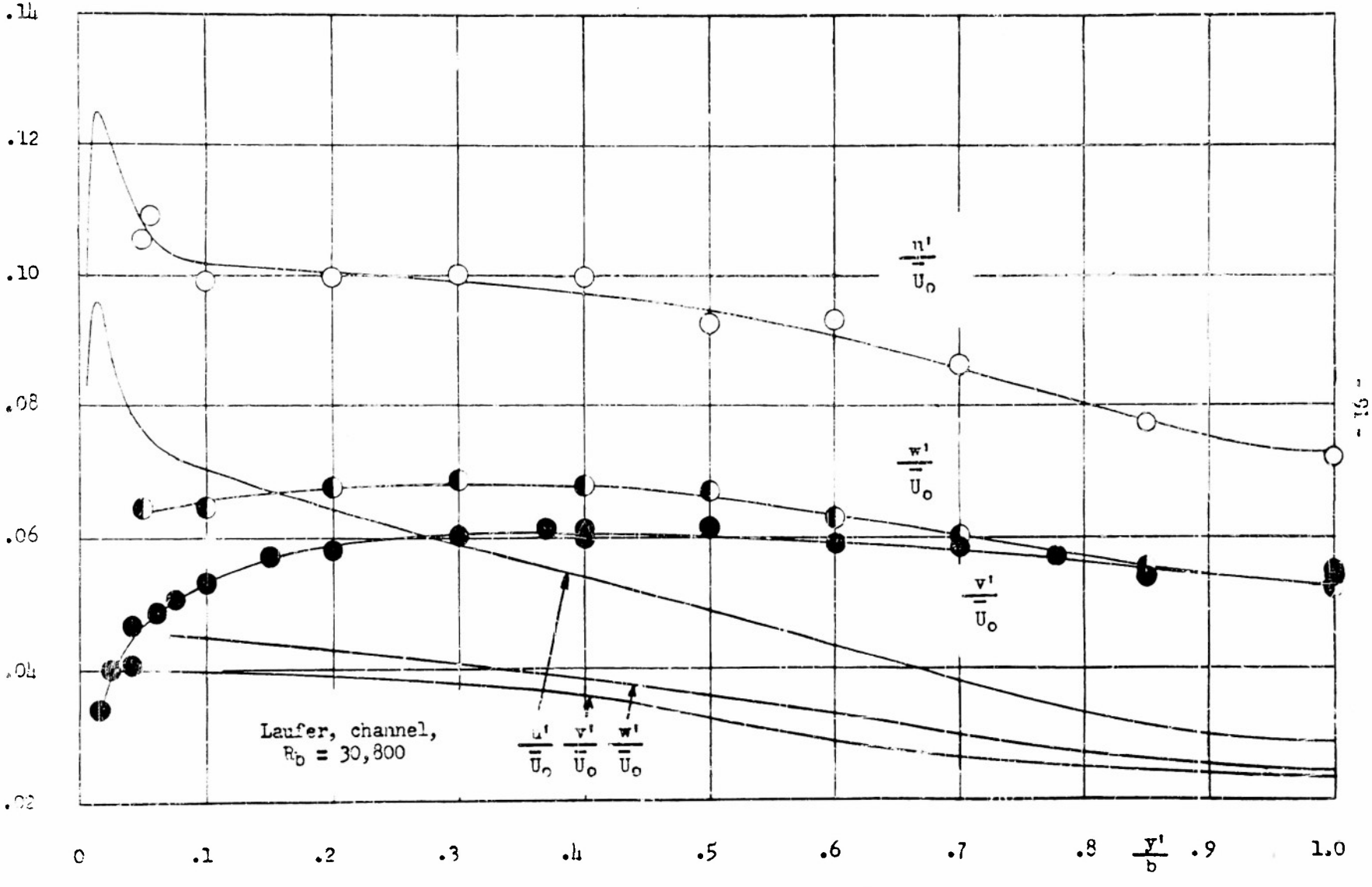

Figure 14.- Distribution of u', v', and w'.

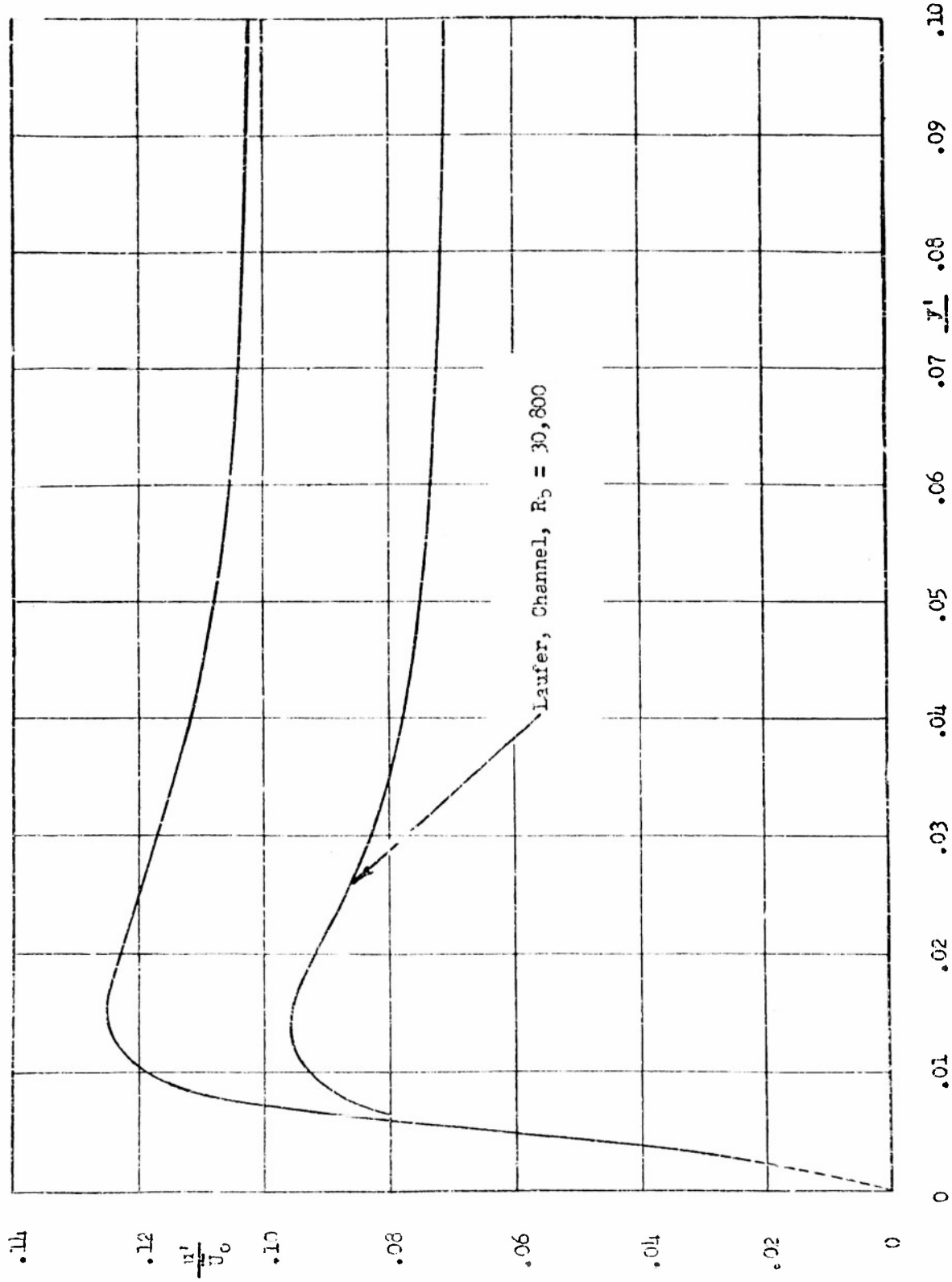

Figure 15.- Distribution of u' near wall.

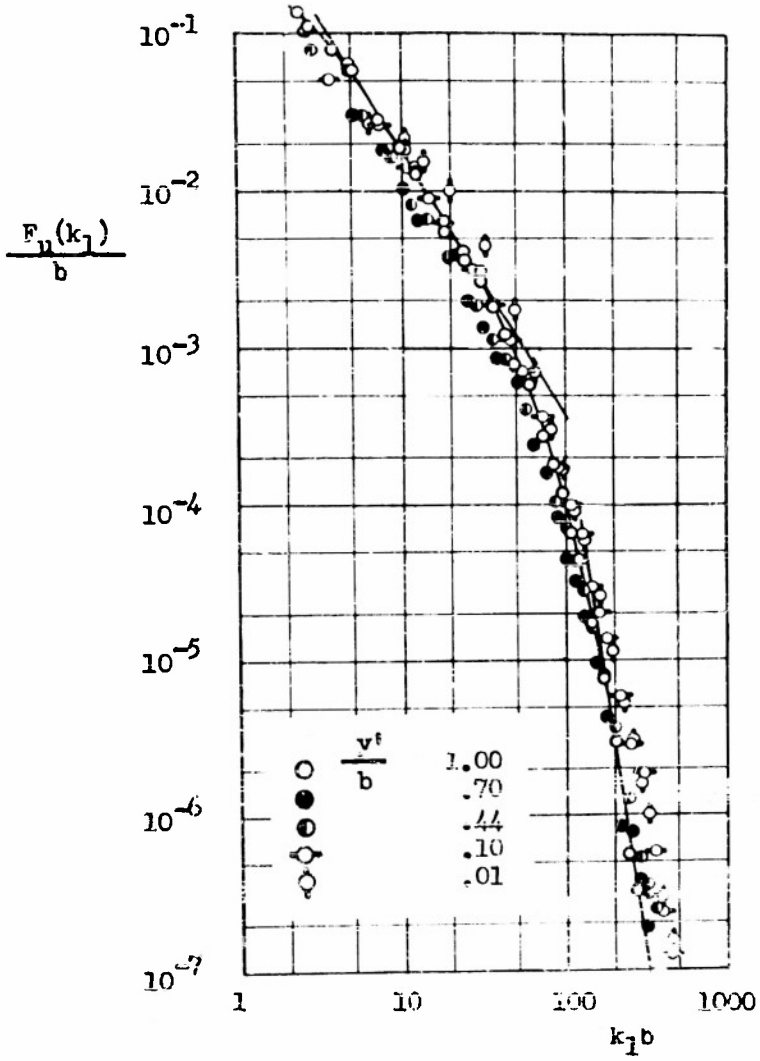

Figure 16.- u'-spectra.

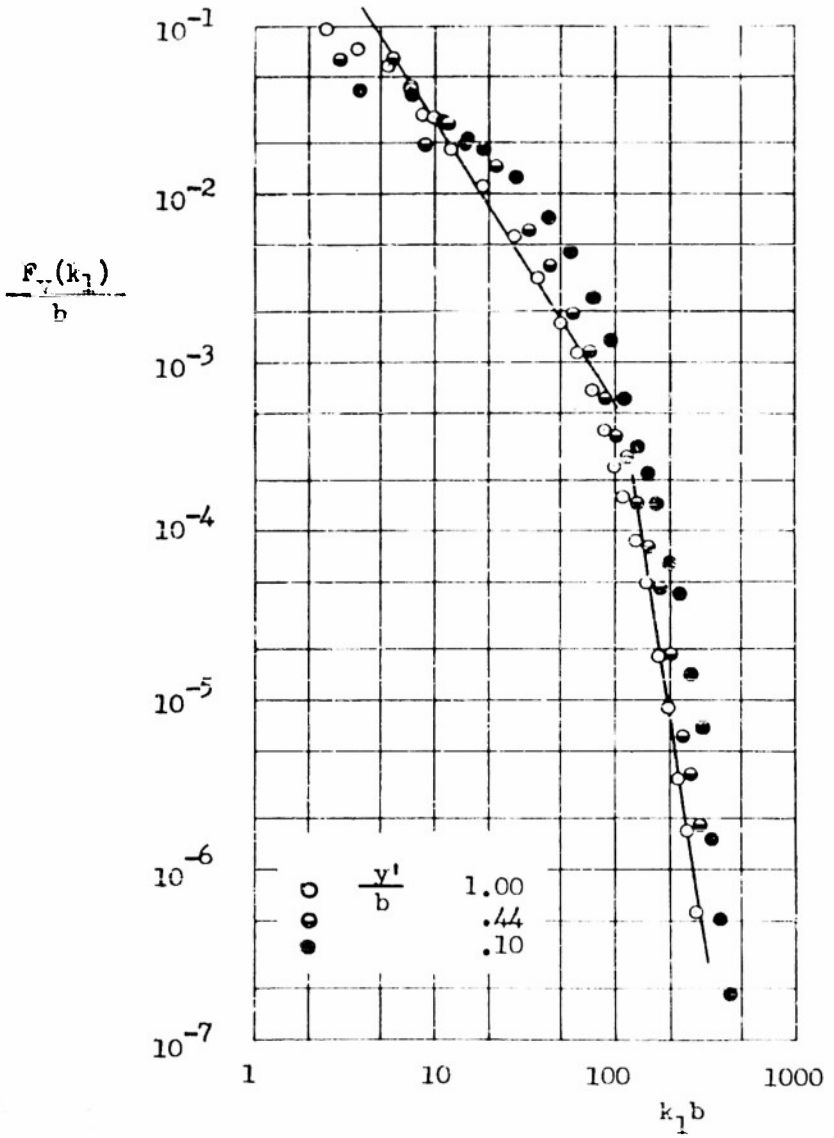

Figure 17.- v'-spectra.

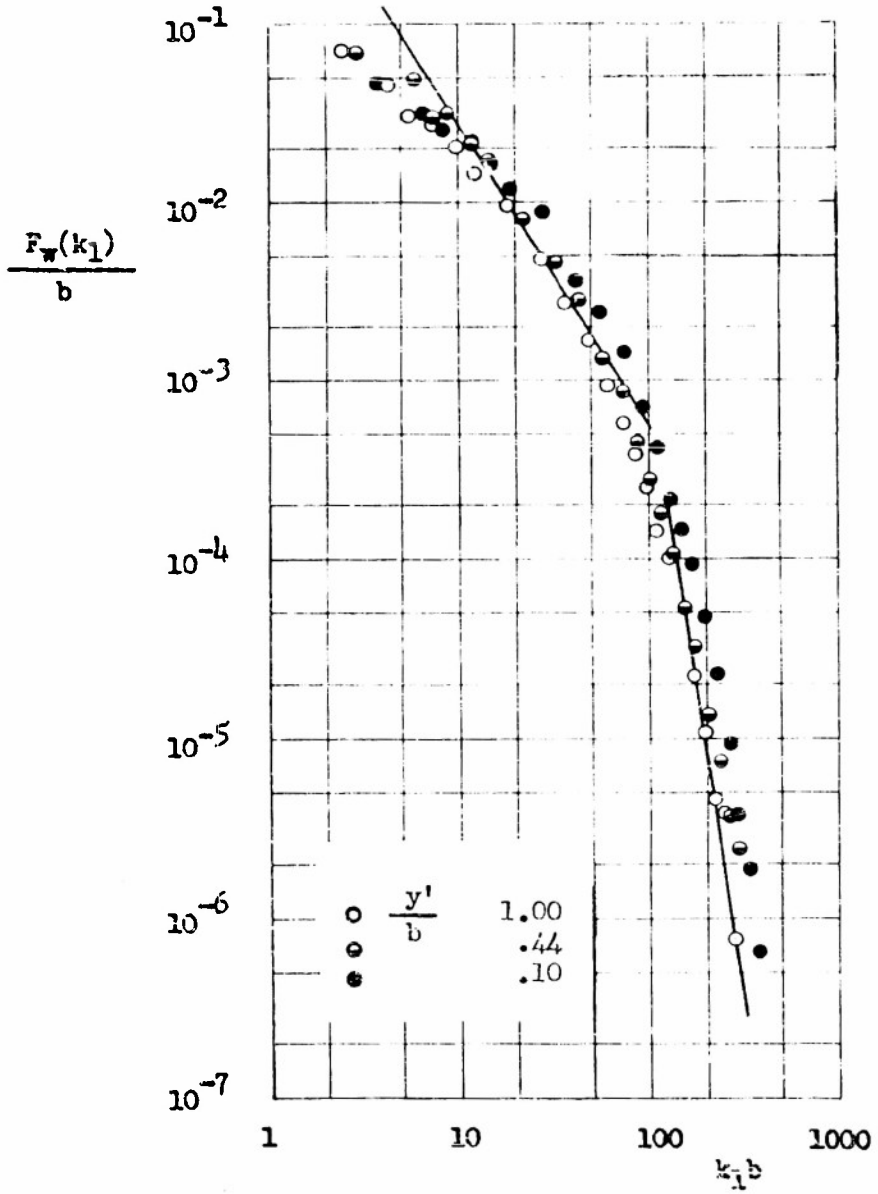

Figure 18.- w'-spectra.

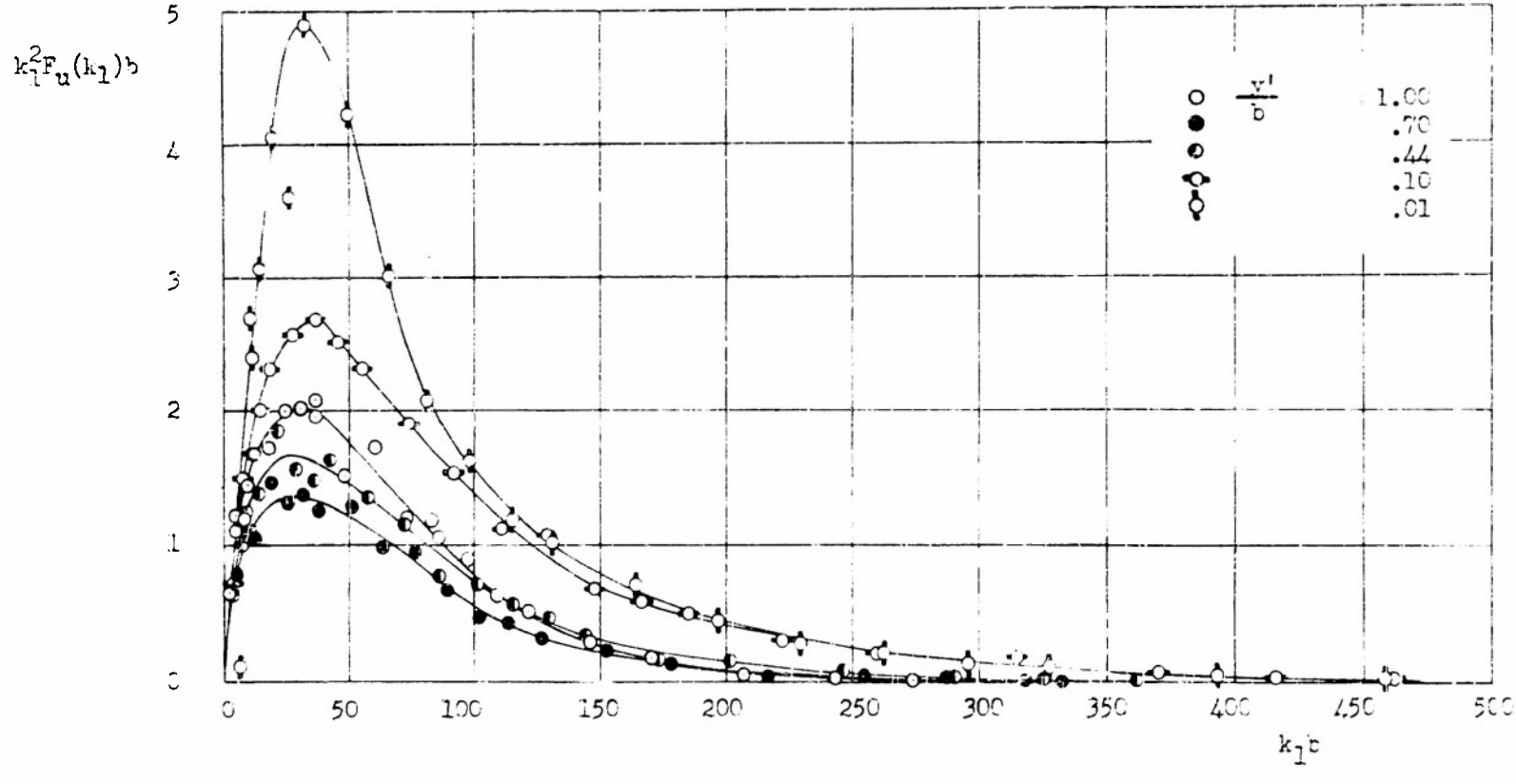

Figure 19.- Spectra distribution.

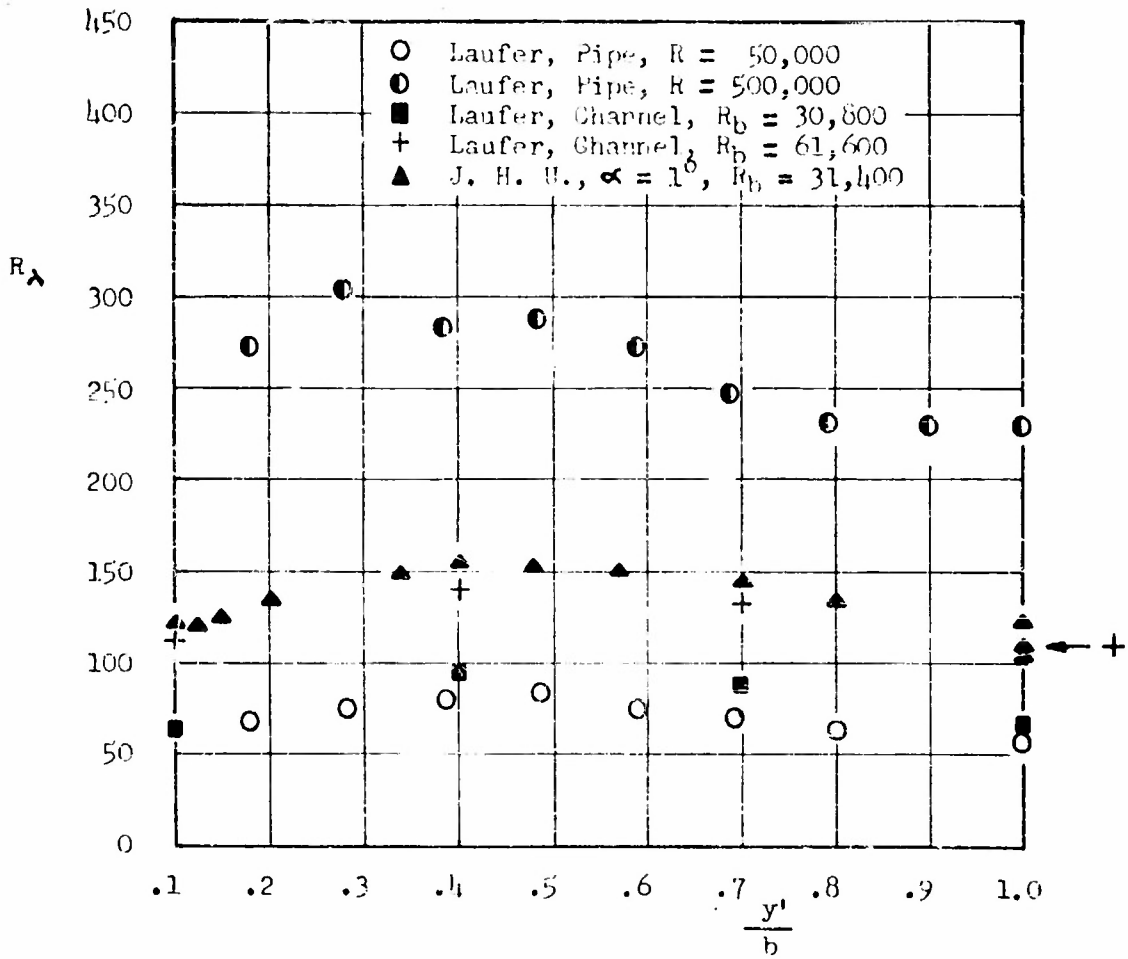

Figure 20.- Comparison of R_λ distributions in the pipe, channel, and diffuser.

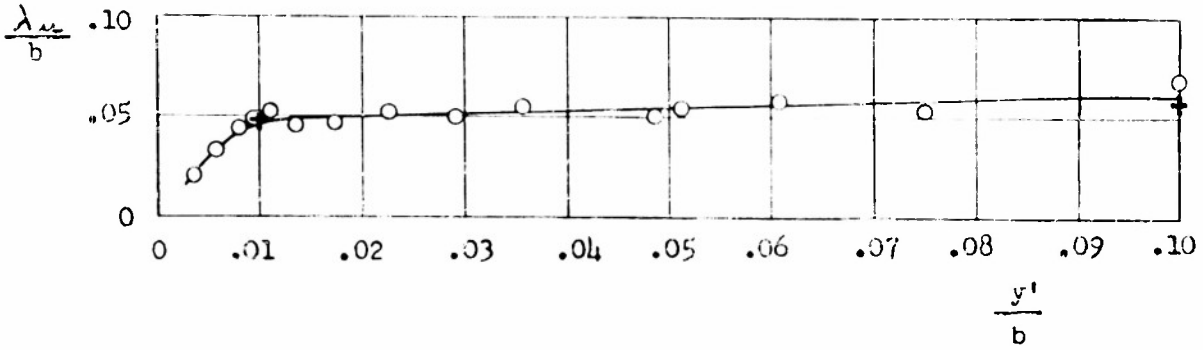

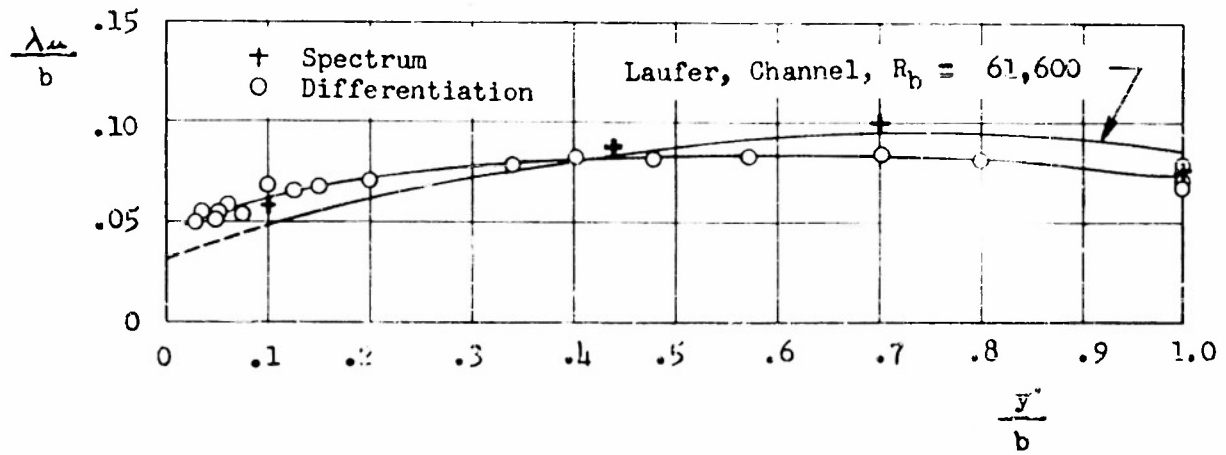

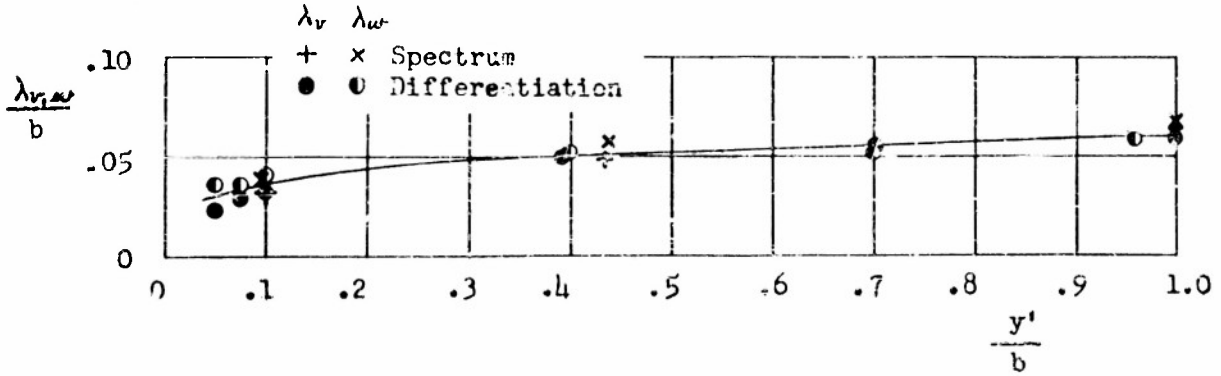

Figure 21.- Distribution of Microscales.

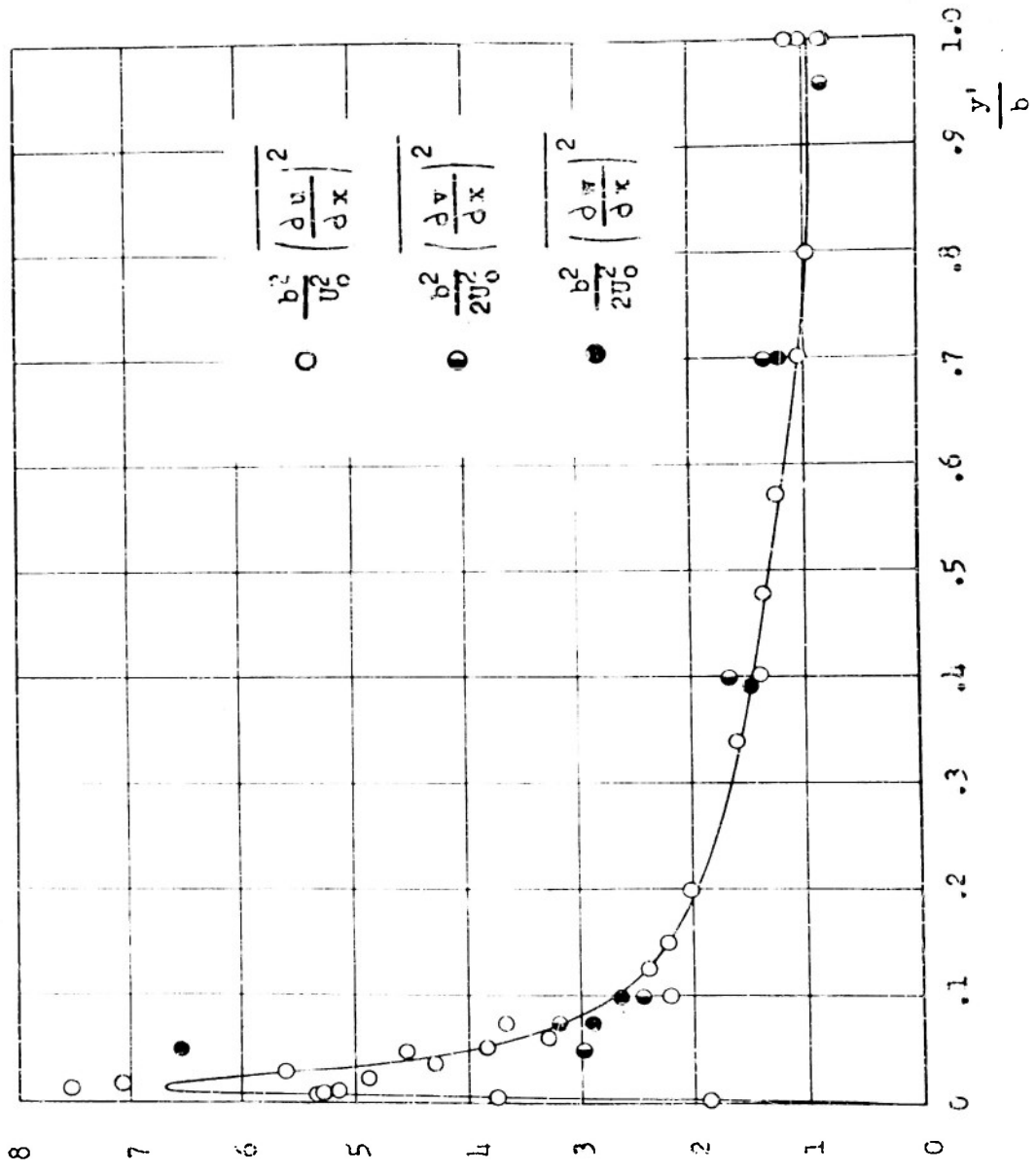

Figure 22.- Distribution of dissipation terms.

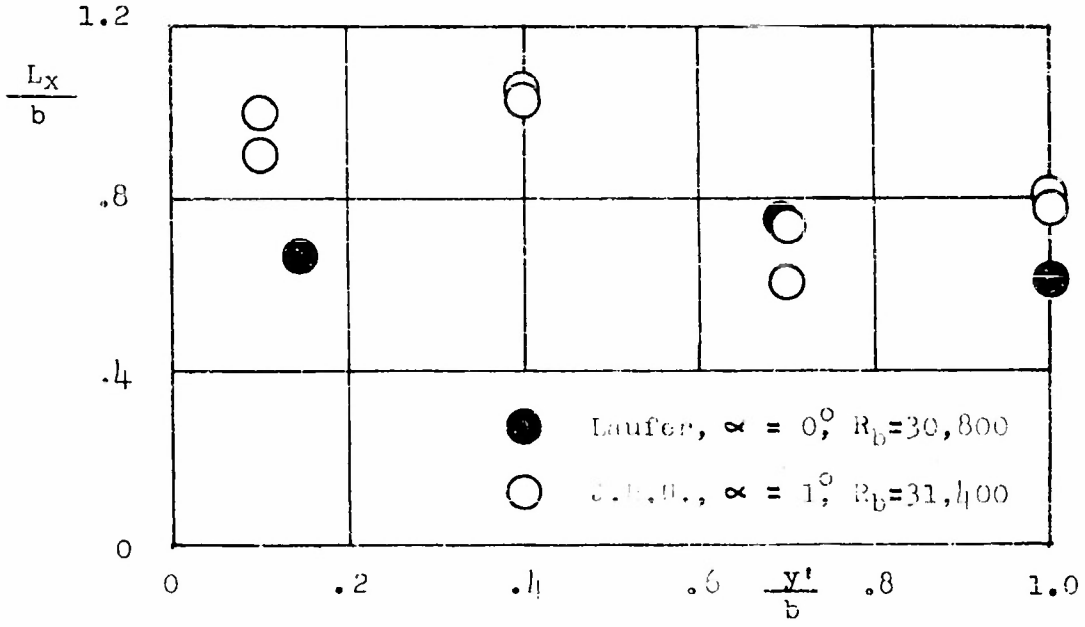

Figure 23.- Scale of Turbulence.

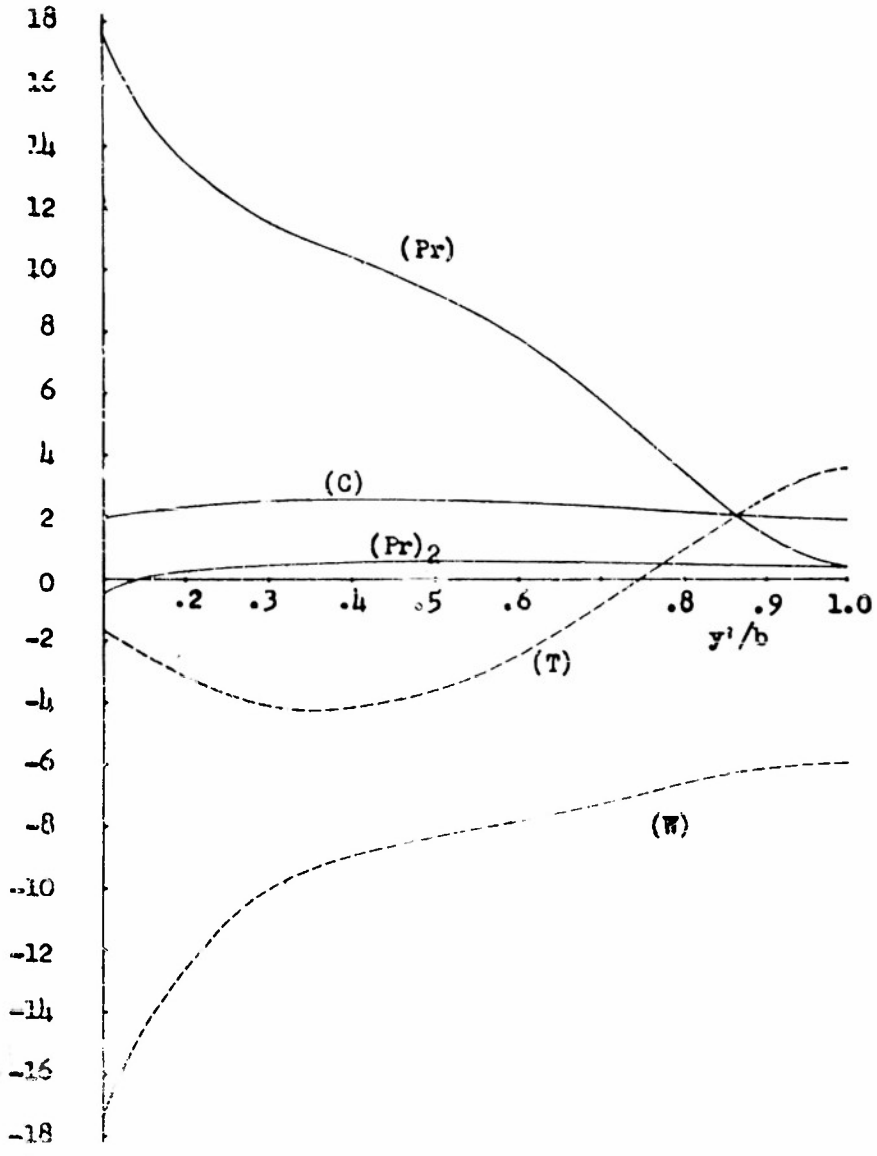

Figure 24.- Turbulent-energy balance.
Dashed lines are estimated.

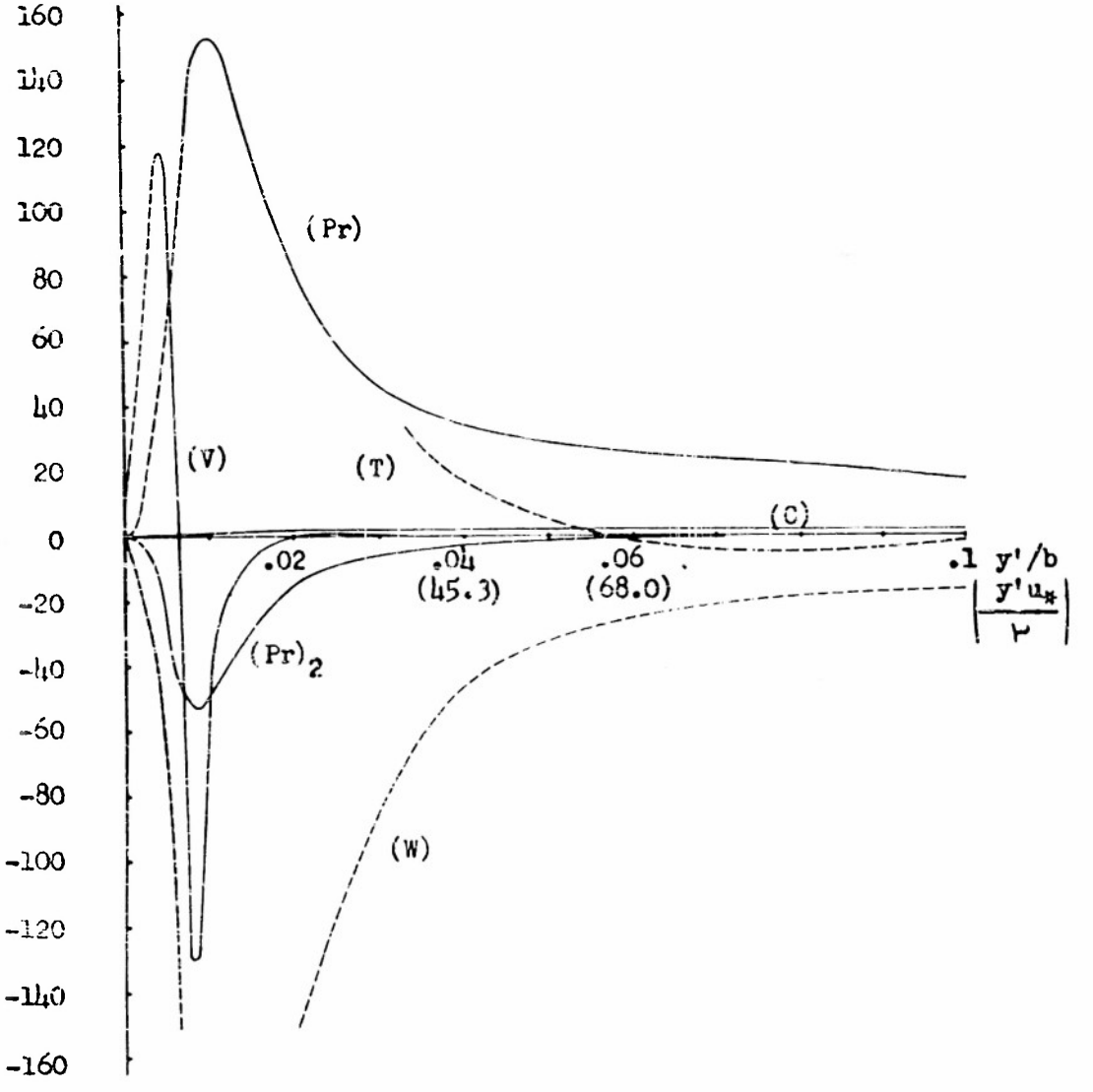

Figure 25.- Turbulent-energy balance near wall.
Dashed lines are estimated.

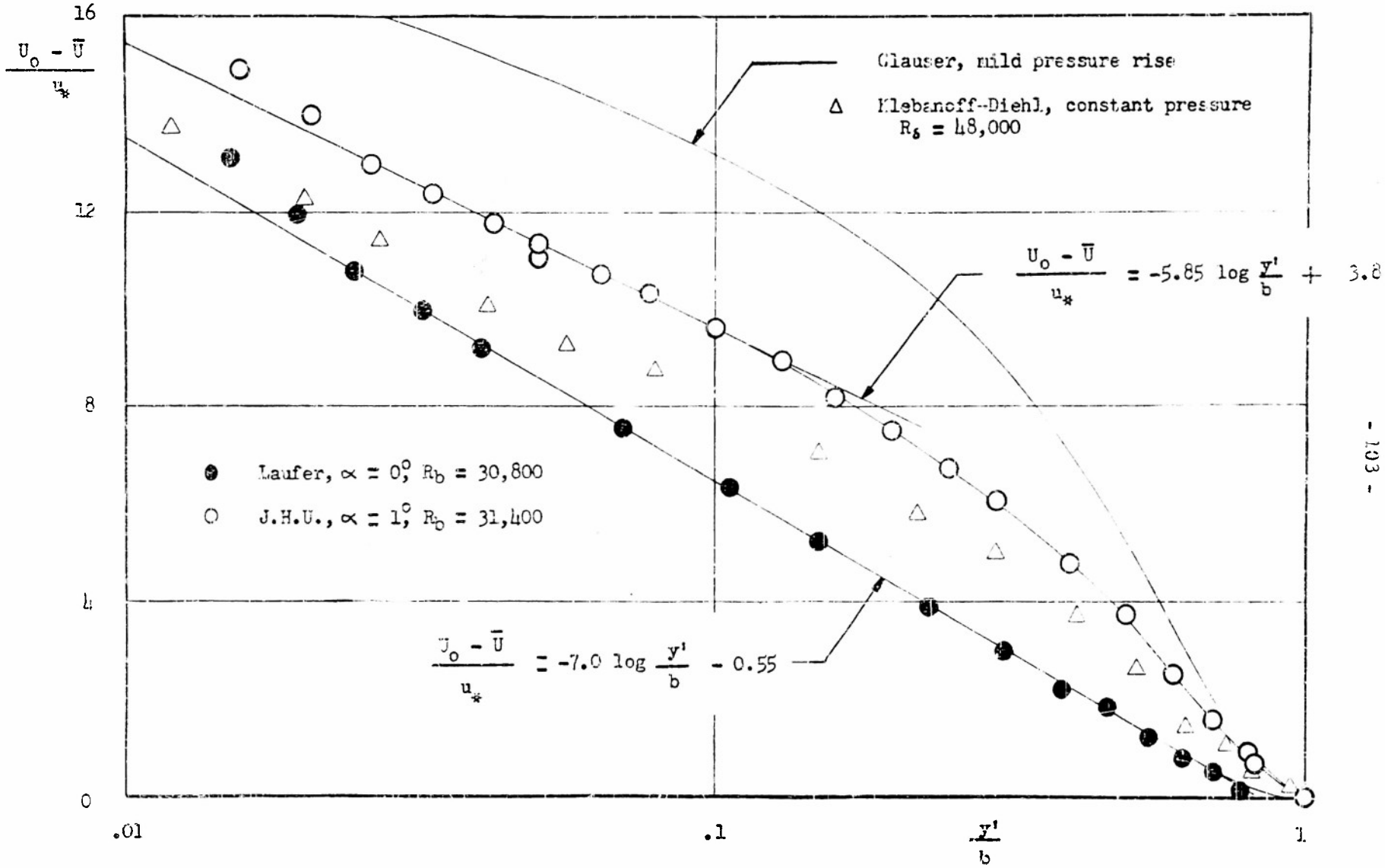

Figure 26.- Channel and boundary-layer mean velocities compared on basis of velocity-defect law.

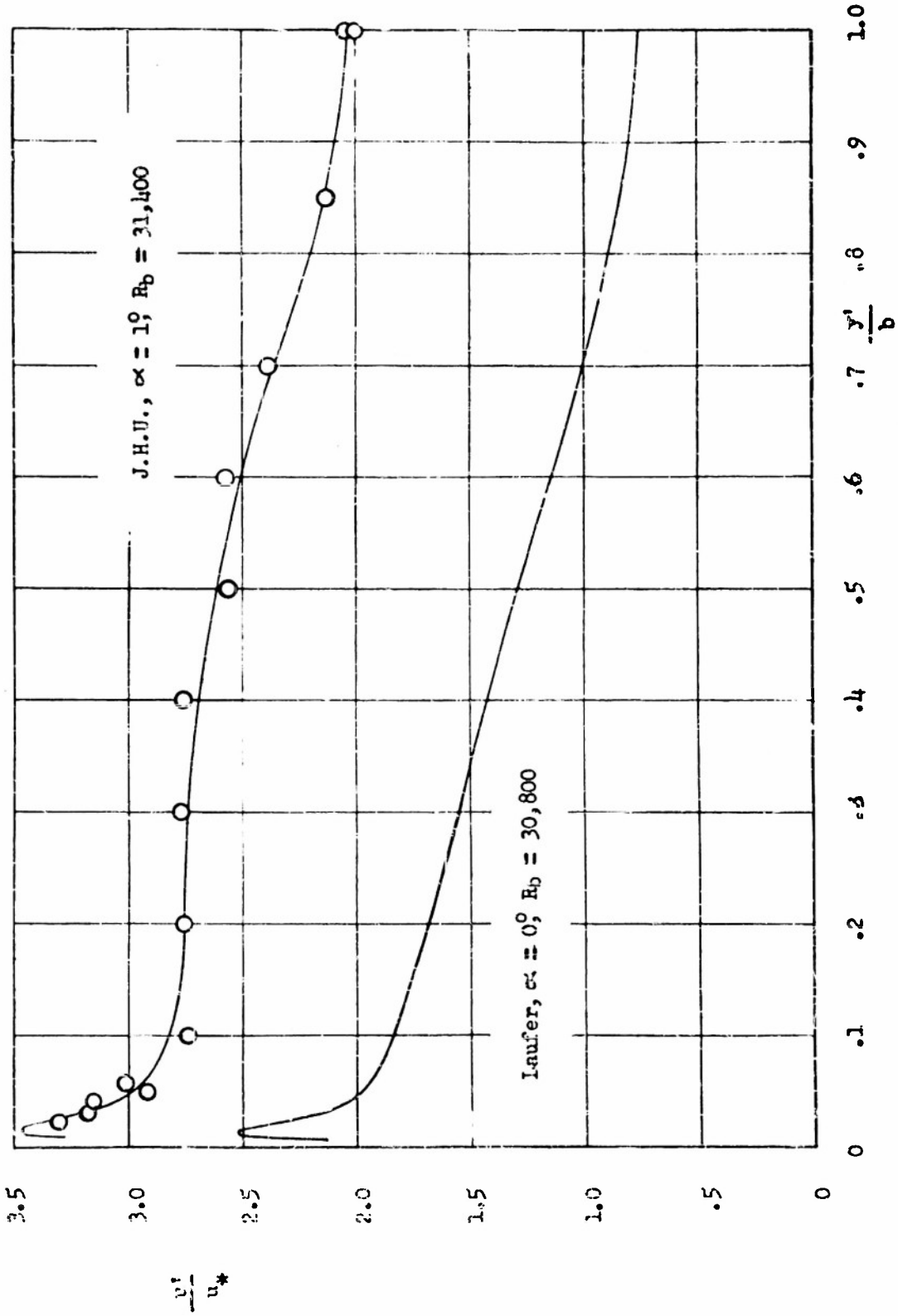

Figure 27.- u' distribution in center of channel.

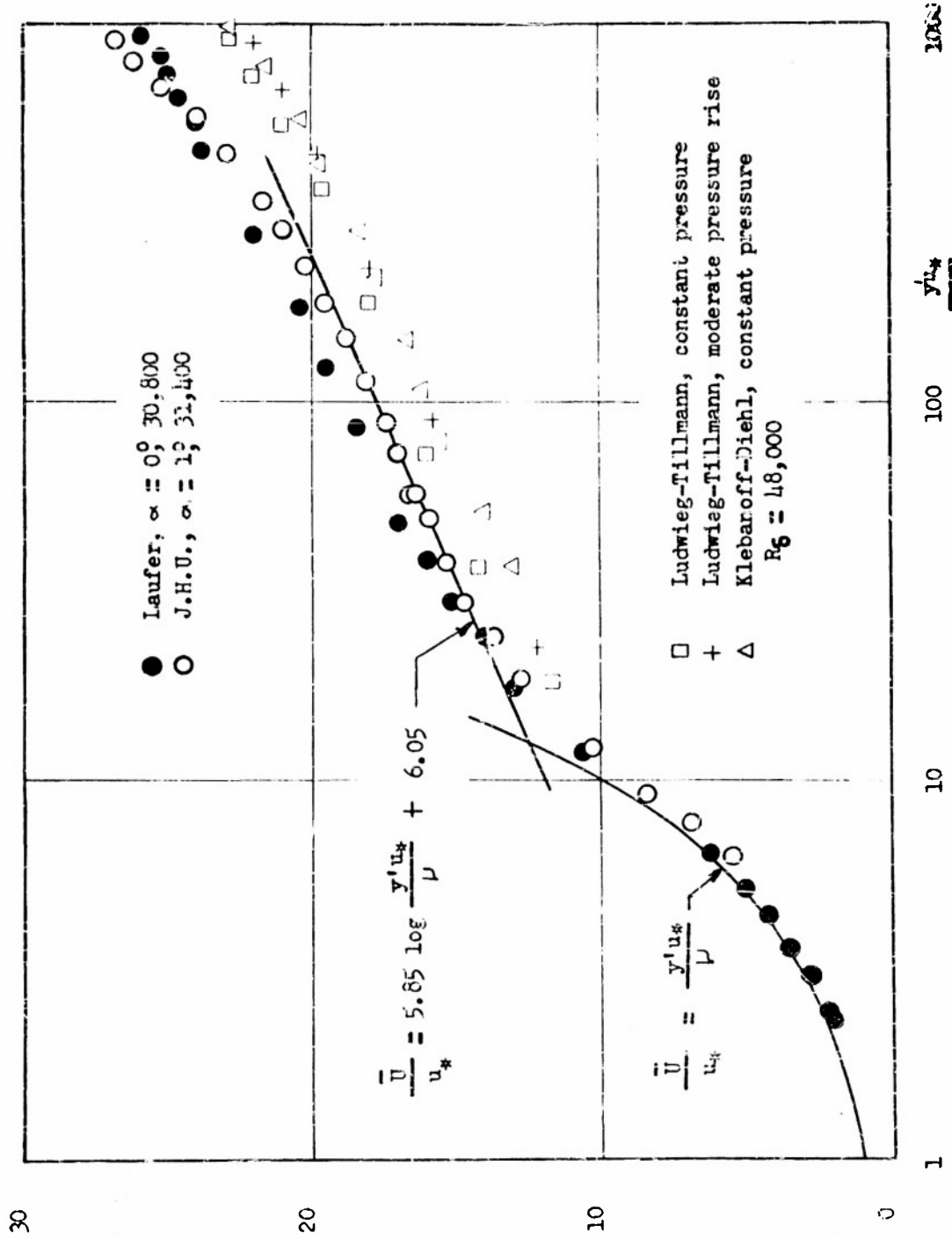

Figure 28.- Channel and boundary-layer mean velocities compared on basis of logarithmic law.

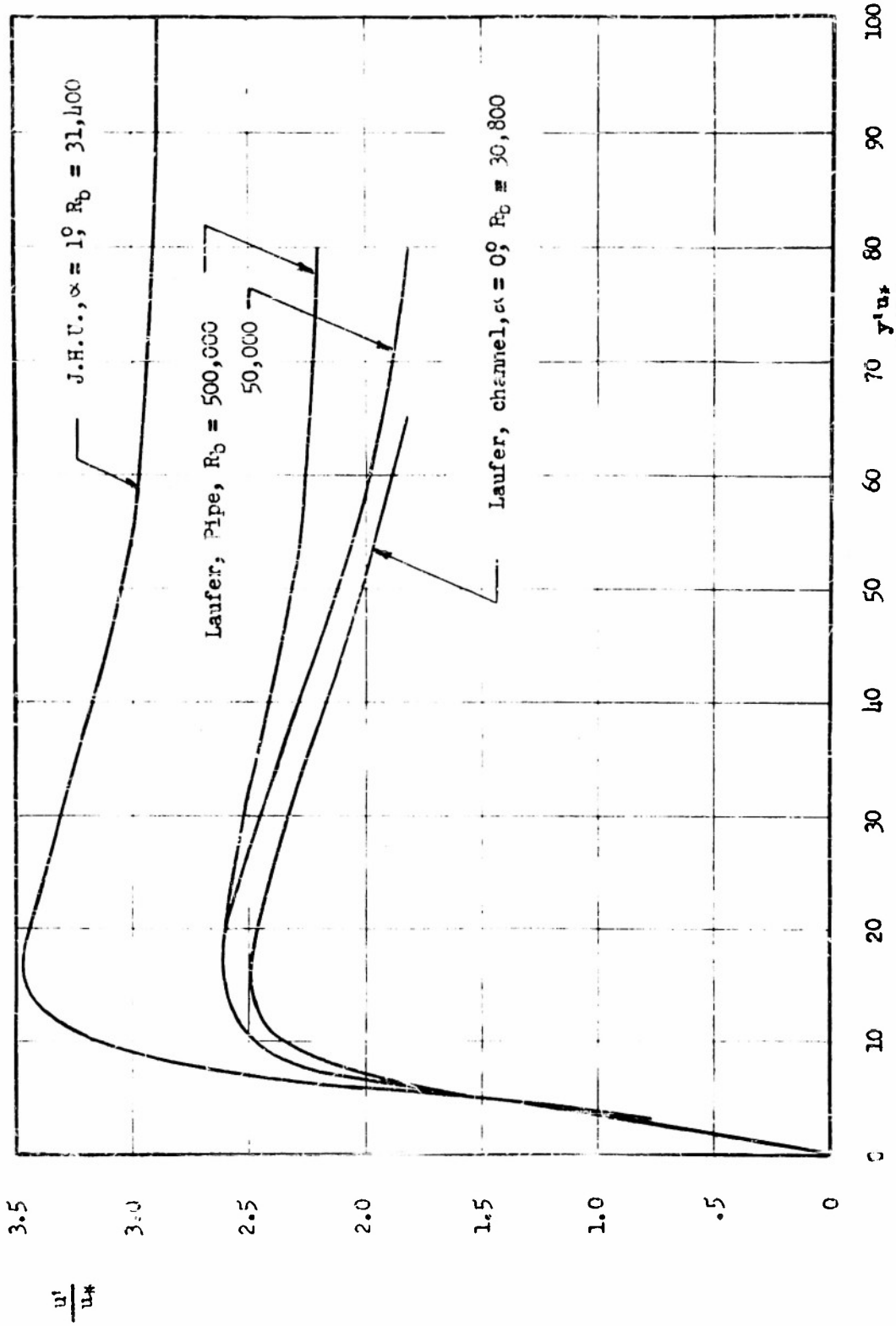

Figure 29.- u' distribution near wall.

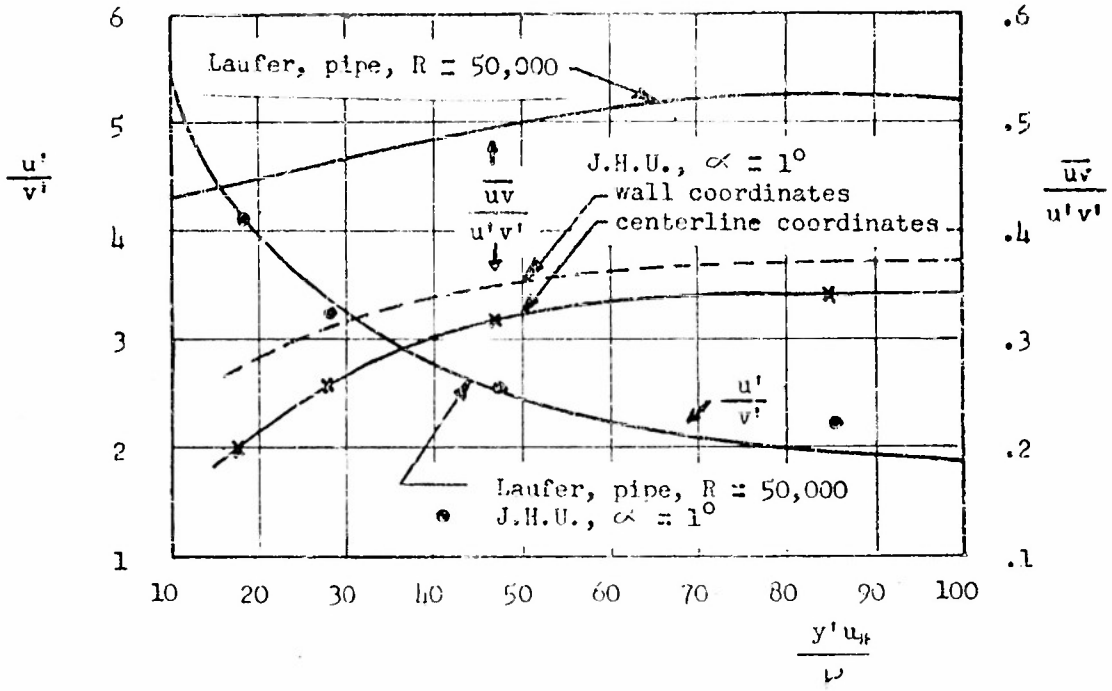

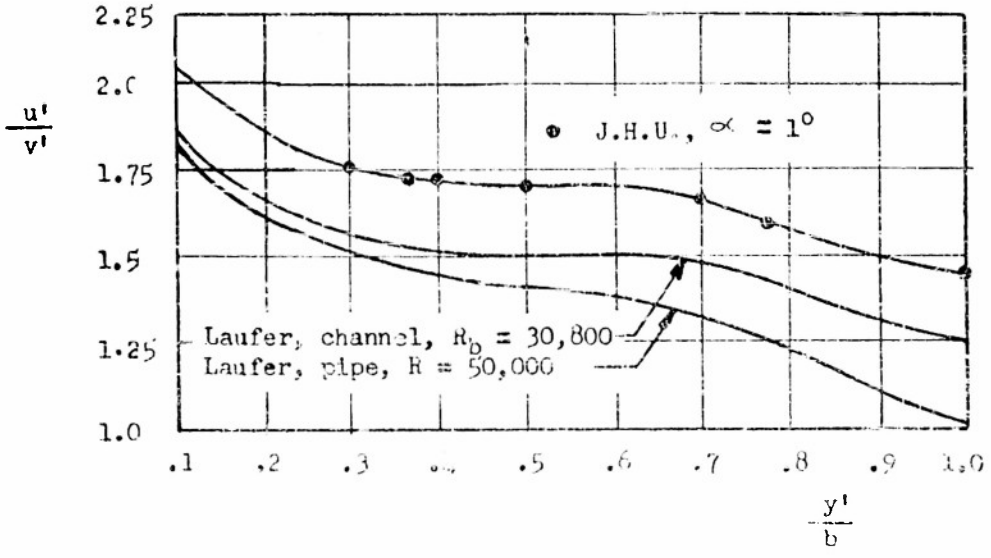

Figure 30.- Comparison of local turbulence quantities.

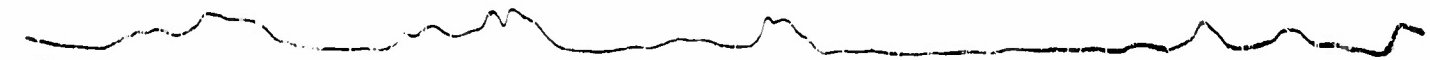

$\longleftarrow$ $\frac{1}{20}$ second $\longrightarrow$

(a) $\frac{y' u_*}{\nu} = 5.0$

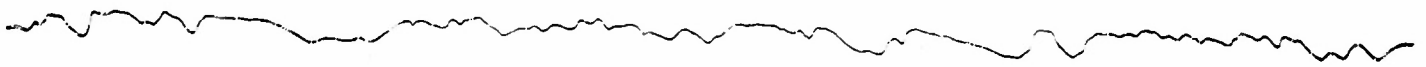

(b) $\frac{y' u_*}{\nu} = 11.7$

Figure 31.- Oscillograms of u-fluctuations near wall.
Velocity increases upward.

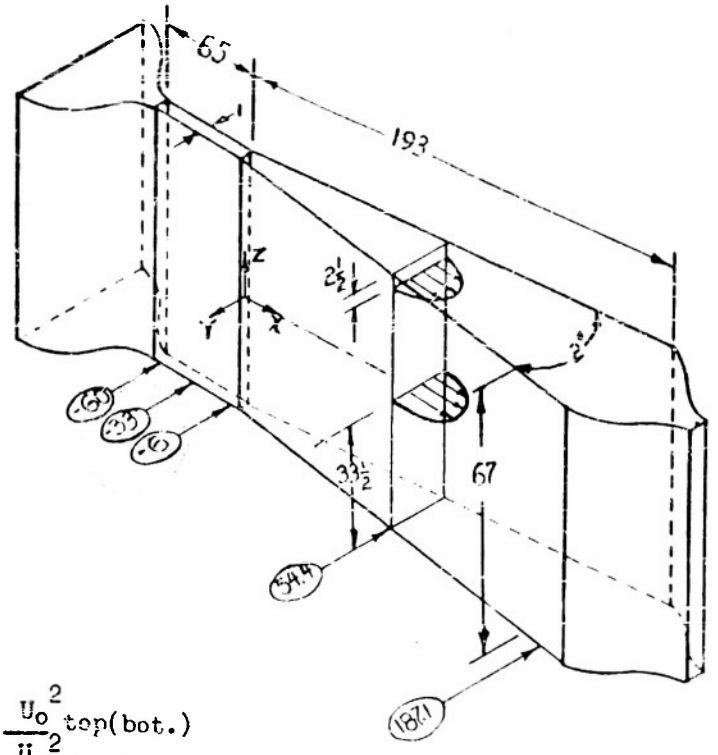

$$P_r \equiv \frac{U_o^2}{U_o^2}_{\text{top(bot.)}}_{\text{midplane}}$$

	Parallel-wall Approach Section			Sta. no. 2	Sta. no. 5
x, in.	-60	-33	-6	54.4	187.1
2b, in.	1.00	1.00	1.00	2.90	7.50
P_r Before modification of approach section	.995	.955	.95	.67	.17
After modification of approach section			top 1.00 bot. .985		.55

Figure 32.- A two-dimensionality test of dynamic pressure.

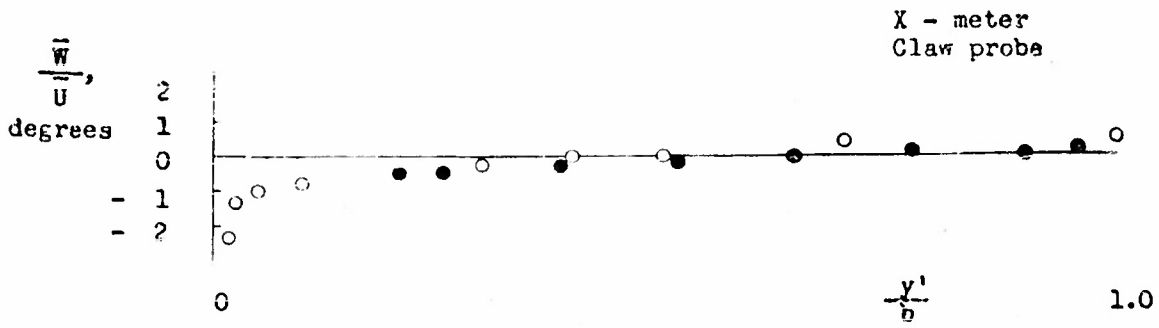

Distribution of $\bar{W}$ relative to $\bar{U}$ at station 5, midplane.

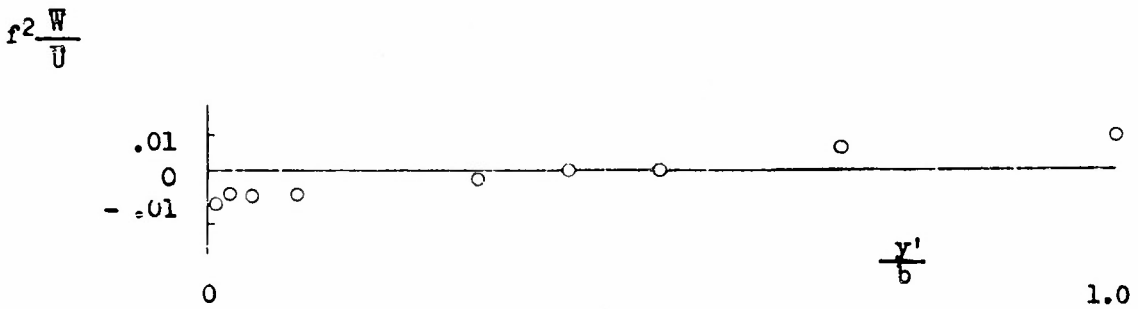

Distribution of $f^2\frac{\bar{W}}{\bar{U}}$ at station 5, midplane.

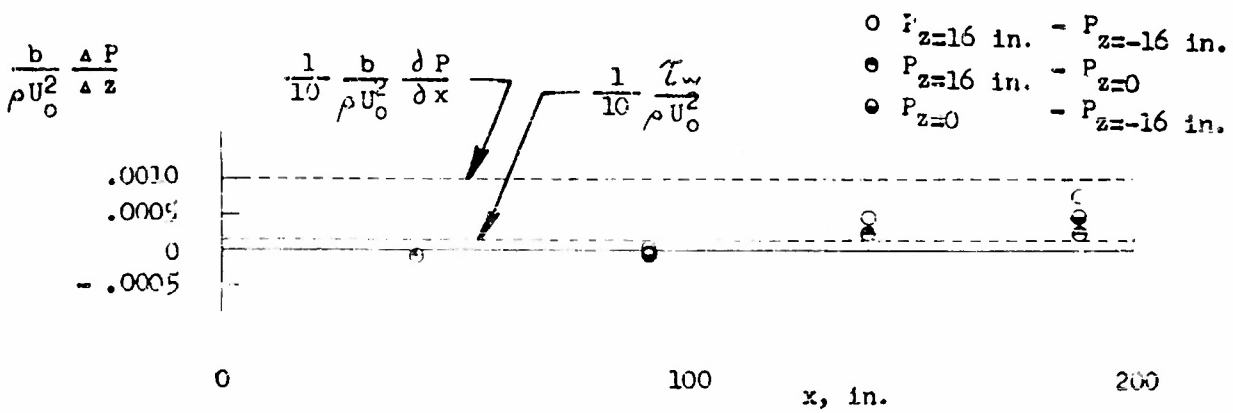

Longitudinal distribution of vertical pressure gradient.

Figure 33.- Quantities to establish test conditions.

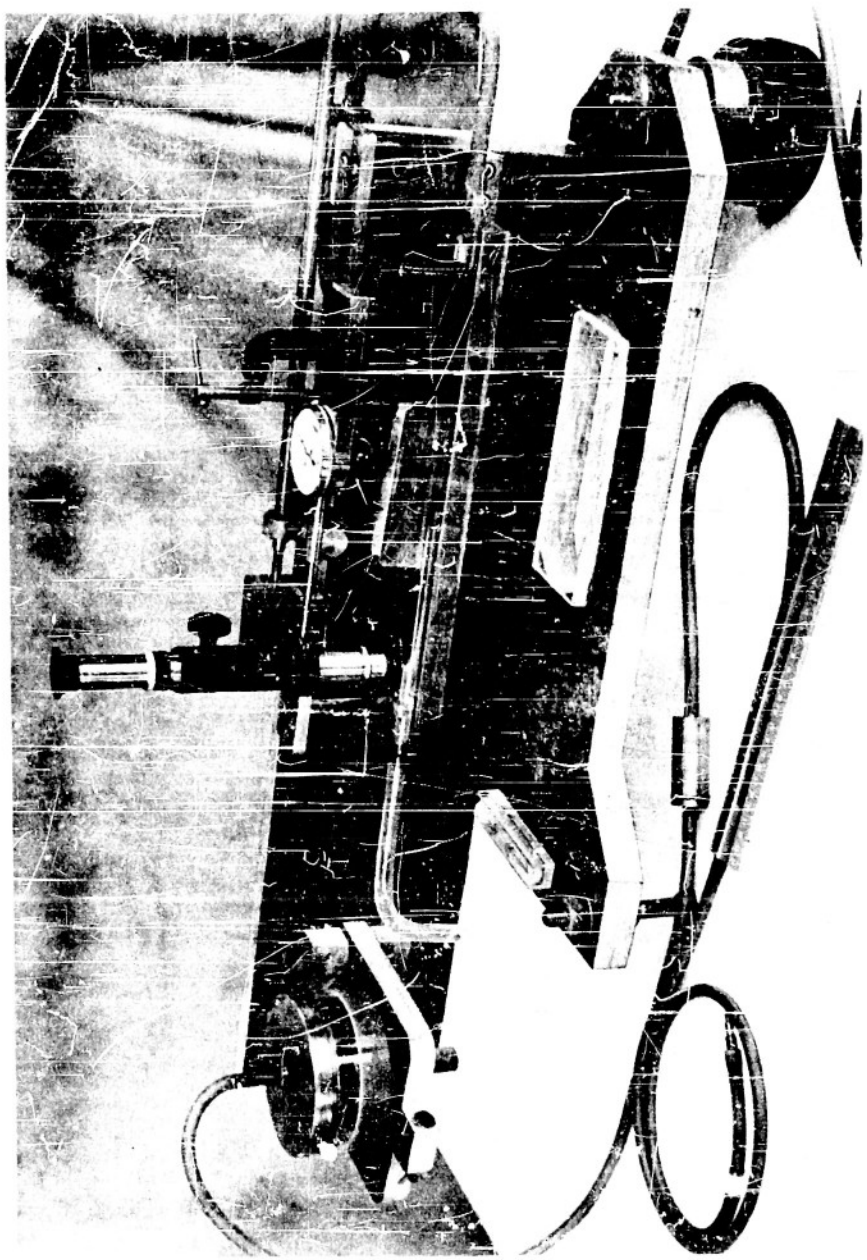

Figure 34.- Precision inclined manometer.

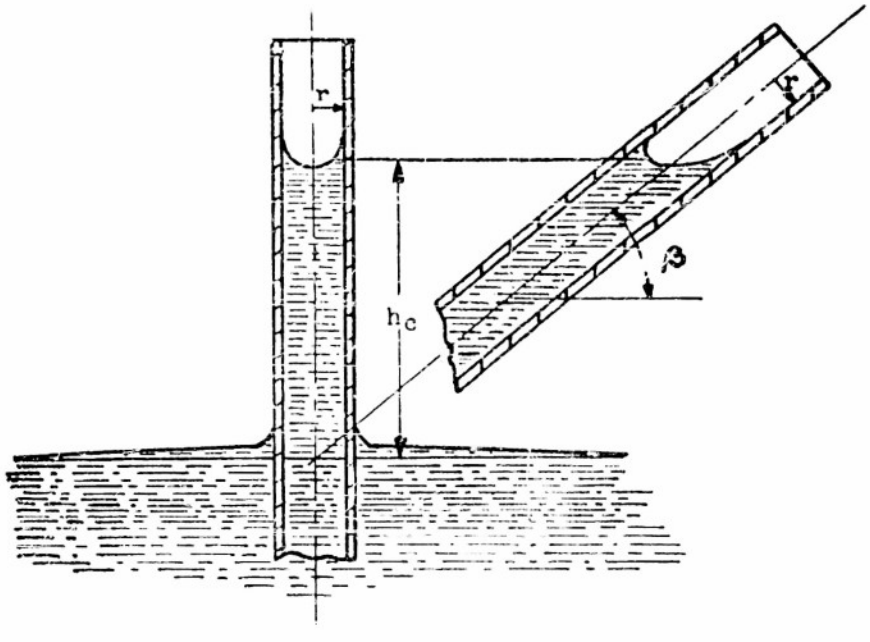

Figure 35.- Capillary rise in a tube.

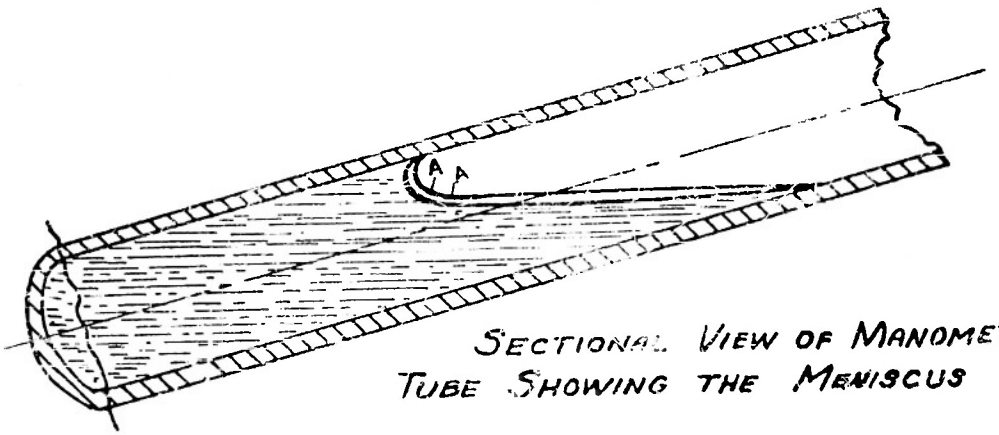

SECTIONAL VIEW OF MANOMETER TUBE SHOWING THE MENISCUS

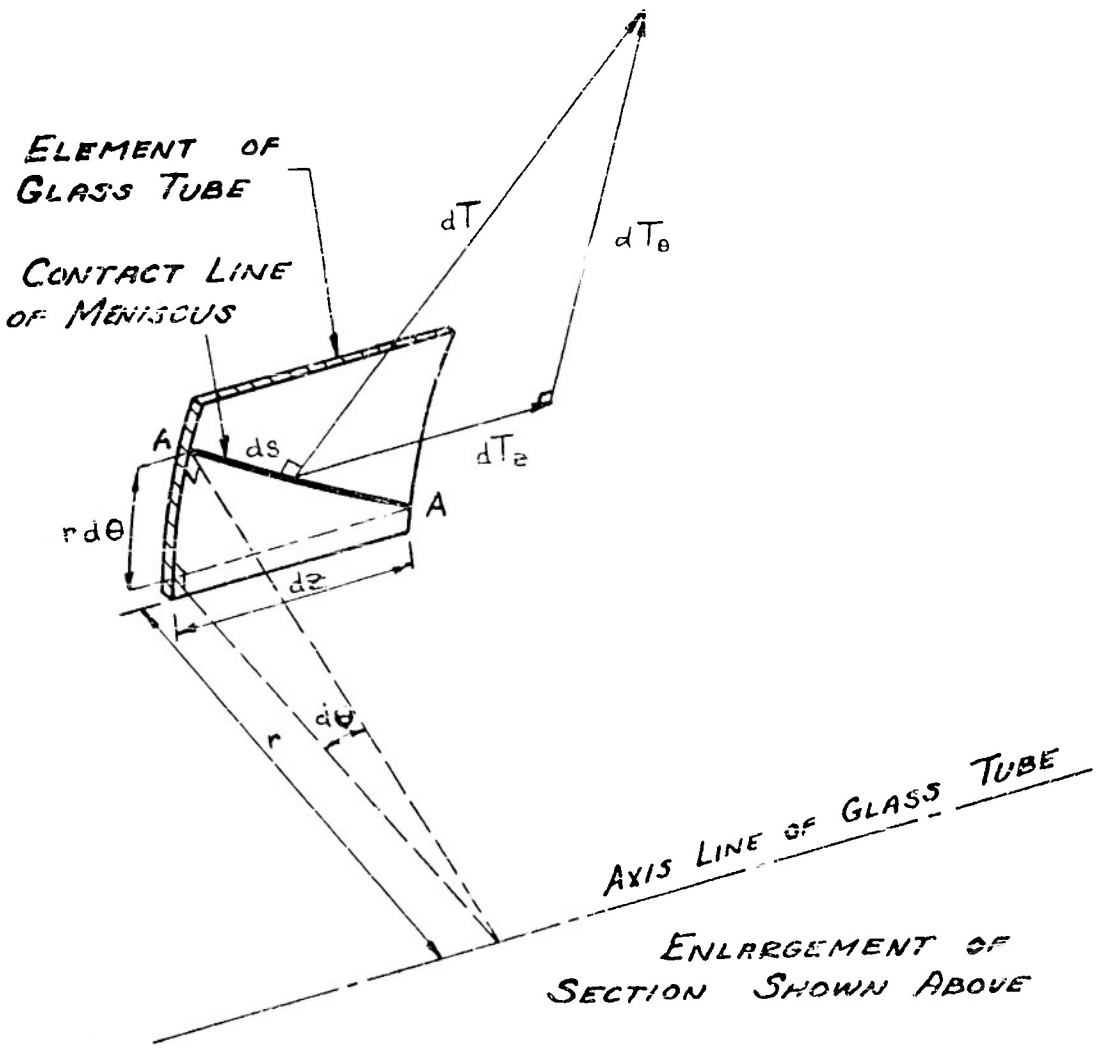

ENLARGEMENT OF SECTION SHOWN ABOVE

FIGURE: 36 - DIAGRAMS SHOWING MANOMETER MENISCUS

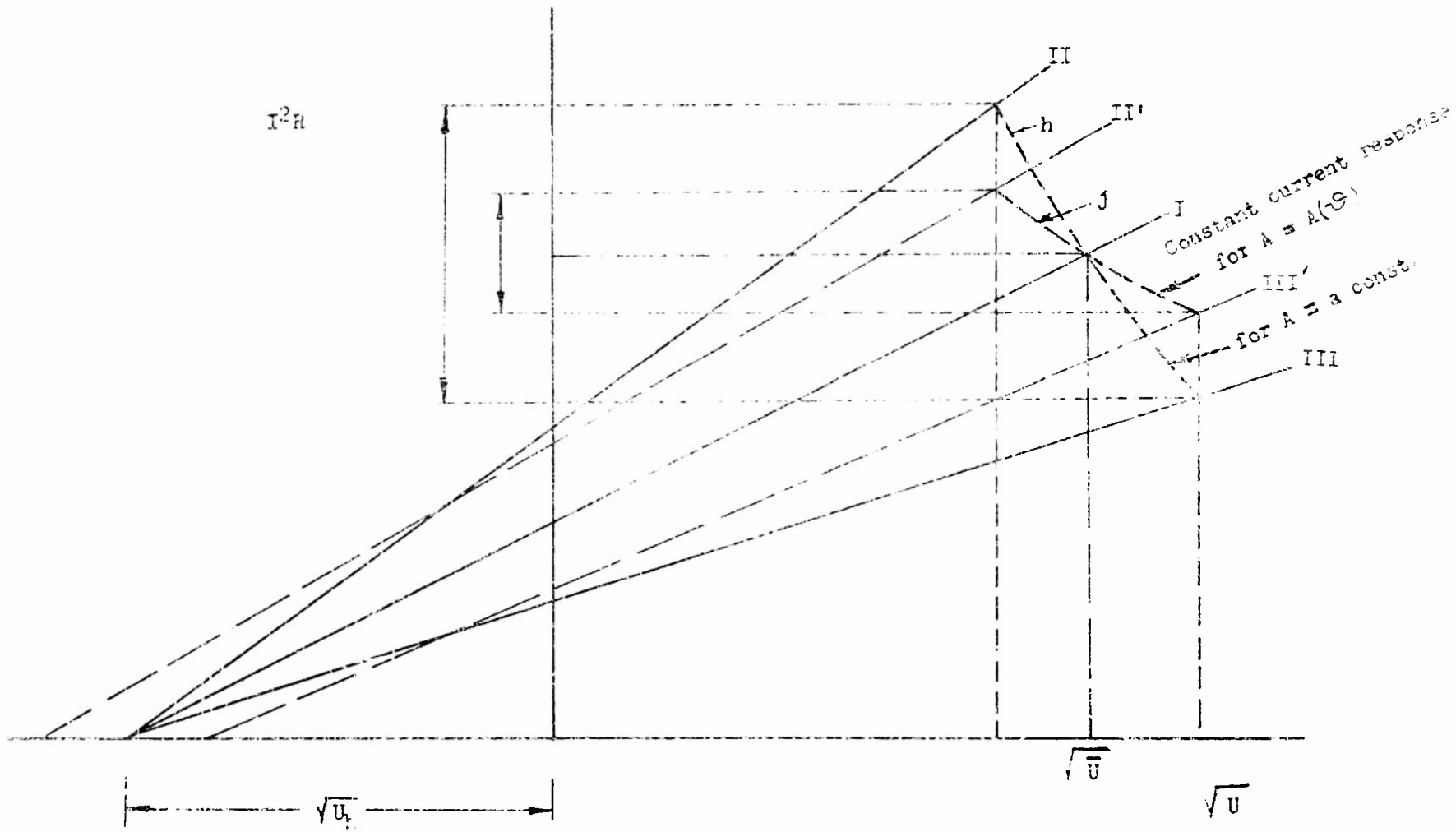

Figure 37.- Hot-wire heat loss curves.

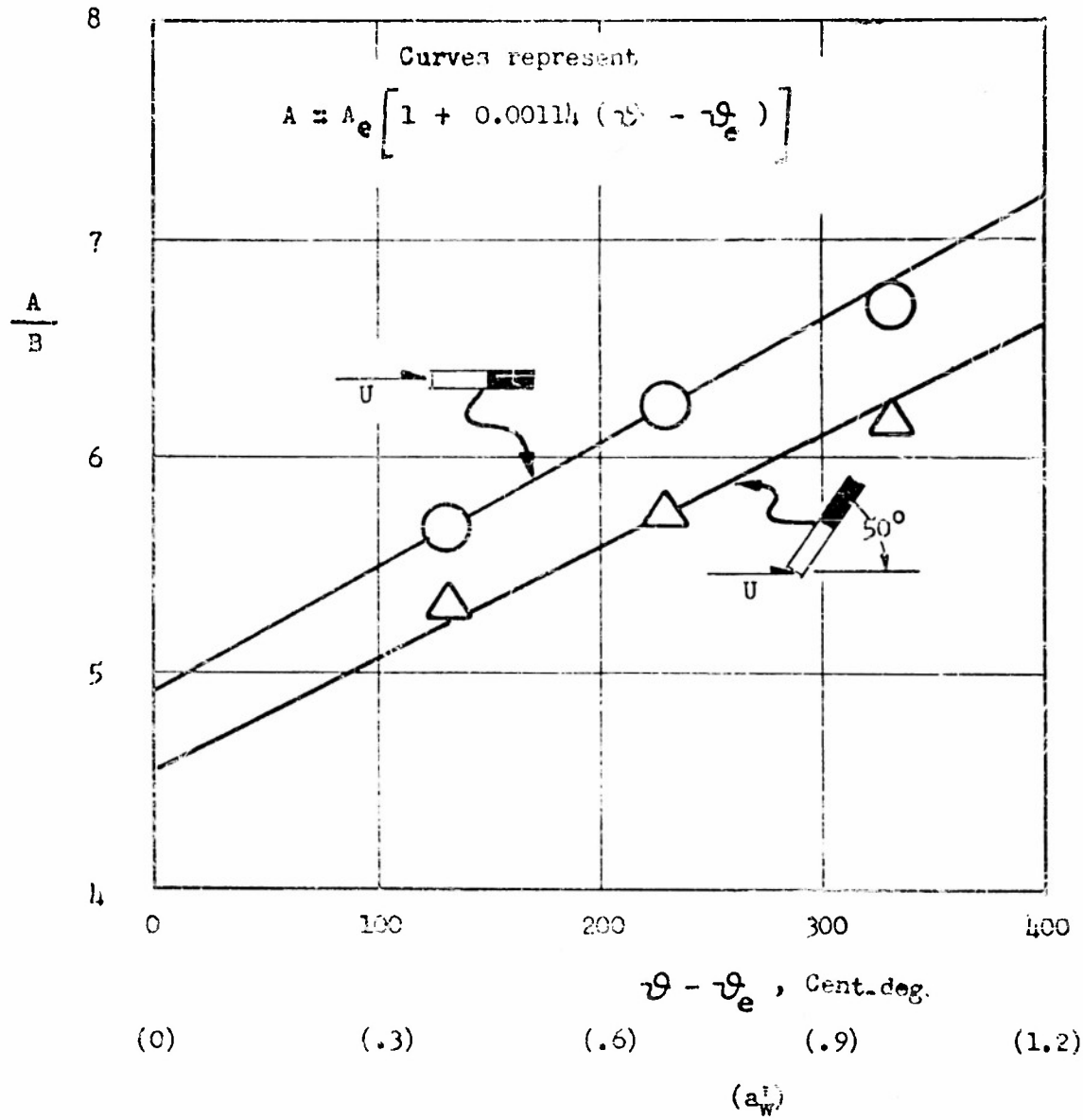

Figure 38.- Experimental verification of King's expression for $A = A(\vartheta)$ for a normal and inclined platinum wire.

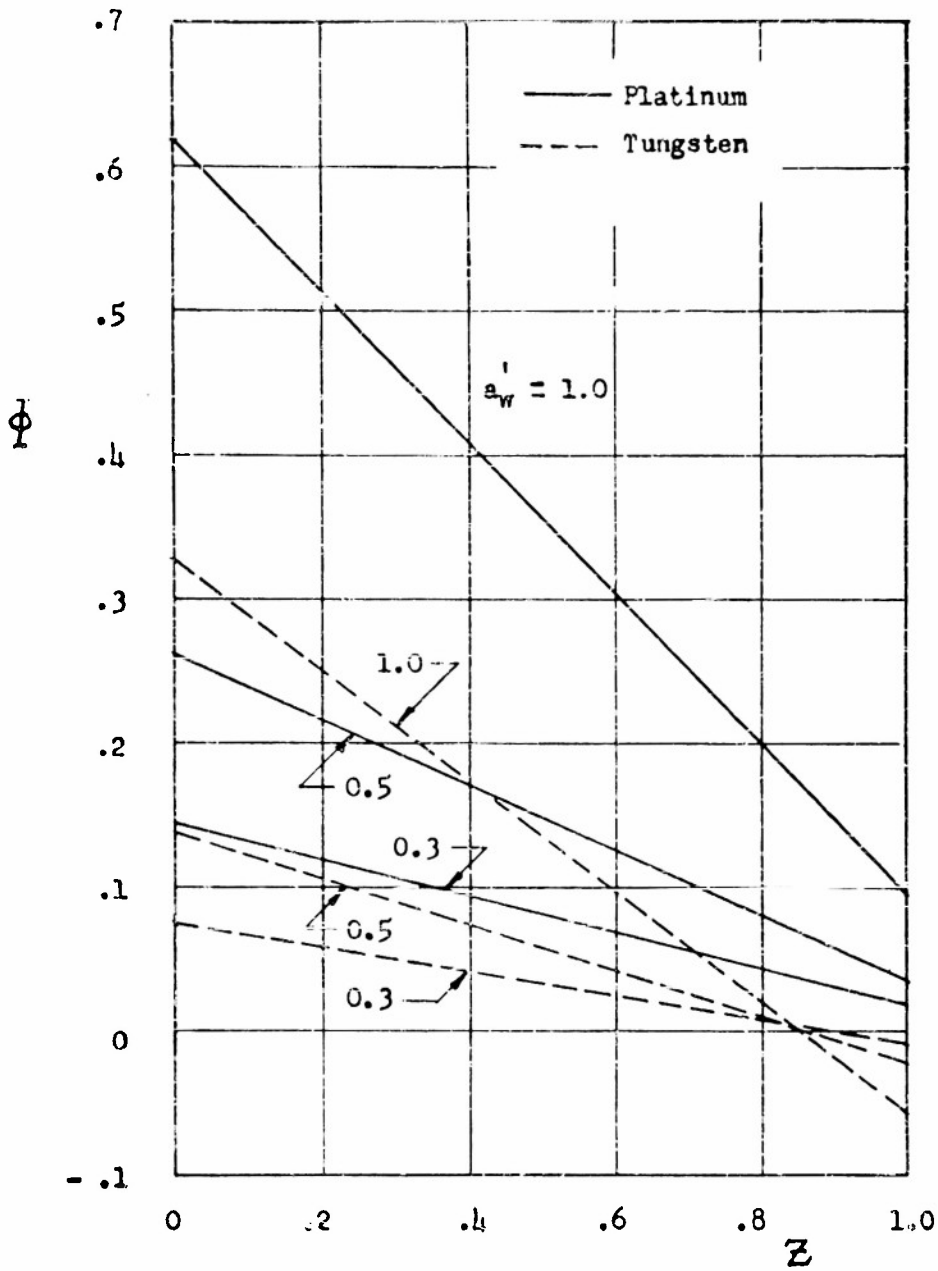

Figure 39.- Hot-wire ϕ correction based upon equation (22). Parameter is a_w'. $\vartheta_e = 80^\circ$ F.

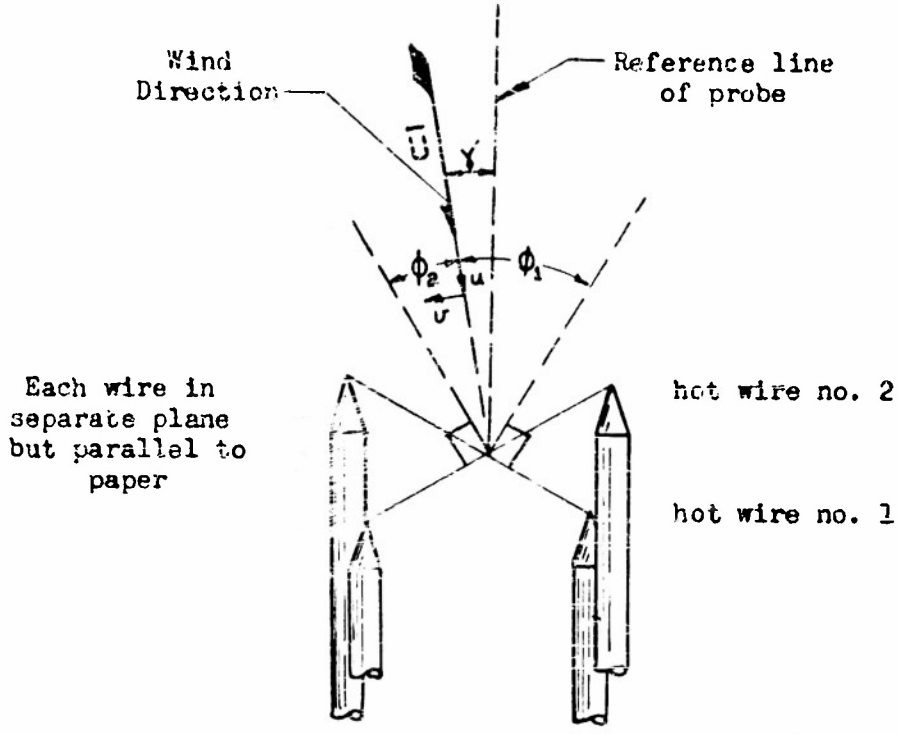

Orientation of x-meter wires

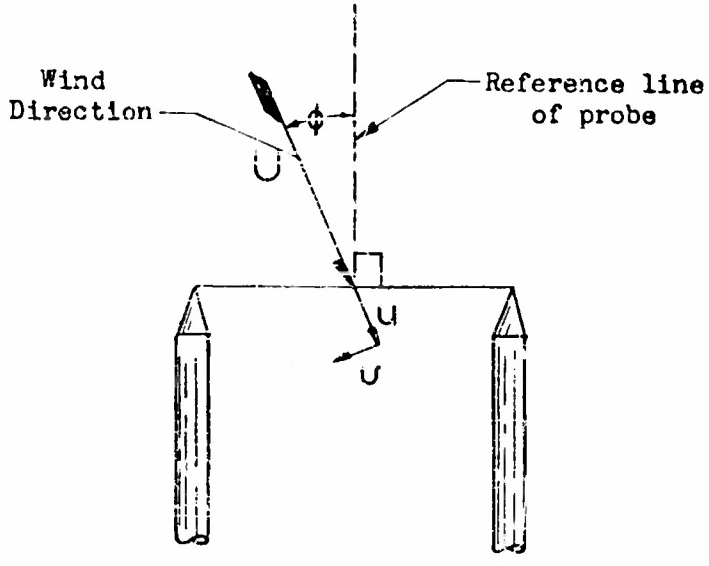

Orientation of a single wire

Figure 40.- Diagrams of hot-wire orientation in stream.

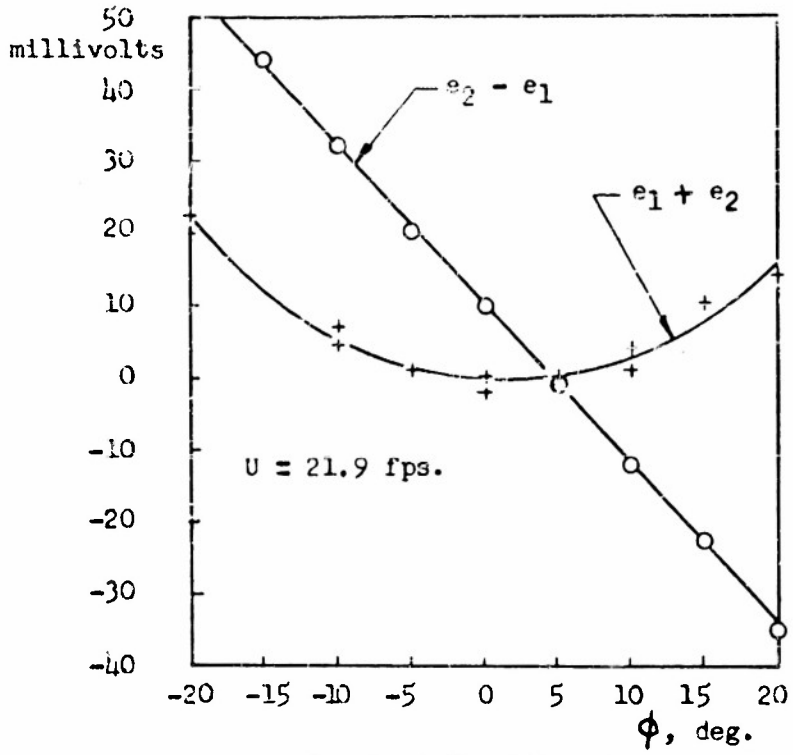

Constant U calibration

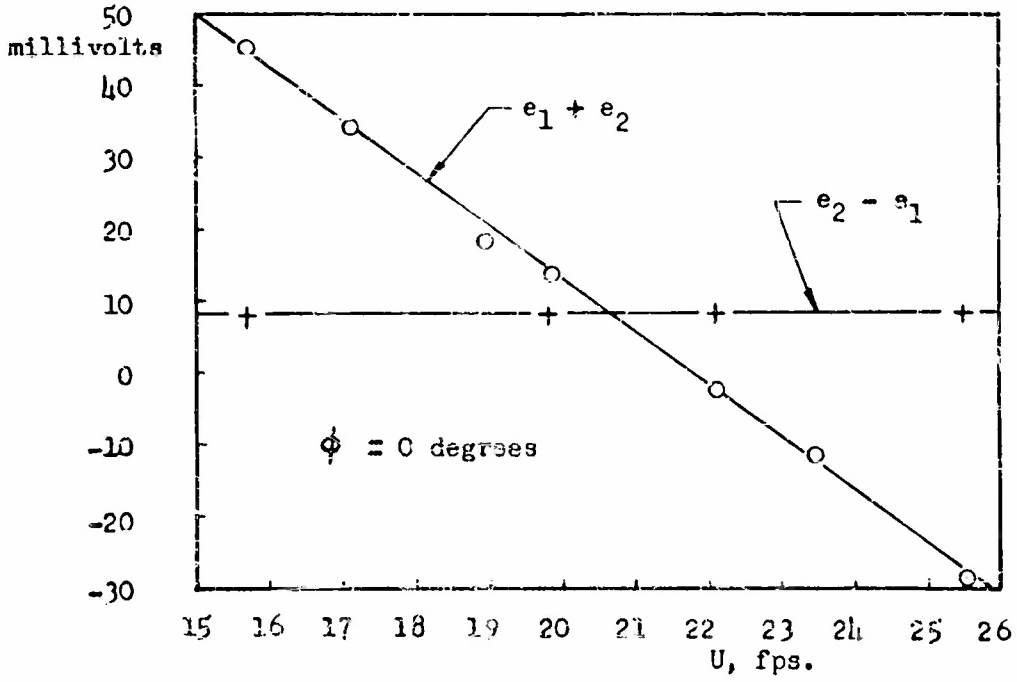

Constant ϕ calibration

Figure 41.- X-meter calibration curves.

DISTRIBUTION LIST

Chief of Naval Research
Department of the Navy
Washington 25, D. C.
Attn: Code 438 (2)

Commanding Officer
Office of Naval Research
Branch Office
150 Causeway Street
Boston, Massachusetts (1)

Commanding Officer
Office of Naval Research
Branch Office
The John Crerar Library Bldg.
86 East Randolph Street
Chicago 1, Illinois (1)

Commanding Officer
Office of Naval Research
Branch Office
346 Broadway
New York 13, New York (1)

Commanding Officer
Office of Naval Research
Branch Office
1031 East Green Street
Pasadena, California (1)

Commanding Officer
Office of Naval Research
Branch Office
1000 Geary Street
San Francisco, California (1)

Commanding Officer
Office of Naval Research
Navy #100, Fleet Post Office
New York, New York (2)

Director
Naval Research Laboratory
Washington 25, D. C.
Attn: Code 2021 (6)

Documents Service Center
Armed Services Technical
Information Agency
Knott Building
Dayton 2, Ohio (5)

Chief, Bureau of Aeronautics
Department of the Navy
Washington 25, D. C.
Attn: Research Division (1)

Chief, Bureau of Ordnance
Department of the Navy
Washington 25, D. C.
Attn: Research and Development
ment Division (1)

Office of Ordnance Research
Department of the Army
Washington 25, D. C. (1)

Commander
Air Research and Development
Command
Office of Scientific Research
P.O. Box 1395
Baltimore 18, Maryland
Attn: Fluid Mechanics Division (1)

Director of Research
National Advisory Committee
for Aeronautics
1724 F Street, Northwest
Washington 25, D. C. (1)

Director
Langley Aeronautical Laboratory
National Advisory Committee
for Aeronautics
Langley Field, Virginia (1)

Director
National Bureau of Standards
Washington 25, D. C.
Attn: Fluid Mechanics Section (1)

Professor R. Courant
Institute for Mathematics and Mechanics
New York University
45 Fourth Avenue
New York 3, New York (1)

Professor G. Kuerti
Department of Mechanical Engineering
Case Institute of Technology
Cleveland, Ohio (1)

Professor W. R. Sears, Director
Graduate School of Aeronautical Engineering
Cornell University
Ithaca, New York (1)

Chief, Bureau of Yards and Docks
Department of the Navy
Washington 25, D. C.
Attn: Research Division (1)

Director
Underwater Sound Laboratory
Fort Trumbull
New London, Connecticut (1)

Director
Waterways Experiment Station
Box 631
Vicksburg, Mississippi (1)

Office of the Chief of Engineers
Department of the Army
Gravelly Point
Washington 25, D. C. (1)

Beach Erosion Board
U. S. Army Corps of Engineers
Washington 25, D. C. (1)

Commissioner
Bureau of Reclamation
Washington 25, D. C. (1)

Dr. G. H. Keulegan
National Hydraulic Laboratory
National Bureau of Standards
Washington 25, D. C. (1)

Chief, Bureau of Ships
Department of the Navy
Washington 25, D. C.
Attn: Research Division (1)
Code 420 (Preliminary Design Division) (1)

Commander
Naval Ordnance Test Station
3202 E. Foothill Blvd.
Pasadena, California (1)

Commanding Officer and Director
David Taylor Model Basin
Washington 7, D. C.
Attn: Hydromechanics Lab. (1)
Hydrodynamics Div. (1)
Library (1)

California Institute of Technology
Hydrodynamic Laboratory
Pasadena, California (1)

Professor V. L. Streeter
Civil Engineering Department
University of Michigan
Ann Arbor, Michigan (1)

Chief, Bureau of Ordnance
Department of the Navy
Washington 25, D. C.
Attn: Code Re6a (1)

Commanding Officer
Naval Torpedo Station
Newport, Rhode Island (1)

Commanding Officer and Director
David Taylor Model Basin
Washington 7, D. C.
Attn: Ship Division (1)

Commanding Officer
Naval Ordnance Laboratory
White Oak, Maryland
Attn: Underwater Ordnance Department (1)

Director
Lewis Flight Propulsion Laboratory
National Advisory Committee for Aeronautics
21000 Brookpark Road
Cleveland 11, Ohio (1)

Professor C. H. Wu
Department of Mechanical Engineering
Polytechnic Institute of Brooklyn
99 Livingston Street
Brooklyn 2, New York (1)

Professor H. Reissner
Department of Aeronautical Engineering and Applied Mechanics
Ploytechnic Institute of Brooklyn
99 Livingston Street
Brooklyn 2, New York (1)

Professor P. F. Maeder
Division of Engineering
Brown University
Providence 12, Rhode Island (1)

Professor D. Rannie
Department of Mechanical Engineering
California Institute of Technology
Pasadena 4, California (1)

Professor J. V. Charyk
Forrestal Research Center
Princeton University
Princeton, New Jersey (1)

Director
Jet Propulsion Laboratory
California Institute of Technology
Pasadena 4, California (1)

Professor J. L. Hooper
Alden Hydraulic Laboratory
Worcester Polytechnic Institute
Worcester, Massachusetts (1)

Dean K. E. Schoenherr
College of Engineering
University of Notre Dame
Notre Dame, Indiana (1)

Professor J. R. Weske
Institute for Fluid Dynamics and Applied Mathematics
University of Maryland
College Park, Maryland (1)

Dr. J. M. Robertson
Ordnance Research Laboratory
Pennsylvania State University
State College, Pennsylvania (1)

Massachusetts Institute of Technology
Department of Naval Architecture
Cambridge 39, Massachusetts (1)

California Institute of Technology
Hydrodynamics Laboratory
Pasadena 4, California
Attn: Professor A. Hollander (1)
Professor R. T. Knapp (1)
Professor M. S. Plesset (1)

Professor V. A. Vanoni
Hydrodynamics Laboratory
California Institute of Technology
Pasadena 4, California (1)

Hydrographer
Department of the Navy
Washington 25, D. C. (1)

Professor M. L. Albertson
Department of Civil Engineering
Colorado A & M College
Fort Collins, Colorado (1)

Professor H. A. Thomas
Pierce Hall
Harvard University (1)
Cambridge 38, Massachusetts

Dr. F. N. Frenkiel
Applied Physics Laboratory
Johns Hopkins University
8621 Georgia Avenue
Silver Spring, Maryland (1)

Professor A. T. Ippen
Hydrodynamics Laboratory
Massachusetts Institute of
Technology (1)
Cambridge 39, Massachusetts

Dr. R. R. Revelle
Scripps Institute of Oceanography
La Jolla, California (1)

Professor J. K. Vennard
Department of Mechanical
Engineering
Stanford University
Stanford, California (1)

Dr. Hunter Rouse, Director
Iowa Institute of Hydraulic
Research
State University of Iowa
Iowa City, Iowa (1)

Stevens Institute of Technology
Experimental Towing Tank
711 Hudson Street
Hoboken, New Jersey (1)

Professor J. W. Johnson
Fluid Mechanics Laboratory
University of California
Berkeley 4, California (1)

Professor H. A. Einstein
Department of Engineering
University of California
Berkeley 4, California (1)

Dr. L. G. Straub
St. Anthony Falls Hydraulic
Laboratory
University of Minnesota
Minneapolis 14, Minnesota (1)

Dr. G. H. Hickox
Engineering Experiment Station
University of Tennessee
Knoxville, Tennessee (1)

Director
Woods Hole Oceanographic
Institute
Woods Hole, Massachusetts (1)

Mr. C. A. Gongwer
Aerojet General Corporation
6352 N. Irwindale Avenue
Azusa, California (1)

Chief, Bureau of Aeronautics
Department of the Navy
Washington 25, D. C.
Attn: Airframe Design Div. (1)

Chief, Bureau of Ordnance
Department of the Navy
Washington 25, D. C.
Attn: Code Re9a (1)

Commanding Officer
Naval Ordnance Laboratory
White Oak, Maryland
Attn: Aerophysics Division (1)

Commander
Naval Ordnance Test Station
Inyokern
China Lake, California (1)

Director
Ames Aeronautical Laboratory
National Advisory Committee
for Aeronautics
Moffett Field, California (1)

Professor A. Ferri
Department of Aeronautical
Engineering and Applied
Mechanics
Polytechnic Institute of Brooklyn
99 Livingston Street
Brooklyn 2, New York (1)

Brown University
Graduate Division of Applied
Mathematics (1)
Providence 12, Rhode Island

California Institute of Technology
Guggenheim Aeronautical Laboratory
Pasadena 4, California
Attn: Professor P. A. Lagerstrom
Professor L. Lees
Professor H. W. Liepmann

Professor S. Corrsin
Department of Aeronautical Engineering
Johns Hopkins University
Baltimore 18, Maryland (1)

Professor C. C. Lin
Department of Mathematics
Massachusetts Institute of
Technology (1)
Cambridge 39, Massachusetts

Institute for Fluid Dynamics
and Applied Mathematics
University of Maryland
College Park, Maryland (1)

Professor George F. Carrier
Department of Engineering
Sciences
Harvard University
Cambridge 38, Massachusetts (1)

Dean L. M. K. Boelter
University of California
Los Angeles 24, California (1)

Professor S. A. Schaaf
Low Pressures Research Project
University of California
Berkeley, California (1)

Stanford University
Guggenheim Aeronautical
Laboratory
Stanford, California (1)

Professor H. G. Lew
Department of Aeronautical
Engineering
Pennsylvania State University
State College, Pennsylvania (1)

Massachusetts Institute of
Technology
Department of Mechanical
Engineering
Cambridge 39, Massachusetts
Attn: Professor J. Kaye (1)
Professor A. H. Shapiro (1)
Professor E. S. Taylor (1)

Professor A. M. Kuethe
Department of Aeronautical
Engineering
University of Michigan
Ann Arbor, Michigan (1)

Professor J. D. Akerman
Department of Aeronautical
Engineering
University of Minnesota
Minneapolis 14, Minnesota (1)

University of Washington
Department of Aeronautical
Engineering
Seattle, Washington (1)

Professor C. H. Fletcher
Department of Aeronautical
Engineering
University of Illinois
Urbana, Illinois (1)

Professor M. J. Thompson
Defense Research Laboratory
University of Texas
Austin, Texas (1)

Professor R. P. Harrington
Department of Aeronautical
Engineering
Rensselaer Polytechnic Institute
Troy, New York (1)

Professor S. M. Bogdonoff
Department of Aeronautical
Engineering
Princeton University
Princeton, New Jersey (1)

Professor M. U. Clauser
Department of Aeronautical
Engineering
Purdue University
Lafayette, Indiana (1)

Chief, Bureau of Ships
Department of the Navy
Washington 25, D. C.
Attn: Ship Design Division (1)
Prop & Shafting Branch (1)